MECHANISTIC AND SPECTROSCOPIC INVESTIGATIONS OF RADICAL GENERATION AND EPIMERIZATION PATHWAYS IN RADICAL SAM ENZYMES

by

Andrew Buckley Gleason

A thesis submitted in partial fulfillment
of the requirements for the degree

of

Master of Science

in

Biochemistry

MONTANA STATE UNIVERSITY
Bozeman, Montana

December 2025

©COPYRIGHT

by

Andrew Buckley Gleason

2025

All Rights Reserved

DEDICATION

This work is dedicated to my family. First, my mom, (Shannon) and dad (Mark) who raised me to be the best version of myself through hard work, curiosity and care for others. Secondly, my sister (Abby) who has always been my biggest supporter. Finally, to my grandfather, Dr. Robert Gleason whose lifelong dedication to science inspired my own journey into research.

ACKNOWLEDGEMENTS

First and foremost, I want to extend my deepest thanks and gratitude to Prof. Joan Broderick for introducing me to the world of bioinorganic chemistry and guiding me through two and a half years of graduate school. It has been a pleasure to be a part of Joan's lab and contribute to the meaningful work that she does. I also would like to thank my graduate committee, Prof. Valèrie Copiè and Prof. Christopher Lemon for their guidance and scientific expertise. Sincere thank you to Dr. Will Walls for training me on almost every instrument in the lab. I am grateful for your patience and guidance throughout my time in the Broderick lab and for our helpful discussions over the years. I must also thank Prof. Will Broderick and Dr. Eric Shephard for their wonderful insights and thoughtful discussions throughout my time in the Broderick Lab. Finally, a sincere thank you to MSU College of Letters and Science and the NIH for the funding that made this research possible.

TABLE OF CONTENTS

TABLE OF CONTENTS CONTINUED

LIST OF TABLES

Table Page

LIST OF FIGURES

Figure Page

LIST OF FIGURES CONTINUED

LIST OF FIGURES CONTINUED

LIST OF FIGURES CONTINNUED

LIST OF FIGURES CONTINUED

ABSTRACT

Metalloproteins are ubiquitous biocatalysts that mediate diverse chemical transformations by exploiting the redox flexibility of metal cofactors. Among these, iron–sulfur (FeS) clusters are exceptionally versatile, enabling electron transfer, radical generation, and complex bond-forming reactions. The radical S-adenosyl-L-methionine (rSAM) superfamily represents one of the largest and most functionally diverse groups of enzymes that rely on [4Fe-4S] clusters to catalyze chemically challenging reactions via radical intermediates. In these enzymes, SAM coordinates to the unique iron of the [4Fe-4S] cluster, undergoing reductive cleavage to generate the potent 5′-deoxyadenosyl radical (5′-dAdo•). The work described in this chapter first examines the electronic basis of SAM activation, highlighting the substantial thermodynamic barrier between SAM reduction and cluster redox potentials, and presents evidence implicating the Jahn–Teller effect in determining the regioselectivity of S–C bond cleavage. The latter section focuses on the biochemical and spectroscopic characterization of OpgD, a newly identified radical SAM epimerase belonging to the origamin family. EPR analysis of OpgD reveals an auxiliary [4Fe-4S] cluster (AuxI) that may participate in electron transfer or radical quenching during catalysis. Together, these studies advance our understanding of sulfonium activation and the functional diversity of auxiliary clusters in radical SAM enzymes.

CHAPTER ONE

INTRODUCTION TO RADICAL SAM ENZYMES

Metals in Biology

Metalloproteins are widespread across all kingdoms of life and catalyze a range of reactions, including electron transfer, molecular transport, metallocofactor assembly, nucleotide modification, anaerobic metabolism, and the biosynthesis of natural products.[1-3] The feasibility of these complex reactions arises from the remarkable electronic flexibility of protein-bound metal sites, which can adopt multiple oxidation states to facilitate diverse processes. When properly coordinated, these metal sites can serve as precision tools for performing directed and specific chemistries. However, metals can be potentially toxic when not adequately controlled, leading to the formation of highly reactive radicals and reactive oxygen species (ROS).[4-6] Elucidating the interactions between metal cofactors and their coordination spheres is fundamental to the rational design and engineering of proteins with tailored or enhanced catalytic functions.

Protein-based metal centers can include mono-nuclear, di-nuclear, and complex metallocofactors, which may contain transition metals such as nickel, copper, cobalt, manganese, and iron (Figure 1.1). The work presented here focuses entirely on the iron metal sites of proteins, which can be found in several different forms, including: mononuclear non-heme iron such as in rubredoxin (Figure 1.1A), iron ions bound to organic ligands such as heme in hemoglobin (Figure 1.1B), iron sulfur clusters ([2Fe-2S], [3Fe-4S], [4Fe-4S]) such as in ferredoxins and Rieske proteins (Figure 1.1C), and more complex iron-sulfur clusters including

those with organic molecules bound such as in radical *S*-adenosyl-L-methionine (SAM) enzymes (Figure 1.1D). Proteins form defined coordination spheres around their metal centers—and for FeS clusters the primary and secondary coordination spheres modulate their reduction potentials (E°′) to span a wide range from approximately –650 mV to +450 mV.[7] The most common ligands for FeS clusters are cysteine thiolates, though histidine and occasionally other amino acid side chains can also serve as coordinating ligands. These versatile metallocofactors play central roles in electron transfer in biology, and can also serve as catalytic centers for a wide range of reactions, including carbon–carbon bond formation and cleavage, radical generation, and isomerization.[8] In enzymes that carry out these complex transformations, the small organic molecule S-adenosyl-L-methionine (SAM) acts in concert with the [4Fe–4S] cluster, as the characteristic active site components of the radical SAM (rSAM) enzyme superfamily.[1, 3, 9, 10]

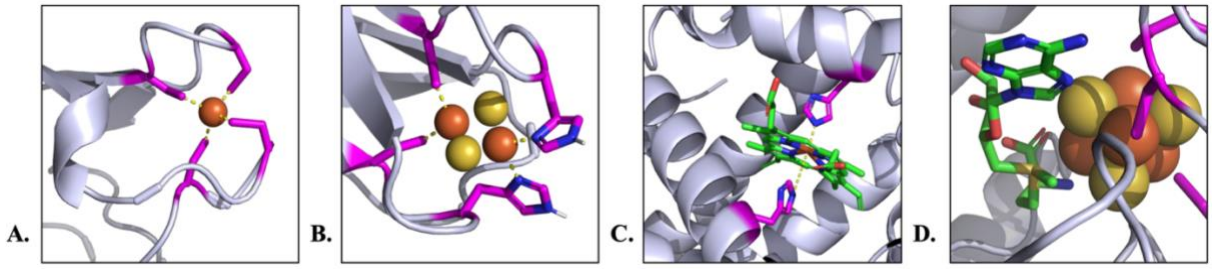

Figure 1.1. Protein Active sites with iron. A) rubredoxin from *Pyrococcus furiosus* (PDB: 1BRF), B) hemoglobin from *Homo sapiens* (PDB: 2DN2), C) Rieske from *Spinacia oleracea* (PDB: 1RFS), D) Radical SAM from *Escherichia coli* (PDB: 8FOL). Color scheme: Fe, rust; S, yellow spheres; coordinating ligands, magenta; protein structure, grey.

Radical SAM Enzymes

Radical SAM enzymes represent one of the largest superfamilies of enzymes in nature, found across all kingdoms of life and consisting of more than 700,000 members.[3, 11, 12] To handle the large sequence space of the family, radicalSAM.org was introduced, which represents the

superfamily as a network of sequence similarity networks.[12] While over 700,00 sequences have been identified encoding rSAM enzymes, only a fraction of these enzymes have been experimentally investigated, and fewer still have been characterized. Radical SAM enzymes all consist of a catalytically essential [4Fe-4S] cluster and have been shown to adopt a triose phosphate isomerase (TIM) barrel fold, which comprises alternating alpha-helices and beta strands connected by loop regions (Figure 1.2). The barrel fold is consistent throughout rSAM enzymes but varies in the number of alternating secondary structures with a full TIM barrel consisting of 8 alternating units, although some structures have been observed to consist of 6 repeating units.[2] Generally, the cavity created by the TIM barrel fold correlates with the size of the substrate, with smaller folds used for smaller substrates and larger folds for larger substrates.[2, 13]

Despite low primary sequence similarity among the rSAM family, they share some characteristic motifs, most notably a CX_3CX_2C motif, with the cysteine thiolates coordinating three out of four of the irons in the [4Fe-4S] cluster. This unique motif is one of the primary diagnostic criteria for determining if an enzyme belongs to the radical SAM (rSAM) superfamily.[1, 3, 13, 14] However, some enzymes deviate from this canonical pattern and are thus considered outliers within the group. One such example is ThiC, a thiamin pyrimidine synthase possessing a CX_2CX_4C motif located near the C-terminus of its sequence rather than at the N-terminus, where the conventional motif would reside.[15] Another exception is PhnJ, an enzyme responsible for catalyzing the cleavage of Carbon-phosphorus (C-P) bonds in phosphonates. Its catalytically essential [4Fe-4S] cluster is coordinated by a $CX_2CX_{21}CX_5C$ motif, which is placed near the C-terminal region of the protein.[16] Yet another example is QueE, a 7-carboxy-7-

deazaguanine synthase, which also deviates from consensus in that it employs a $CX_{14}CX_2C$ cluster-binding motif.[17] Collectively, these enzymes illustrate the structural diversity existing in the rSAM superfamily, despite their shared reliance on iron-sulfur chemistry.

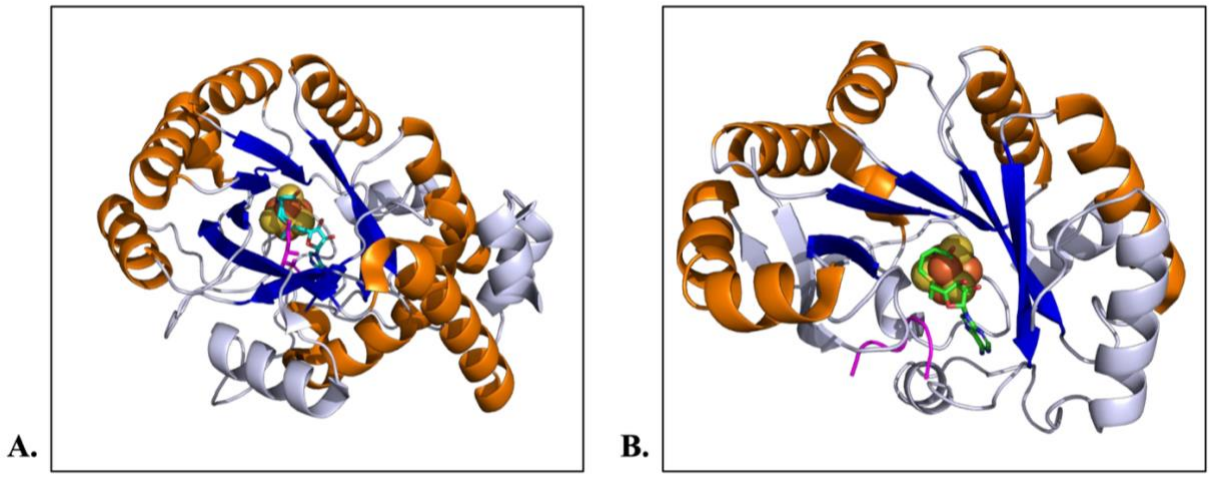

Figure 1.2. Radical SAM enzymes with full or partial TIM barrel folds. In all structures, the alpha-helices of the TIM barrel are shown in orange, the beta strands are displayed in dark blue, and the rest of the protein structure in grey. In the center of the TIM barrel, essential components of radical SAM enzymes are displayed: the [4Fe-4S] cluster (Sulphur, yellow spheres; iron, rust-colored spheres), SAM (green/light blue sticks), and substrate (magenta sticks, when present). (A) The full TIM barrel fold $(\beta\alpha)_8$ is methylornithine synthase, PlyB (PDB: 3T7V). (B) PFL-AE's partial TIM barrel fold $(\beta\alpha)_6$ houses the cluster, SAM, and a peptide (magenta sticks) representing the arm of PFL that sits in the PFL-AE active site (PDB: 3CB8).

Interaction of SAM with [4Fe-4S] clusters

An essential interaction for radical SAM enzymes is the coordination of the SAM molecule to the [4Fe-4S] cluster. Typically, three out of the four irons of the [4Fe-4S] cluster are coordinated by cysteine thiolates, with the fourth iron of the site-differentiated cluster referred to as the unique iron. The unique iron of the [4Fe-4S] cluster is labile, as evidenced by the observations that the cluster in an as-isolated enzymes frequently exists partially as the inactive $[3Fe\text{-}4S]^+$ state, and this state can also readily be generated from the $[4Fe\text{-}4S]^{2+}$ state upon

exposure to oxygen. With the addition of iron and a mild reducing agent like dithiothreitol (DTT), the $[3Fe\text{-}4S]^{+}$ can be converted to the $[4Fe\text{-}4S]^{2+}$ state.[1] The $[4Fe\text{-}4S]^{2+}$ cluster can be reduced to the $[4Fe\text{-}4S]^{+}$ state *in vitro* chemically using sodium dithionite (NaDT) or through a photochemical process by using 5'-deazariboflavin.[1, 18] Because the [4Fe-4S] cluster is readily oxidized, radical SAM enzymes are highly oxygen-sensitive; therefore, their purification, biochemical assays, and spectroscopic analyses must be performed under strictly anaerobic conditions. Within the active site, SAM coordinates to the unique iron in a bidentate fashion through its amine and carboxylate moieties, forming a 5-membered ring chelate, thereby placing the sulphonium in orbital overlap with the unique iron (Figure 1.4).[19-21]

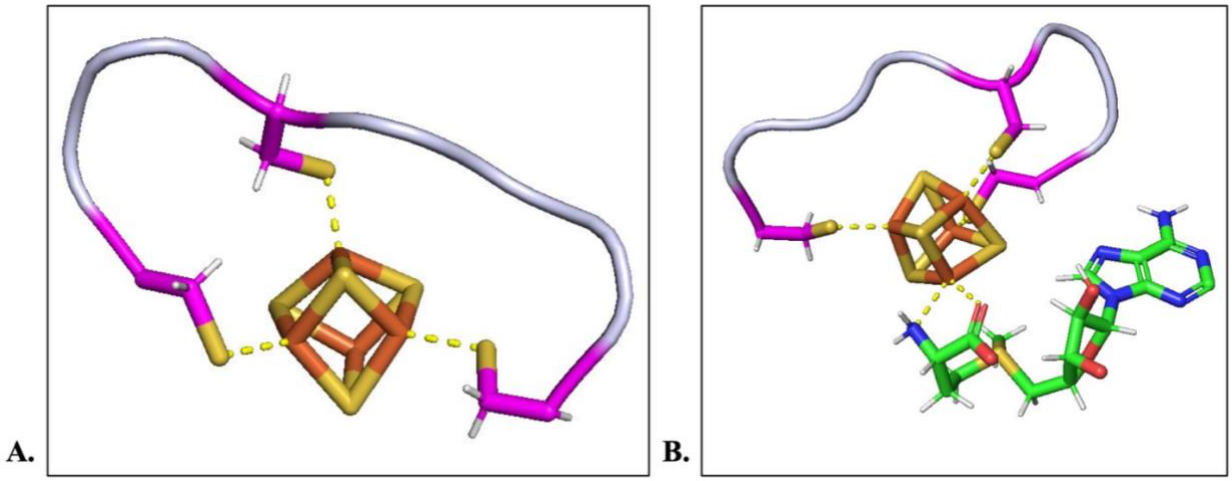

Figure 1.3. Coordination of the radical SAM [4Fe-4S] cluster in radical SAM enzyme pyruvate formate lyase activating enzyme (PDB: 3CB8). A) Cysteine thiolates in a CXXXCXXC motif coordinate three out of four irons. Each sulfur is 2.3 Å from the iron it coordinates. B) SAM coordinates to the unique iron via its carboxylate and amine moieties. The oxygen of the carboxylate and nitrogen of the amine are 2.2 Å and 2.3 Å from the iron, respectively. Irons represented in orange, sulfurs in yellow, and coordinating cysteine residues in magenta.

Some rSAM enzymes have been shown to contain a C-terminal extension known as either a twitch or SPASM (named for its founding member) domain which can coordinate one

(twitch) or two (SPASM) additional FeS clusters.[22] Additional [4Fe–4S] clusters coordinated through the SPASM domain are designated AuxI and AuxII, with AuxI positioned proximal to the radical SAM cluster and AuxII located more distally. The twitch domain is a truncated variant of the SPASM domain and coordinates a single auxiliary [4Fe–4S] cluster. These auxiliary clusters play different roles depending on the protein and can include electron transfer, substrate coordination, or structural stabilization.[23-25] Mutating the cysteine residues ligating one or both Fe–S clusters typically results in protein insolubility or loss of activity, thereby restricting functional characterization of these clusters. These clusters are not always able to be reduced chemically, making their activity difficult to track spectroscopically.[25, 26] Radical SAM enzymes containing SPASM or twitch domains are most often associated with the biosynthesis of ribosomally synthesized and post-translationally modified peptides (RiPPs).[27-29]

Radical Initiation Mechanism

Despite their large catalytic and structural diversity, all rSAM enzymes are proposed to undergo the same radical initial mechanism, involving the generation of a highly reactive intermediate, 5'-dAdo•, followed by hydrogen atom abstraction from the substrate (Figure 1.3).[1] *In vivo* initiation of radical SAM enzymes occurs through a single-electron transfer from flavodoxin, ferredoxin, or other electron donors to the $[4Fe\text{-}4S]^{2+}$ cluster, which is chelated by SAM, thereby reducing it to the $[4Fe\text{-}4S]^{+}$ state.[30] *In vitro,* this reduction can be achieved using strong reductants such as sodium dithionite or photoreduced 5-deazariboflavin. Coordination of SAM and/or substrate triggers electron transfer from the cluster to the sulphonium center, resulting in homolytic cleavage of the S-C(5') bond of SAM. The complex rearranges to form the organometallic intermediate, **Ω**, featuring a covalent bond between the C(5') of dAdo and the

unique iron, with the amino and carboxylate moieties still bound.[31, 32] Homolysis of this Fe-C bond generates the highly reactive and oxidizing radical intermediate, 5'-dAdo•, which regio- and stereoselectively abstracts a hydrogen atom from the substrate. This generates a substrate radical intermediate, which can then perform its own specific chemistry (Figure 1.3).[33] The resulting methionine and dAdoH diffuse from the active site, and the oxidized $[4Fe\text{-}4S]^{2+}$ cluster can be regenerated for further catalysis via further reduction by ferredoxin, flavodoxin, or NADPH to the $[4Fe\text{-}4S]^{1+}$ state. When a second equivalent of SAM binds to the unique iron, the enzyme is primed for further catalysis.[33-35]

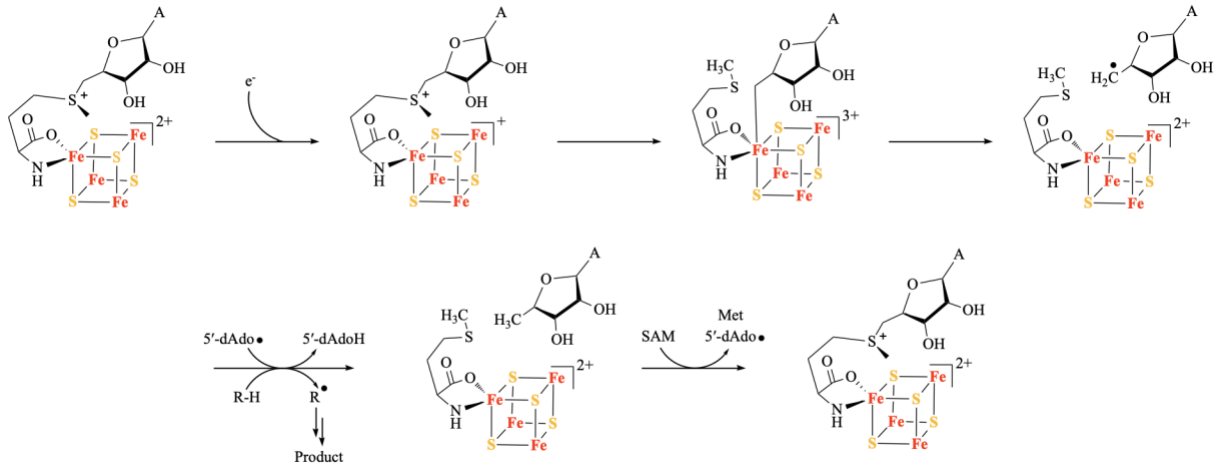

Figure 1.4. Proposed mechanism for radical initiation in radical SAM enzymes.

Glycyl Radical Enzyme — Activating Enzymes

One of the founding members of the radical SAM superfamily is pyruvate formate lyase activating enzyme (PFL-AE). PFL-AE is also a member of a subclass of radical SAM enzymes called glycyl radical enzyme activating enzymes (GRE-AE).[36-38] Glycyl radical enzymes utilize a post-translationally installed backbone glycyl radical to initiate a wide range of reactions

involved in anaerobic glucose metabolism, anaerobic metabolism of hydrocarbons, and glucose dehydration.[39-41] The backbone glycyl radical is installed by a GRE-AE, which abstracts the pro-*S* hydrogen from a conserved glycine residue on the "Gly loop," which can move or flip into the active site of the activating enzyme for radical installation.[42] After installation, the Gly loop flips back into the GRE, and the glycyl radical abstracts a hydrogen from a conserved Cys residue near the Gly loop. [36, 37] The cysteine radical then abstracts a hydrogen from the substrate to form a substrate base radical, which then converts into a product radical. This radical is quenched by reabstracting a hydrogen atom from the conserved Cys residue, which in turn abstracts a hydrogen from the conserved glycine radical to reform the stable glycyl radical (Figure 1.5)

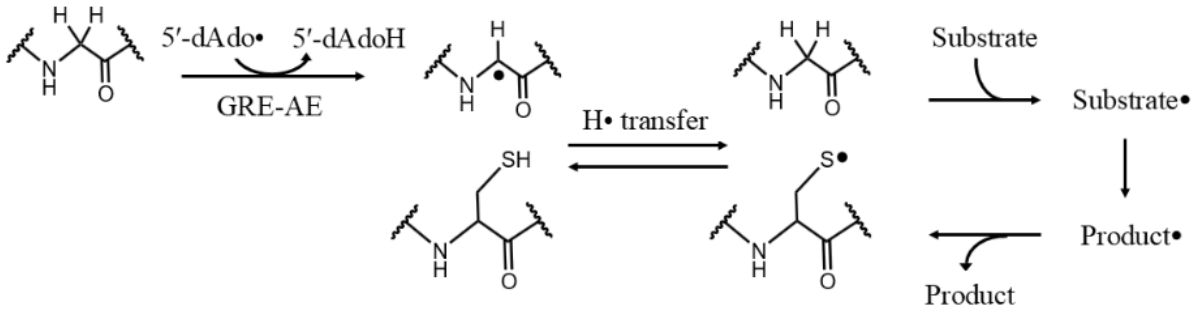

Figure 1.5. Activation and general mechanism of the GRE family. Activation of the GRE begins with a radical SAM enzyme generating 5'-dAdo•, generating the catalytic glycyl radical. Figure from reference.[43]

HydG and Hydrogenase maturation.

[FeFe]-hydrogenases catalyze the reversible conversion of two protons and electrons to form molecular hydrogen. These enzymes are extremely efficient catalysts in generating hydrogen gas, making them an appealing target for biohydrogen production technologies.[44, 45] The [FeFe] hydrogenase, HydA, contains a unique metallocofactor in the active site called the H-

cluster (Figure 1.6), which consists of a [4Fe-4S] cluster ligated via a bridging cysteine thiolate ligand to a 2Fe subcluster. The subcluster irons are ligated by two carbon monoxide (CO) and two cyanide (CN) ligands with a bridging dithiomethylamine (DTMA).[45]

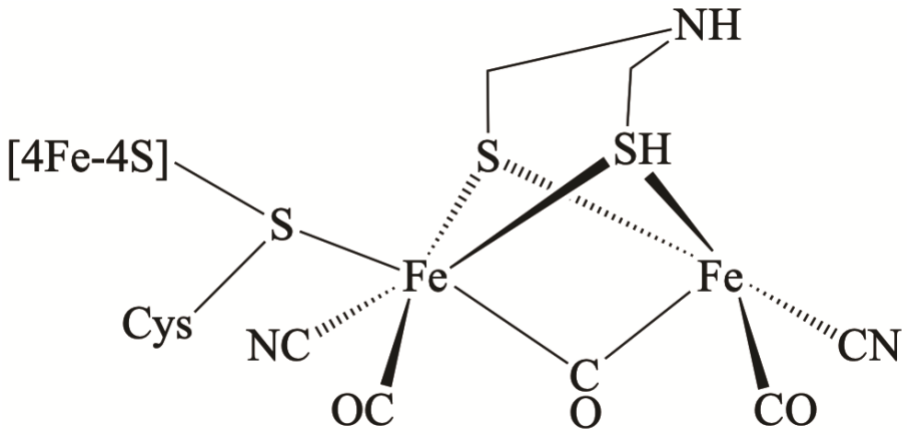

Figure 1.6. The active site HydA metal cluster contains a [4Fe-4S] cubane bridged to a 2Fe subcluster. The two irons of the subcluster a ligated by 2 carbon monoxide, a cyanide, and a dithiomethylamine (DTMA) ligand each.

Early studies on the [FeFe]-hydrogenase metallocofactor revealed that its synthesis and activation requires three dedicated maturation proteins: HydG, HydE, and HydF.[46, 47] Both HydG and HydE are radical SAM enzymes, and HydF is a GTPase that coordinates FeS clusters.[1, 47-50] These three maturases biochemically synthesize the 2Fe subcluster and transfer it to HydA, where it binds to the [4Fe-4S] cluster, resulting in the bioactive H-cluster.[51] The current model for maturation of HydA is depicted in Figure 1.7. HydG catalyzes the radical SAM-dependent cleavage of tyrosine to generate CO and CN^- ligands that bind an FE center, forming the organometallic synthon used in the [2FE] subcluster assembly.[52, 53] HydE uses radical SAM chemistry to couple two of these Fe-CO-CN synthons and install bridging sulfur atoms,

completing the formation of the [2Fe] subcluster precursor that is later incorporated into the H-cluster of [FeFe]-hydrogenase.[52, 54]

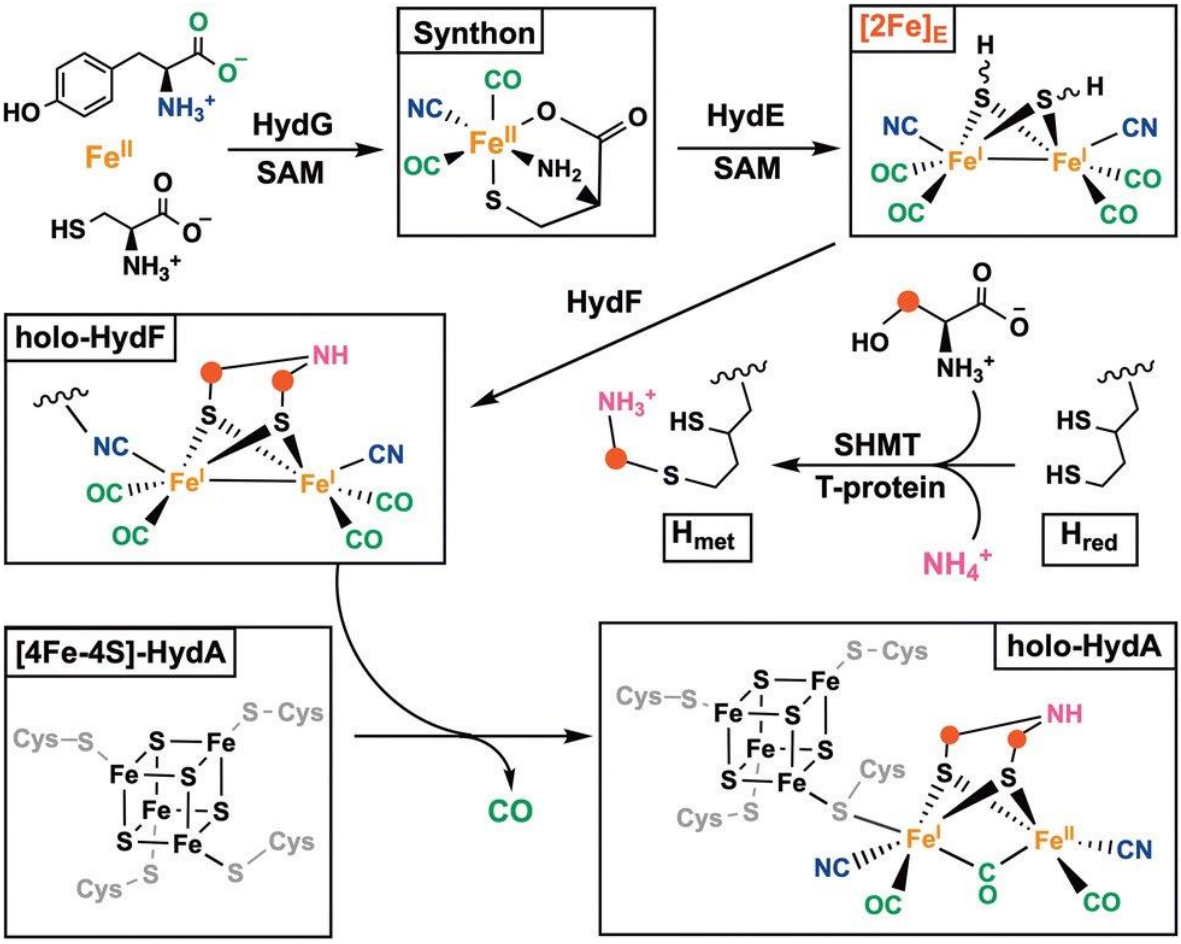

Figure 1.7. In the current model of [FeFe]-hydrogenase (HydA) maturation, the radical SAM enzyme HydG initiates assembly of the catalytic H-cluster by synthesizing a small organometallic synthon that serves as a precursor to the $[2Fe]^E$ subcluster. The radical SAM enzyme HydE subsequently couples two of these synthons to generate the complete $[2Fe]^E$ unit, which is then transferred to the scaffold protein HydF. Within HydF, the dithiomethylamine (DTMA) ligand is incorporated, finalizing maturation of the $[2Fe]^E$ moiety prior to its delivery to the apo-HydA protein. The DTMA ligand itself is synthesized through the glycine cleavage system, involving the coordinated activity of serine hydroxymethyltransferase (SHMT), T-protein, and H-protein (in both the reduced and methylated forms, Hred/Hmet). Unpublished figure used with permission from A. Marlott.

Biosynthesis of RiPP Natural Products

Organisms produce natural products to provide themselves with an ecological advantage intended to defend against threats, compete for resources, communicate, or adapt to environmental stress.[55, 56] These products can be produced by two separate pathways: ribosomally synthesized and non-ribosomally synthesized. The latter pathway is composed of large, multienzyme complexes, where each module appends a specific amino acid to the growing polypeptide chain.[57] The former synthesis pathway of natural products—which is the focus of this section—occurs at the ribosome. These natural products are referred to as ribosomally synthesized and post-translational modified peptides (RiPPs), and are a diverse class of natural products with a broad range of bioactivities, including antimicrobial, antiviral, and apoptosis-inducing properties.[58-61]

Maturation of RiPP natural products begins with the ribosomal synthesis of the precursor peptide. This precursor generally contains an N-terminal leader region and a C-terminal core region, with the leader region comprising recognition elements that recruit and bind maturation enzymes, which install post-translational modifications (PTMs) on the C-terminal core. The core is then cleaved from the N-terminal leader region, typically by a dedicated protease, and the bioactive core can then be excreted from the cell.

A major post-translational modification observed in RiPP natural products is epimerization, a process that alters the stereochemistry of amino acid residues at the Cα position, converting the naturally occurring L-configuration into the D-form. D-amino acids are known for their stability against proteases because the proteases are unable to recognize the non-natural configuration.[62] Epimerization of the precursor peptide can occur through either polar or radical-based mechanisms—the latter often involving radical SAM enzymes. The proposed mechanism

of radical-based epimerization of amino acids is shown in Figure 1.8, and begins with the reductive cleavage of SAM, releasing 5'-dAdo•, which abstracts the Cα hydrogen, forming a Cα radical intermediate. A cysteine residue in the primary sequence of the epimerase then stereospecifically quenches the radical through a hydrogen atom transfer step to yield a D-amino acid and a thiyl radical, which is quenched by solvent or electron transfer from an auxiliary FeS cluster.

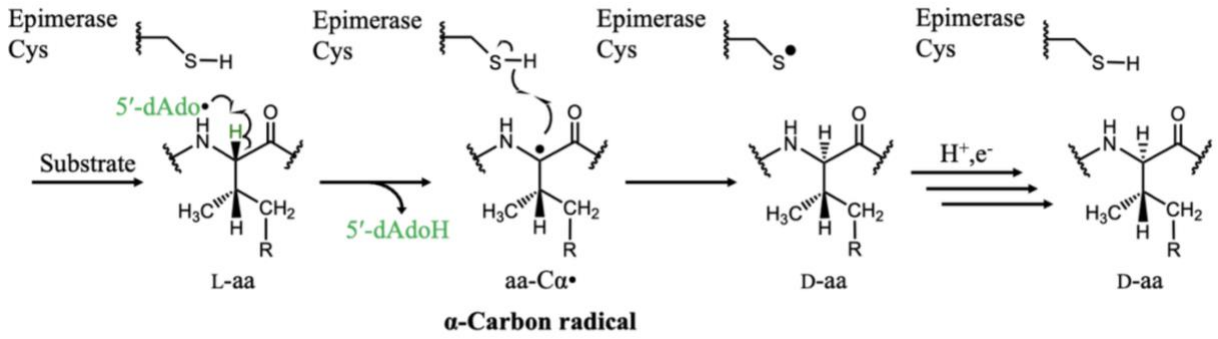

Figure 1.8. General mechanism of radical epimerization. 5'-dAdo• abstracts a hydrogen from the Cα, which is in turn quenched by a cysteine residue of the epimerase on the backside of the peptide, thus inverting the stereochemistry about the Cα. For this figure, R is either -CH_3 representing an isoleucine residue, or a hydrogen indicating a valine residue.

Several classes of epimerases have been discovered, including proteusins, eppipeptides, and origamins. The proteusin family of enzymes usually acts on large peptides and produces, complex products with numerous PTMs, including C- and N-methylations, aminations, cysteine crosslinks, and epimerizations.[63] Eppipeptide epimerases generally act on smaller peptides and install fewer PTMs, and the enzymes often harbor a twitch domain harboring an auxiliary [4Fe-4S] cluster. To date, the only crystal structures of radical SAM epimerases are of the rSAM enzyme EpeE with and without a truncated version of its substrate (EpeX) bound in the active site (PDB 8AI1 and 8AI2). Origamins are a newly discovered family of epimerases with

biosynthetic gene clusters found widespread in the human microbiome. There is currently no published work on this class of epimerases; however, origamins are proposed to consist of attributes found in both proteusins and eppipeptides. The enzyme family was discovered by Jorn Piel's lab out of ETH Zurich and is proposed to act on large substrates like proteusins but has predicted structural similarity to eppipeptides.

The work presented in the following two chapters focuses on fundamental aspects of the radical initiation mechanism in radical SAM enzymes and the characterization of a newly discovered radical SAM origamin epimerase, OpgD. The first chapter focuses on the regioselectivity of sulphonium reductive cleavage in the generation of 5'-dAdo•. We use an anhydrous analogue of SAM and using substrate-free photolysis provide evidence for the role of the Jahn-Teller effect in determining which of the S-C bonds is cleaved. The second chapter discusses the biochemical characterization of OpgD, and we provide evidence of SAM binding, and an EPR active AuxI cluster which could provide useful insights into the roles of auxiliary [4Fe-4S] clusters in radical SAM epimerases.

References

(1) Broderick, J. B.; Duffus, B. R.; Duschene, K. S.; Shepard, E. M. Radical S-Adenosylmethionine Enzymes. *Chem. Rev.* **2014**, *114* (8), 4229-4317, Review.

(2) Nicolet, Y. Structure-function relationships of radical SAM enzymes. *Nat. Catal.* **2020**, *3* (4), 337-350, Review.

(3) Sofia, H. J. Radical SAM, a novel protein superfamily linking unresolved steps in familiar biosynthetic pathways with radical mechanisms: functional characterization using new analysis and information visualization methods. *Nucleic Acids Research* **2001**, *29* (5), 1097-1106.

(4) Wang, Y.; Li, D.; Xu, K.; Wang, G.; Zhang, F. Copper homeostasis and neurodegenerative diseases. *Neural Regeneration Research* **2025**, *20* (11), 3124-3143.

(5) Burdette, S. C.; Lippard, S. J. Meeting of the minds: Metalloneurochemistry. *Proceedings of the National Academy of Sciences* **2003**, *100* (7), 3605-3610.

(6) Valko, M.; Jomova, K.; Rhodes, C. J.; Kuča, K.; Musílek, K. Redox- and non-redox-metal-induced formation of free radicals and their role in human disease. *Archives of Toxicology* **2016**, *90* (1), 1-37.

(7) Fontecave, M. Iron-sulfur clusters: ever-expanding roles. *Nature Chemical Biology* **2006**, *2* (4), 171-174.

(8) Finkelstein, J. Metalloproteins. *Nature* **2009**, *460* (7257), 813-813.

(9) Frey, P. A.; Hegeman, A. D.; Ruzicka, F. J. The Radical SAM Superfamily. *Critical Reviews in Biochemistry and Molecular Biology* **2008**, *43* (1), 63-88.

(10) Booker, S. J.; Lloyd, C. T. Twenty Years of Radical SAM! The Genesis of the Superfamily. *ACS Bio & Med Chem Au* **2022**, *2* (6), 538-547.

(11) Blum, M.; Andreeva, A.; Laise; Sara; Grego, T.; Hobbs, E.; Beatriz; Orr, A.; Paysan-Lafosse, T.; Ponamareva, I.; et al. InterPro: the protein sequence classification resource in 2025. *Nucleic Acids Research* **2025**, *53* (D1), D444-D456.

(12) Oberg, N.; Precord, T. W.; Mitchell, D. A.; Gerlt, J. A. RadicalSAM.org: A Resource to Interpret Sequence-Function Space and Discover New Radical SAM Enzyme Chemistry. *ACS Bio & Med Chem Au* **2022**, *2* (1), 22-35.

(13) Vey, J. L.; Drennan, C. L. Structural Insights into Radical Generation by the Radical SAM Superfamily. *Chem. Rev.* **2011**, *111* (4), 2487-2506. DOI: 10.1021/cr9002616.
(14) Layer, G.; Heinz, D. W.; Jahn, D.; Schubert, W.-D. Structure and function of radical SAM enzymes. *Current Opinion in Chemical Biology* **2004**, *8* (5), 468-476.

(15) Fenwick, M. K.; Mehta, A. P.; Zhang, Y.; Abdelwahed, S. H.; Begley, T. P.; Ealick, S. E. Non-canonical active site architecture of the radical SAM thiamin pyrimidine synthase. *Nat. Commun.* **2015**, *6* (1), 6480.

(16) Kamat, S. S.; Raushel, F. M. PhnJ – A novel radical SAM enzyme from the C–P lyase complex. *Perspectives in Science* **2015**, *4*, 32-37.

(17) Dowling, D. P.; Bruender, N. A.; Young, A. P.; McCarty, R. M.; Bandarian, V.; Drennan, C. L. Radical SAM enzyme QueE defines a new minimal core fold and metal-dependent mechanism. *Nature Chemical Biology* **2014**, *10* (2), 106-112.

(18) Byer, A. S.; McDaniel, E. C.; Impano, S.; Broderick, W. E.; Broderick, J. B. Mechanistic Studies of Radical SAM Enzymes: Pyruvate Formate-Lyase Activating Enzyme and Lysine 2,3-Aminomutase Case Studies. In *Radical Sam Enzymes*, Bandarian, V. Ed.; Methods in Enzymology, Vol. 606; Elsevier Academic Press Inc, 2018; pp 269-318.

(19) Walsby, C. J.; Ortillo, D.; Broderick, W. E.; Broderick, J. B.; Hoffman, B. M. An anchoring role for FeS clusters: Chelation of the amino acid moiety of S-adenosylmethionine to the unique iron site of the 4Fe-4S cluster of pyruvate formate-lyase activating enzyme. *J. Am. Chem. Soc.* **2002**, *124* (38), 11270-11271.

(20) Walsby, C. J.; Hong, W.; Broderick, W. E.; Cheek, J.; Ortillo, D.; Broderick, J. B.; Hoffman, B. M. Electron-nuclear double resonance spectroscopic evidence that S-adenosylmethionine binds in contact with the catalytically active 4Fe-4S + cluster of pyruvate formate-lyase activating enzyme. *J. Am. Chem. Soc.* **2002**, *124* (12), 3143-3151.

(21) Krebs, C.; Broderick, W. E.; Henshaw, T. F.; Broderick, J. B.; Huynh, B. H. Coordination of adenosylmethionine to a unique iron site of the 4Fe-4S of pyruvate formate-lyase activating enzyme: A Mossbauer spectroscopic study. *J. Am. Chem. Soc.* **2002**, *124* (6), 912-913.

(22) Grell, T. A. J.; Goldman, P. J.; Drennan, C. L. SPASM and Twitch Domains in S-Adenosylmethionine (SAM) Radical Enzymes. *Journal of Biological Chemistry* **2015**, *290* (7), 3964-3971.

(23) Rush, K. W.; Eastman, K. A. S.; Kincannon, W. M.; Blackburn, N. J.; Bandarian, V. Peptide Selenocysteine Substitutions Reveal Direct Substrate–Enzyme Interactions at Auxiliary Clusters in Radical S-Adenosyl-<scp>l</scp>-methionine Maturases. *J. Am. Chem. Soc.* **2023**, *145* (18), 10167-10177.

(24) Eastman, K. A. S.; Jochimsen, A. S.; Bandarian, V. Intermolecular electron transfer in radical SAM enzymes as a new paradigm for reductive activation. *Journal of Biological Chemistry* **2023**, *299* (9), 105058.

(25) Balo, A. R.; Caruso, A.; Tao, L.; Tantillo, D. J.; Seyedsayamdost, M. R.; Britt, R. D. Trapping a cross-linked lysine–tryptophan radical in the catalytic cycle of the radical SAM enzyme SuiB. *Proceedings of the National Academy of Sciences* **2021**, *118* (21), e2101571118.

(26) Lanz, N. D.; Booker, S. J. Auxiliary iron–sulfur cofactors in radical SAM enzymes. *Biochimica et Biophysica Acta (BBA) - Molecular Cell Research* **2015**, *1853* (6), 1316-1334.

(27) Latham, J. A.; Barr, I.; Klinman, J. P. At the confluence of ribosomally synthesized peptide modification and radical S-adenosylmethionine (SAM) enzymology. *Journal of Biological Chemistry* **2017**, *292* (40), 16397-16405.

(28) Benjdia, A.; Balty, C.; Berteau, O. Radical SAM Enzymes in the Biosynthesis of Ribosomally Synthesized and Post-translationally Modified Peptides (RiPPs). *Frontiers in Chemistry* **2017**, *5*.

(29) Mahanta, N.; Hudson, G. A.; Mitchell, D. A. Radical S-Adenosylmethionine Enzymes Involved in RiPP Biosynthesis. *Biochemistry* **2017**, *56* (40), 5229-5244.

(30) Bruender, N. A.; Young, A. P.; Bandarian, V. Chemical and Biological Reduction of the Radical SAM Enzyme CPH₄ Synthase. *Biochemistry* **2015**, *54* (18), 2903-2910.

(31) Horitani, M.; Shisler, K.; Broderick, W. E.; Hutcheson, R. U.; Duschene, K. S.; Marts, A. R.; Hoffman, B. M.; Broderick, J. B. Radical SAM catalysis via an organometallic intermediate with an Fe–[5′-C]-deoxyadenosyl bond. *Science* **2016**, *352* (6287), 822-825.

(32) Byer, A. S.; Yang, H.; McDaniel, E. C.; Kathiresan, V.; Impano, S.; Pagnier, A.; Watts, H.; Denler, C.; Vagstad, A. L.; Piel, J.; et al. Paradigm Shift for Radical S-Adenosyl-L-methionine Reactions: The Organometallic Intermediate Ω Is Central to Catalysis. *J. Am. Chem. Soc.* **2018**, *140* (28), 8634-8638.

(33) Hoffman, B. M.; Broderick, W. E.; Broderick, J. B. Mechanism of Radical Initiation in the Radical SAM Enzyme Superfamily. *Annu. Rev. Biochem.* **2023**, *92*, 333-349, Review.

(34) McCarthy, E. L.; Booker, S. J. Biochemical Approaches for Understanding Iron–Sulfur Cluster Regeneration in Escherichia coli Lipoyl Synthase During Catalysis. Elsevier, 2018; pp 217-239.

(35) Broderick, J. B.; Broderick, W. E.; Hoffman, B. M. Radical SAM enzymes: Nature's choice for radical reactions. *FEBS Letters* **2023**, *597* (1), 92-101.

(36) Knappe, J.; Blaschkowski, H. P. Pyruvate formate-lyase from Escherischia coli and its activation system. *Methods in enzymology* **1975**, *41*, 508-518.

(37) Rodel, W.; Plaga, W.; Frank, R.; Knappe, J. PRIMARY STRUCTURES OF ESCHERICHIA-COLI PYRUVATE FORMATE-LYASE AND PYRUVATE-FORMATE-LYASE-ACTIVATING ENZYME DEDUCED FROM THE DNA NUCLEOTIDE-SEQUENCES. *European Journal of Biochemistry* **1988**, *177* (1), 153-158.

(38) Broderick, J. B.; Duderstadt, R. E.; Fernandez, D. C.; Wojtuszewski, K.; Henshaw, T. F.; Johnson, M. K. Pyruvate formate-lyase activating enzyme is an iron-sulfur protein. *J. Am. Chem. Soc.* **1997**, *119* (31), 7396-7397.

(39) Backman, L. R. F.; Funk, M. A.; Dawson, C. D.; Drennan, C. L. New tricks for the glycyl radical enzyme family. *Critical Reviews in Biochemistry and Molecular Biology* **2017**, *52* (6), 674-695.

(40) Shisler, K. A.; Broderick, J. B. Glycyl radical activating enzymes: Structure, mechanism, and substrate interactions. *Archives of Biochemistry and Biophysics* **2014**, *546*, 64-71.

(41) Hioe, J.; Savasci, G.; Brand, H.; Zipse, H. The Stability of C_α Peptide Radicals: Why Glycyl Radical Enzymes? *Chemistry-a European Journal* **2011**, *17* (13), 3781-3789.

(42) Peng, Y.; Veneziano, S. E.; Gillispie, G. D.; Broderick, J. B. Pyruvate Formate-lyase, Evidence for an Open Conformation Favored in the Presence of Its Activating Enzyme. *Journal of Biological Chemistry* **2010**, *285* (35), 27224-27231. DOI: 10.1074/jbc.M109.096875.
(43) Walls, W. Mechanistic Investigation into post-Translational Modifications Catalyzed By Radical S-Adenosylmethionine Enzymes. Montana State Univeristy, 2025.

(44) Mészáros, L. S.; Németh, B.; Esmieu, C.; Ceccaldi, P.; Berggren, G. InVivo EPR Characterization of Semi-Synthetic FeFe Hydrogenases. *Angew. Chem.-Int. Edit.* **2018**, *57* (10), 2596-2599.

(45) Morra, S.; Valetti, F.; Gilardi, G. FeFe -hydrogenases as biocatalysts in bio-hydrogen production. *Rendiconti Lincei-Scienze Fisiche E Naturali* **2017**, *28*, 183-194.

(46) Posewitz, M. C.; King, P. W.; Smolinski, S. L.; Zhang, L. P.; Seibert, M.; Ghirardi, M. L. Discovery of two novel radical S-adenosylmethionine proteins required for the assembly of an active Fe hydrogenase. *Journal of Biological Chemistry* **2004**, *279* (24), 25711-25720.

(47) King, P. W.; Posewitz, M. C.; Ghirardi, M. L.; Seibert, M. Functional studies of FeFe hydrogenase maturation in an Escherichia coli biosynthetic system. *Journal of Bacteriology* **2006**, *188* (6), 2163-2172.

(48) Shepard, E. M.; Mus, F.; Betz, J. N.; Byer, A. S.; Duffus, B. R.; Peters, J. W.; Broderick, J. B. FeFe -Hydrogenase Maturation. *Biochemistry* **2014**, *53* (25), 4090-4104.

(49) Byer, A. S.; Shepard, E. M.; Peters, J. W.; Broderick, J. B. Radical S-Adenosyl-L-methionine Chemistry in the Synthesis of Hydrogenase and Nitrogenase Metal Cofactors. *Journal of Biological Chemistry* **2015**, *290* (7), 3987-3994.

(50) Brazzolotto, X.; Rubach, J. K.; Gaillard, J.; Gambarelli, S.; Atta, M.; Fontecave, M. The Fe-Fe -hydrogenase maturation protein HydF from Thermotoga maritima is a GTPase with an iron-sulfur cluster. *Journal of Biological Chemistry* **2006**, *281* (2), 769-774.

(51) Mulder, D. W.; Ortillo, D. O.; Gardenghi, D. J.; Naumov, A. V.; Ruebush, S. S.; Szilagyi, R. K.; Huynh, B.; Broderick, J. B.; Peters, J. W. Activation of HydA^{ΔEFG} Requires a Preformed 4Fe-4S Cluster. *Biochemistry* **2009**, *48* (26), 6240-6248.

(52) Rubach, J. K.; Brazzolotto, X.; Gaillard, J.; Fontecave, M. Biochemical characterization of the HydE and HydG iron-only hydrogenase maturation enzymes from Thermatoga maritima. *Febs Letters* **2005**, *579* (22), 5055-5060.

(53) Kuchenreuther, J. M.; Myers, W. K.; Suess, D. L. M.; Stich, T. A.; Pelmenschikov, V.; Shiigi, S. A.; Cramer, S. P.; Swartz, J. R.; Britt, R. D.; George, S. J. The HydG Enzyme Generates an Fe(CO)2(CN) Synthon in Assembly of the FeFe Hydrogenase H-Cluster. *Science* **2014**, *343* (6169), 424-427.

(54) Rao, G.; Tao, L.; Yu, X.; Rauchfuss, T. B.; Britt, R. D. The Radical S-Adenosyl-<scp>l</scp>-methionine Enzyme HydE Forms an Fe(I)Fe(I) Dimer En Route to the [FeFe] Hydrogenase H-Cluster. *J. Am. Chem. Soc.* **2025**, *147* (36), 32737-32744.

(55) Singh, K. S.; van der Hooft, J. J. J.; van Wees, S. C. M.; Medema, M. H. Integrative omics approaches for biosynthetic pathway discovery in plants. *Natural Product Reports* **2022**, *39* (9), 1876-1896.

(56) Amelia, T. S. M.; Suaberon, F. A. C.; Vad, J.; Fahmi, A. D. M.; Saludes, J. P.; Bhubalan, K. Recent Advances of Marine Sponge-Associated Microorganisms as a Source of Commercially Viable Natural Products. *Marine Biotechnology* **2022**, *24* (3), 492-512.

(57) Ruijne, F.; Kuipers, O. P. Combinatorial biosynthesis for the generation of new-to-nature peptide antimicrobials. *Biochemical Society Transactions* **2021**, *49* (1), 203-215.

(58) Ayikpoe, R. S.; Shi, C. Y.; Battiste, A. J.; Eslami, S. M.; Ramesh, S.; Simon, M. A.; Bothwell, I. R.; Lee, H.; Rice, A. J.; Ren, H. Q.; et al. A scalable platform to discover antimicrobials of ribosomal origin. *Nat. Commun.* **2022**, *13* (1), 15.

(59) Pfeiffer, I. P. M.; Schröder, M. P.; Mordhorst, S. Opportunities and challenges of RiPP-based therapeutics. *Natural Product Reports* **2024**, *41* (7), 990-1019. DOI: 10.1039/d3np00057e.
(60) Montalbán-López, M.; Scott, T. A.; Ramesh, S.; Rahman, I. R.; van Heel, A. J.; Viel, J. H.; Bandarian, V.; Dittmann, E.; Genilloud, O.; Goto, Y.; et al. New developments in RiPP discovery, enzymology and engineering. *Natural Product Reports* **2021**, *38* (1), 130-239.

(61) Arnison, P. G.; Bibb, M. J.; Bierbaum, G.; Bowers, A. A.; Bugni, T. S.; Bulaj, G.; Camarero, J. A.; Campopiano, D. J.; Challis, G. L.; Clardy, J.; et al. Ribosomally synthesized and post-translationally modified peptide natural products: overview and recommendations for a universal nomenclature. *Natural Product Reports* **2013**, *30* (1), 108-160.

(62) Lu, J. G.; Xu, H. J.; Xia, J. H.; Ma, J.; Xu, J.; Li, Y. N.; Feng, J. D- and Unnatural Amino Acid Substituted Antimicrobial Peptides With Improved Proteolytic Resistance and Their Proteolytic Degradation Characteristics. *Frontiers in Microbiology* **2020**, *11*.

(63) Freeman, M. F.; Gurgui, C.; Helf, M. J.; Morinaka, B. I.; Uria, A. R.; Oldham, N. J.; Sahl, H. G.; Matsunaga, S.; Piel, J. Metagenome Mining Reveals Polytheonamides as Posttranslationally Modified Ribosomal Peptides. *Science* **2012**, *338* (6105), 387-390.

CHAPTER TWO

PROBING THE REGIOSELECTIVITY OF SULFONIUM REDUCTIVE CLEAVAGE IN RADICAL SAM ENZYMES

Abstract

Radical S-adenosyl-L-methionine (RS) enzymes catalyze a wide variety of radical-mediated reactions by using a [4Fe–4S] cluster to generate highly reactive intermediates. The canonical mechanism involves electron transfer from the reduced [4Fe–4S] cluster to S-adenosyl-L-methionine (SAM), promoting homolytic cleavage of a specific sulfur–carbon bond to produce the 5′-deoxyadenosyl radical (5′-dAdo•), which abstracts a hydrogen atom from substrate. Although all RS enzymes produce 5′-dAdo• catalytically, recent photolysis studies in the absence of substrate revealed divergent cleavage patterns in model enzymes: PFL-AE forms primarily 5′-dAdo•, whereas HydG produces the methyl radical (•CH_3). The structural basis for this regioselectivity remains unclear. To investigate the role of ribose conformation in directing S–C bond cleavage, we performed cryogenic photolysis experiments using SAM and a more rigid analogue, anhydroadenosylmethionine (anSAM), which contains a 3′–4′ double bond and lacks the 3′ hydroxyl group. Photolysis of SAM-bound PFL-AE yielded both 5′-dAdo• and •CH_3 radicals, with 5′-dAdo• predominating. When anSAM was used, the product distribution shifted toward increased formation of •CH_3, consistent with reduced ribose flexibility influencing bond selectivity. In HydG, photolysis produced exclusively the •CH_3 radical regardless of whether SAM or anSAM was bound. These results indicate that ribose ring conformation in SAM can

influence the regioselectivity of photolytic S–C bond cleavage in some RS enzymes, such as PFL-AE, but not in others, like HydG. Restricting ribose flexibility through the 3′,4′ double bond alters the geometric and electronic interactions that guide radical formation, highlighting the importance of active-site contacts and cofactor conformation in controlling radical outcomes in RS enzymes.

Introduction

Radical S-adenosyl-L-methionine (RS) enzymes use SAM as a cofactor or cosubstrate to initiate an impressive diversity of radical reactions.[1-4] In the active site, SAM binds to the catalytically essential $[4Fe{-}4S]^{+}$ cluster, with the amino and carboxylate moieties of SAM coordinated to the cluster's unique iron.[5-8] Catalysis was traditionally thought to proceed via electron transfer from the reduced $[4Fe\text{-}4S]^{+}$ cluster to SAM, inducing homolytic cleavage of the 5′C−S bond generating the 5′-deoxyadenosyl radical (5′-dAdo•), which abstracts a hydrogen atom from substrate. This model was refined with the discovery of an organometallic intermediate, Ω, in which the 5′C of 5′-dAdo• forms a bond with the unique iron of the cluster; [9, 10] subsequent Fe−C bond homolysis liberates 5′-dAdo•, directly analogous to Co−C5′ bond cleavage in adenosylcobalamin (coenzyme B12) enzymes (Figure 2.1).[11-13] Coenzyme B_{12}, first identified as a radical generator in the late 1950s, also produces 5′-dAdo• to initiate substrate hydrogen abstraction, and although the radical is too reactive to trap directly, kinetic, spectroscopic, and labeling studies have elucidated its behavior.[11-13] The discovery of Ω highlights the mechanistic parallel between RS and B_{12} enzymes, demonstrating that both families generate 5′-dAdo• via controlled organometallic bond cleavage, establishing this radical as a central species in enzymatic radical chemistry.

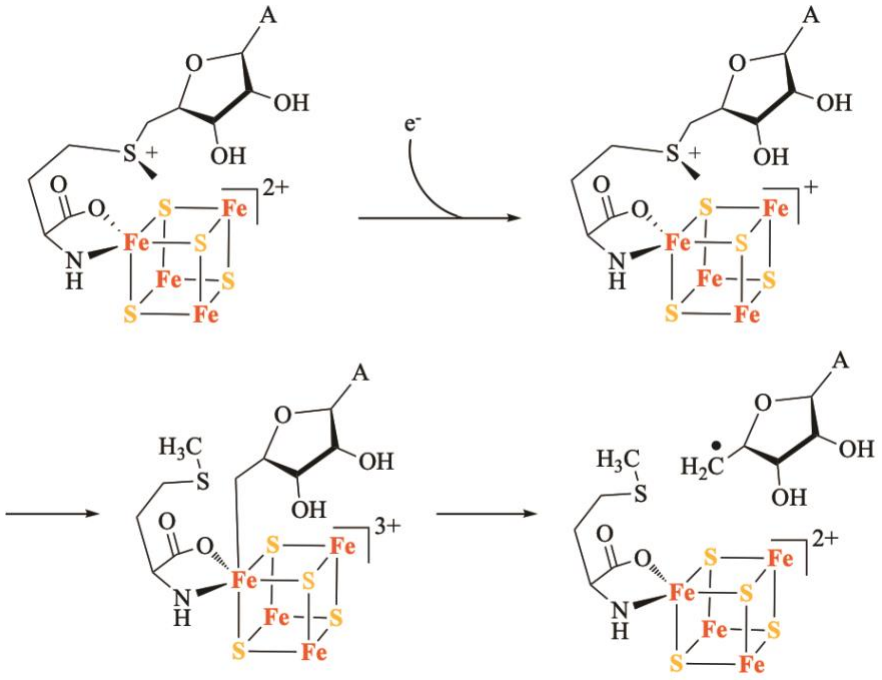

Figure 2.1. Proposed mechanism of radical initiation in radical SAM enzymes. Initiation begins with the 1-electron reduction of the $[4Fe\text{-}4S]^{2+}$ cluster to the $[4Fe\text{-}4S]^{+}$ state. Upon reduction, the cluster can then reduce the sulfonium center promoting the reductive cleavage of the S-C5' bond. This complex rearranges to form the organometallic intermediate, Ω. When the Fe-C5' bond is homolytically cleaved, the highly reactive intermediate 5'-dAdo• radical is released to abstract a hydrogen from the substrate.

Initial attempts to trap the 5'dAdo• radical under turnover conditions proved futile as the 5'-dAdo• radical was too reactive and would immediately abstract a hydrogen from the substrate. Observations that the $[4Fe\text{-}4S]^{+}$-SAM cluster was photochemically active introduced new ways to try to trap this radical.[14] Under cryogenic, substrate free conditions, the cluster could be excited photochemically, inducing electron transfer to the sulfonium center thus promoting reductive cleavage of the S-C5' bond. At cryogenic temperatures (<75 K), the 5'-dAdo• radical was trapped and characterized within the active site of PFL-AE.[14] When these photolysis experiments were repeated with HydG, a different radical was observed and further characterized as a methyl radical.[15]

Initial observations and photolysis experiments on PFL-AE[14] and HydG[15] with SAM showed strict regioselectivity in the cleavage of S-C bonds with the S-5'C bond cleaved in PFL-AE, and S-CH_3 bond cleaved in HydG. Follow up work performed in 2021 points out that reduction of the sulfonium center renders it Jahn-Teller active by adding an electron into a doubly degenerate LUMO. The bifurcation of product regioselectivity observed is likely due to active site influences that localize Jahn-Teller distortions onto one S-C priority bond. Catalytically all these enzyme produce 5'-dAdo• but outside of its catalytic relevance, the regioselectivity of this cleavage and why it is different when substrate isn't present is unknown.[16] Further examination of published radical SAM enzyme crystal structures revealed a correlation between the conformation of the SAM ribose ring and the type of radical generated upon photolysis of the SAM-bound $[4Fe\text{-}4S]^+$ cluster. Specifically, SAM molecules adopting a 2′-endo ribose conformation with an axial C4′–C5′ bond are associated with formation of the 5′-deoxyadenosyl radical (5′-dAdo•)**,** whereas those adopting a 3′-endo conformation with an equatorial C4′–C5′ bond correlate with formation of the methyl radical, $\bullet CH_3$ (Figure 2.2).[16]

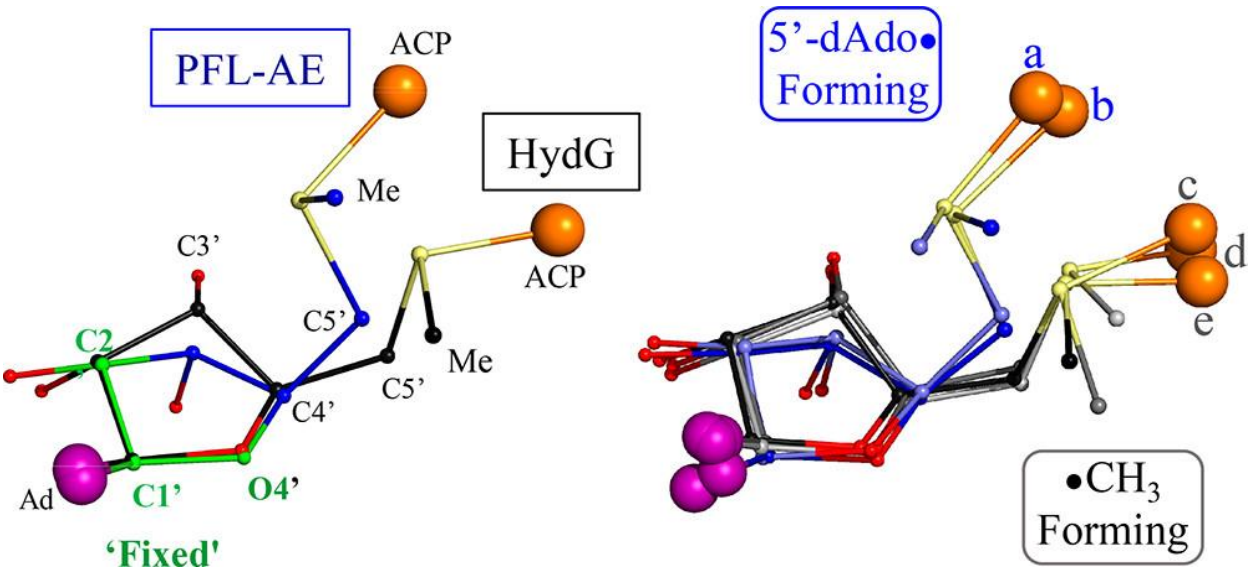

Figure 2.2. Comparisons of SAM configurations that yield photoinduced cleavage to form 5′-dAdo· or ·CH_3, with orientation adjusted so that in all cases the ribose C2′, C1′, and ring O atoms overlay. (Left) Overlay of PFL-AE (3cb8.pdb) and HydG (4wcx.pdb). (Right) Overlay of (a) SPL (4fhf.pdb), (b) PFL-AE, (c) HydE (3iiz.pdb), (d) LAM (2a5h.pdb), (e) HydG, demonstrating the axial orientation of the C4′–C5′ bond in 5′-dAdo· formers and the equatorial orientation in ·CH_3 formers. Figure and caption from source (16).

Here we employ a SAM analogue, anhyroadenosylmethione (anSAM), which harbors a double bond between the 3'C and 4'C and is missing the 3'-OH to probe the idea that ring pucker of the ribose ring influences regioselectivity of the sulfonium reductive cleavage (Figure 2.3). The anSAM analogue was first used by Perry Frey's group when trying to provide evidence that the radical SAM enzyme, lysine 2,3-ammino mutase (LAM), produced the 5'-dAdo• radical.[17, 18] Introducing a double bond in the ribose moiety of SAM should eliminate the flexibility of the ribose ring to adopt the 2'-endo and 3'-endo conformations, which we hypothesize may result in decrease of regioselectivity during photolytic reductive cleavage of SAM. The use of anSAM in our photolysis experiments could thus lead to the observation of both photolysis products, 5'-dAdo• and •CH_3 radicals for both PFL-AE and HydG

To test this prediction, anSAM was utilized in photolysis experiments using both a 5'-dAdo• former (PFL-AE) and a •CH_3 former (HydG), two representative radical SAM used in previous photolysis studies with radical SAM enzymes.[14, 15] We provide evidence that the earlier photolysis experiments may have had signals hidden within the published results as we found both 5'-dAdo• and •CH_3 radical signals when PFL-AE was photolyzed with SAM. However, when anSAM is used, the ratio of these two signals shifts and more •CH_3 radical is produced. When the photolysis experiments were conducted with HydG, regardless of SAM/anSAM used as a cosubstrate, only the •CH_3 radical was observed. These results demonstrate that constraining the ribose ring through the 3′,4′ double bond alters the outcome of photolytic bond cleavage in PFL-AE but not in HydG, providing new insights into the origins of regioselectivity in the two enzyme classes.

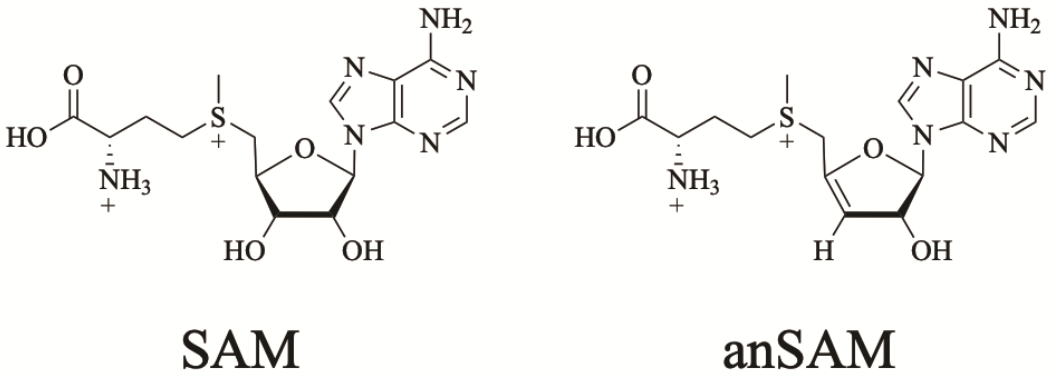

Figure 2.3. Chemical structures of SAM and anhydroadenosylmethionine analogue (anSAM). The anSAM analogue features a double bond between the 3' and 4' carbons and is lacking a hydroxyl group on the 3'C.

Materials and Methods

Enzymatic SAM and anSAM Synthesis

Natural abundant SAM and anSAM were synthesized, purified, and characterized according to previously published methods.[9, 19]

Preparation of Some Proteins

Growth and purification of PFL, adenosine kinase, and preparation of adenylate kinase (rabbit muscle) were carried out following previously published methods without modification.[19] The adenylate kinase from yeast is supplied as a lyophilized powder and does not require any preparation before use in anSAM synthesis.

Plasmid Transformation

For all plasmid transformations, 50-100 ng of plasmid DNA was added to thawed BL21(DE3) cells and incubated on ice for 30 min. The mixture was then heat-shocked in a 42°C water bath for 45 s before another incubation on ice for 2 minutes. Following this incubation, 250 μL of super optimal broth (SOC) was added, and the mixture was incubated with shaking at 37°C and 220 rpm. 50 μL of the mixture was added to an agar plate supplemented with the appropriate antibiotics. The plate was placed in an oven at 37°C and transformants were left to grow overnight.

Preparation of *s.o.*HydG

HydG from *Shewanella oneidensis* was expressed, purified, and reconstituted following previously published protocols with minor modifications.[20] 3L of LB medium was prepared and supplemented with ampicillin (100 μg/mL), kanamycin (50 μg/mL), 0.5% w/v glucose, 100 mM

MOPS/NaOH, and the pH was adjusted to 7.4. The media was inoculated with 1% v/v of the preculture, and the cells were grown at 37°C with shaking at 180 rpm until an OD_{600} of 0.3-0.5 was reached. Cultures were then supplemented with 2 mM ferrous ammonium citrate and transferred to an anaerobic chamber (COY Laboratory Products). Subsequently, L-cysteine and sodium fumarate (5 mM and 10 mM, respectively) were added, and the cultures were stirred anaerobically at 25°C for 1 hour before the addition of 0.5 mM IPTG. Cell cultures were allowed to grow overnight at 25°C and harvested the next morning by centrifugation at 6000 rpm, 12 min, 4°C. Cell pellet was collected, flash frozen in liquid nitrogen, and stored at -80°C.

Protein purification and reconstitution were performed together in a stepwise fashion. In Phase one, cells were thawed and lysed in buffer A (50 mM HEPES pH 7.5, 250 mM KCl, 5% glycerol) containing 1% Triton X-100, 50 mg/mL lysozyme, ~0.01 mg DNAse, 2 mg/mL $MgCl_2$, and 1 Pierce protease inhibitor tablet in 50 mL lysate for 60 minutes. Lysate was clarified via centrifugation at 15,000 rpm for 45 min at 4°C. The fifth "dangler" iron site of HydG was loaded by incubating the lysate with 2 mM NaDT for 10 min, followed by the sequential addition of 80 μM Fe^{3+}, 800 μM S^{2-}, and 2 mM L-cysteine. The mixture was incubated for 45 min and centrifuged (15,000 rpm, 30 min, 4°C). The supernatant was loaded onto a 7.5 mL Strep-Tactin affinity column, which was equilibrated in buffer A, and then washed with 5 column volumes. Protein was eluted with buffer B (50 mM HEPES, pH 7.5, 250 mM KCl, 50 mM biotin), then desalted into buffer A. The desalted protein was concentrated using 30 kDa centrifugal spin filters (Amicon), aliquoted, flash frozen in liquid nitrogen, and stored at -80°C.

PFL-AE Growth and Purification

PFL-AE was expressed following previously published protocols,[19] however, purification diverged from published methods. Clarified lysate was loaded onto a 5 x 26 cm, Waters AP-5 column packed with sephacryl 5-200 resin and equilibrated in 50 mM tris, 150 mM KCl, 1 mM DTT, pH 7.5. The same buffer was run through the column at 1.5 mL/min and collection of PFL-AE began when a brown band was observed entering the bottom of the column. These fractions were collected and concentrated with 10 kDa spin filters (Amicon), then loaded back onto the column. Fractions were collected, pooled and concentrated as the brown band entered the bottom of the column following the same protocol established by Byer and coworkers.[19]

Chemical Reconstitution

Aliquots of purified protein were thawed in an anaerobic chamber, pooled, and diluted to 100 μM in their respective buffers. DTT was added to a final concentration of 5 mM, and the solution was stirred on ice for 5 minutes. Ferrous ammonium sulfate was added over a period of 10 minutes to a final concentration of 800 μM and left to stir on ice for 10 minutes. Lithium sulfide was then added in the same fashion, and the protein solution was left to stir anaerobically on ice for 3 hours. The reaction was then filtered through a 0.2 μm filter and desalted into their respective buffers using a Sephadex G25 desalting column. The protein was then concentrated using a 30 kDa spin filter (Amicon), flash frozen in liquid nitrogen, and stored at -80°C. Following the chemical reconstitution, Fe/monomer protein increased from around 2 Fe/ monomer to nearly 4 Fe/monomer. The success of the reconstitution was analyzed quantitatively via iron analysis and qualitatively using an Agilent Cary 60 UV-vis spectrometer, which scanned

from 800 to 200 nm at 600 nm/min. Samples were measured in Spectrosil Quartz cuvettes (Starna Cells, CA, USA) with a 10 mm path length.

Protein Quantification

Proteins were quantified according to the protocol from Zor and Selinger using Pierce bovine serum albumin (ThermoFisher) as a standard.[21]

Iron Analysis

The iron content of the purified protein was determined using an Agilent 240FS atomic absorption spectrometer. A standard curve was created with an iron atomic absorption standard (Ricca, 1000 ppm in 3% HNO_3) diluted in MQ water, ranging from 0.4 ppm to 2.0 ppm. Protein samples were diluted to 1-2 μM in buffer, in triplicate for analysis. Any absorption from the buffer was subtracted from the sample absorption, and iron content per protein was calculated by dividing the moles of iron by the moles of protein.

anATP Synthesis and Purification

anATP was prepared following previously published protocols with some modifications.[19] Anhydoadenosine, phosphocreatine, and GTP were combined with bovine serum albumin (0.1% w/v), phosphocreatine kinase (40 U/mL), adenylate kinase (20 U/mL), and adenosine kinase (0.18 mg/mL) in 25 mM PIPES, 1.25 mM $MgCl_2$, pH 7 buffer. The reaction was left stirring overnight. Reaction progress was monitored via HPLC using a method that baseline separates anATP from anADP, anAMP, and GTP adopted from Juarez-Facio and coworkers.[22] The technique employs a Kinetex XB-C_{18} (2.6 μm, 100 Å, 150 x 4.6 mm) column with buffer A as 50 mM K_2HPO_4, pH 6.8, and buffer B as HPLC-grade acetonitrile (Fisher

Chemicals). The HPLC method consisted of a 5-minute wash in 0% B, followed by a linear gradient from 0% to 50% B over 5 minutes, and then a final equilibration of 0% B for 5 minutes. Analytes were detected measuring at 254 nm with GTP eluting at 1.7 min, anATP at ~3.4 min, anADP at ~4.0 min, and anATP at ~5.5 min. After the reaction was complete, the mixture was centrifuged at 15,000 rpm for 30 minutes to remove any precipitate. The supernatant was loaded onto a HiPrep Q Sepharose FF 16/10 anion exchange column with buffer A (filtered H_2O) and buffer B (500 mM NH_4HCO_3, pH 6.8). The sample was loaded onto the column via superloop at 1mL/min and washed at a flow rate of 3 mL/min with 50 mM NH_4HCO_3. The sample was eluted at 3 mL/min using a linear gradient from 50 mM NH_4HCO_3 to 350 mM NH_4HCO_3 over 20 column volumes. Reaction intermediates, anAMP and anADP, elute before anATP at 100 mM NH_4HCO_3 and 175 mM NH_4HCO_3, respectively, while anATP elutes around 200 mM NH_4HCO_3. Each peak is collected in a round-bottom flask and rotovapped on a Buchi R-300 Rotavapor to a solid in a water bath set at 28°C and stored at -80°C. Concentrations can be determined via HPLC following the method described above or UV-Vis spectroscopy, measuring at 254 nm.

UV-Visible Spectroscopy

UV-vis spectra were recorded using an Agilent Cary 60 UV-visible spectrophotometer, scanning from 200 to 800 nm at 600 nm/min. Samples were measured in Spectrosil Quartz cuvettes (Starna Cells, CA, USA) with a 10 mm path length.

EPR Sample Preparation

In an anaerobic mBraun chamber, protein samples for intracavity photolysis and EPR spectroscopic analysis were prepared by mixing buffer (50 mM Tris, 150 mM KCl, pH 7.5) with Na-dithionite and dithiothreitol (DTT) to final concentrations of 2 mM and 3 mM, respectively.

Protein was added to final concentrations of 200 μM for Mut12, PFL-AE, and 40 μM for HydG and HydE, and allowed to reduce for 8 minutes. Following the reduction of the [4Fe-4S] cluster, SAM was added to a final concentration of 2 mM. The solution was then mixed, transferred to an EPR tube, and frozen in liquid nitrogen within 45 s to 1 min. For confirming PFL and Mut12 activity, a 200 μL solution was prepared with 150 μM PFL-AE, 340 μM PFL, 3 mM NaDT, 1 mM DTT, and buffer, and allowed to reduce for 8 min. In a separate tube, 2 mM SAM/anSAM was combined with buffer (to 50μL) and 3 mM NaDT. After reduction, the SAM/anSAM solution was added to the protein solution and frozen in liquid nitrogen at 1 min.

EPR Analysis and Photolysis

Continuous wave EPR X-band EPR spectroscopy was performed using a Bruker EMX EPR spectrometer equipped with a Bruker/ColdEdge (Sumitomo Cyrogenics) 10 K waveguide cryogen-free system with an Oxford MercuryiTC controller unit and helium Stinger recirculating unit (Sumitomo Cyrogenics, ColdEdge Technologies). All spectra were recorded at a microwave frequency of 9.378 GHz and a modulation frequency of 100 kHz. The spectrometer was calibrated with an external standard of 2,2-diphenyl-1-picrylhydrazyl (DPPH) with a *g*-value of 2.0036 (Bruker). Experimental spectra were simulated with Easyspin (5.2.35) within the Matlab R2020b software suite (Mathworks, Inc.).[23] Iron-sulfur cluster signals were recorded at 10 K with 10 G modulation amplitude and 1 mW microwave power. Organic radicals were observed at 40 K with 3 G modulation amplitude and 3 mW microwave power. Photolysis experiments were conducted using a 450 nm diode laser (Thorlabs) within the instrument's cavity at 10 K for 30 minutes. The temperature was increased to 40 K and the post-hv spectrum was recorded. The sample was then annealed within the cavity of the EPR at 75 K for 45 minutes before the

temperature was returned to 40 K, where the post-anneal spectrum was recorded. Glycyl radical on PFL was observed at 75 K with 6 G modulation amplitude and 0.053 mW microwave power.

Results

PFL-AE uses SAM/anSAM to Activate PFL

The ability of anSAM to act as a cosubstrate for PFL-AE during activation of PFL has not previously been examined. Before any photolysis experiments were conducted, the viability of anSAM as a cosubstrate was assessed using two approaches: by using EPR spectroscopy to probe the ability of anSAM to bind to the $[4Fe\text{-}4S]^{+}$ cluster, and by carrying out an activity assay to probe whether anSAM supports generation of a glycyl radical on G734 of PFL. Addition of either SAM or anSAM to reduced PFL-AE caused the $[4Fe–4S]^{+}$ EPR signal to shift from axial to rhombic, a change indicative of cofactor binding to the $[4Fe\text{-}4S]^{+}$ cluster (Figure 2.4A & B). Previous studies have shown that anSAM functions as a cofactor during LAM catalysis providing a specific activity of 0.25% of what was observed with SAM.[17] To see if anSAM would function in the same manner as SAM and install a glycyl radical on PFL, an EPR based activity assessment was conducted, in which anSAM and PFL were incubated with reduced PFL-AE and then analyzed by EPR spectroscopy. An axial signal centered at $g = 2.006$ was observed that is characteristic of the PFL based glycyl radial,[19, 24-26] confirming that anSAM can undergo reduction, anAdo• formation, and can carry out subsequent H-atom abstraction from Gly734 (Figure 2.4 C & D).

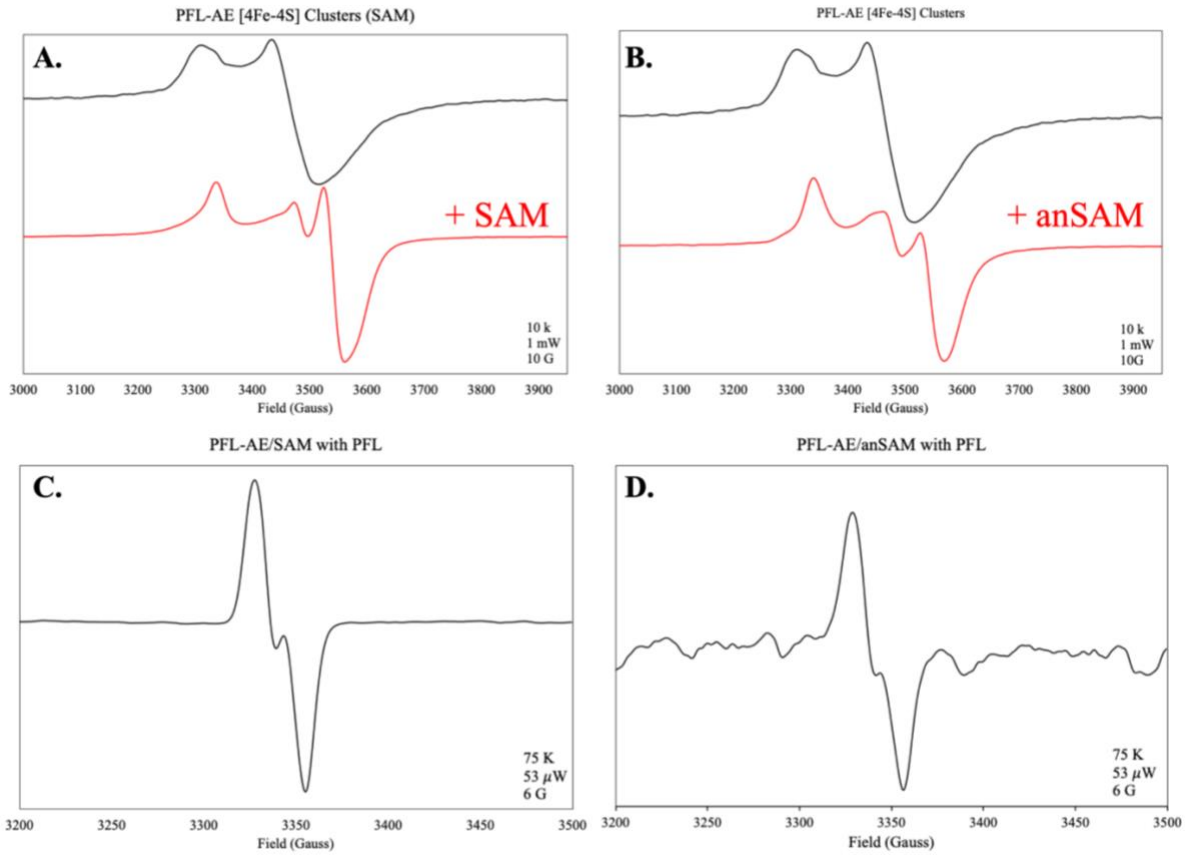

Figure 2.4. EPR spectra of PFL-AE and PFL based radicals. A) PFL-AE $[4Fe\text{-}4S]^{+}$ cluster with and without SAM bound. B) PFL-AE $[4Fe\text{-}4S]^{+}$ cluster with and without anSAM bound. EPR parameters for A & B: 10 K, 1 mW, 10 G. C & D) Glycyl radical observed on PFL generated by both SAM (C) and anSAM (D). EPR parameters: 75 K, 53 μW, 6 G, 9.37 GHz.

Photolysis of PFL-AE/SAM complex

Prior to carrying out photolysis with anSAM attempts were made to recreate the published photolysis results from 2019.[14] When the PFL-AE/SAM complex was photolyzed in triplicate, the resulting spectrum looked different from the previously published dAdo• signals (Figure 2.5A). Upon thermal annealing at 75 K, a portion of the signal appeared to be lost, leaving a spectrum that looked more like previous dAdo• signals (Figure 2.5B). Subtracting the annealed spectrum from the post-photolysis spectrum allowed us to observe the signal that was lost upon annealing, which appears as the distinct 1-3-3-1 splitting pattern associated with

methyl radicals (Figure 2.5C).[15] These results are puzzling considering there was no discussion of other photolysis products in PFL-AE under the substrate free, cryogenic photolysis conditions.[14] When the post-photolysis (dAdo•) and subtracted (•CH_3) spectra were integrated, it was found the signal attributed to the dAdo• accounted for 84.1 $\pm$ 1.7% and the methyl radical accounting for the other 15.6 $\pm$ 1.7% of the initial post-photolysis EPR signal intensity. To probe the source of the discrepancy with earlier reports, we tested multiple variables: different protein preparations, reduced photothermal heating during photolysis, several buffer systems, and varied photolysis times. The same trend persisted under all conditions suggesting this trend is an intrinsic factor to the PFL-AE-SAM complex. Though the initial paper did not comment on this phenomenon, unpublished collaborative work between our lab and the Hoffman lab at Northwestern University reports a species with characteristics of a $[4Fe\text{-}4S]^{+}$-CH_3 signal at roughly the same relative intensity as we observe here that was hidden within the initial published data, confirming that the regioselectivity of SAM cleavage under photolysis conditions is not as strict as originally reported.

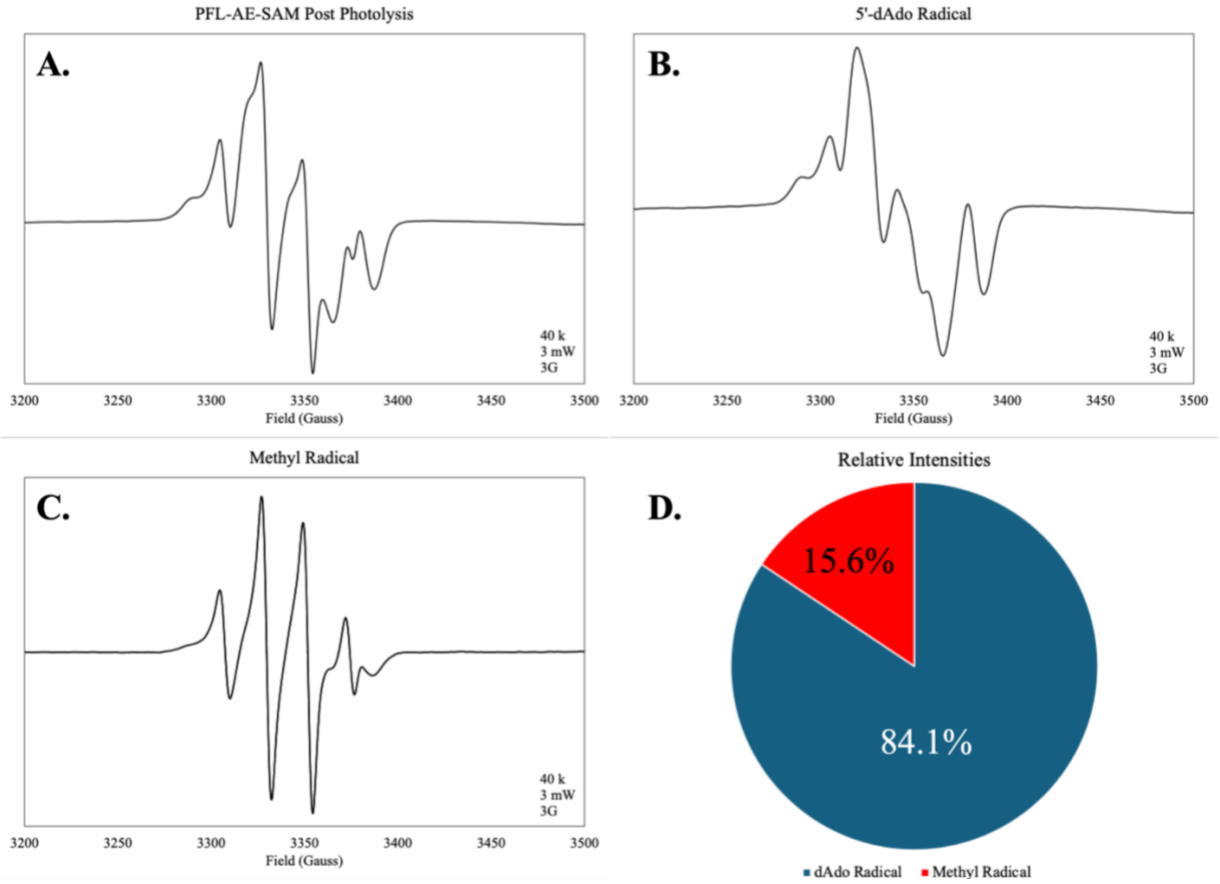

Figure 2.5. EPR Spectra of the $[4Fe\text{-}4S]^{+}$ cluster of PFL-AE with SAM before and after photolysis. A) Reduced PFL-AE and SAM after being photolyzed for 30 min at 10 K. B) Signal after thermal annealing at 75 K for 45 minutes. C) Spectrum resulting from subtracting B from A indicating what species was annealed away at 75 K. D) Comparison of signal intensities of the 5'dAdo (B) and methyl (C) radicals that make up the signal depicted in (A). EPR parameters: 40 K, 3 mW, 3 G, 9.37 GHz.

Photolysis of PFL-AE/anSAM complex

Despite evidence that the regioselectivity of sulfonium reductive cleaved is not as strict as initially reported, anSAM can still be used as a tool to test the hypothesis that the ribose ring pucker correlates to the localization of Jahn-Teller distortions. With a double bond between the 3' and 4' carbons, any pucker of the ring should be eliminated in anSAM, and we would thus expect to see differences in the relative intensities of the species post-photolysis. Photolysis experiments

as described above were repeated with PFL-AE and anSAM in triplicate, revealing a distinct shift in product distribution: the anAdo• radical accounted for $65.6 \pm 0.5\%$ of the total signal, while the methyl radical contributed $34.3 \pm 1.3\%$ (Figure 2.6). These results directly support our hypothesis that the ribose ring pucker influences the photolysis product distribution of the enzyme.

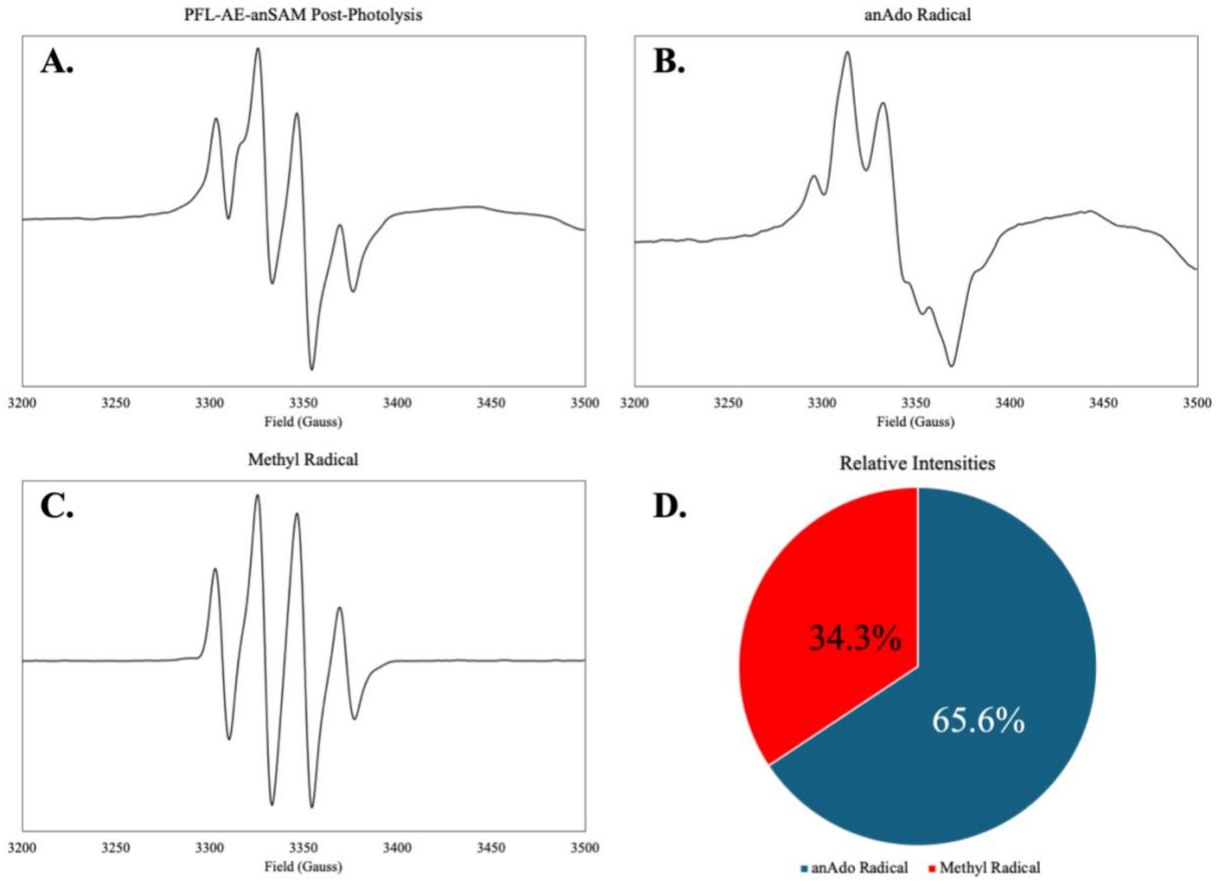

Figure 2.6. EPR Spectra of the $[4Fe\text{-}4S]^{+}$ cluster of PFL-AE with anSAM before and after photolysis. A) Reduced PFL-AE and anSAM after being photolyzed for 30 min at 10 K. B) Signal after thermal annealing at 75 K for 45 minutes. C) Spectrum resulting from subtracting B from A indicating what species was annealed away at 75 K. D) Comparison of signal intensities of the 5'dAdo (B) and methyl (C) radicals that make up the signal depicted in (A). EPR parameters: 40 K, 3 mW, 3 G, 9.37 GHz.

Photolysis of *s.o.*HydG/SAM complex

With evidence supporting the hypothesis that the ribose ring pucker is associated with regioselectivity of reductive SAM cleavage, we next sought to determine whether similar differences in regioselectivity would be observed in one of the methyl radical-forming enzymes, HydG. The prior published work was performed with HydG from *Clostridium acetobutylicum (C.a.)*[16] but we have recently shown that HydG from *Shewenella oneidensis (S.o.)* yields stronger EPR signals and is slightly easier to purify and characterize, so the current work was carried out with the *S.o.*HydG. Our results demonstrate that both SAM and anSAM bind to the $[4Fe\text{-}4S]^+$ cluster of *S.o.*HydG (Figure 2.7) and that the resulting EPR signals closely resemble previously published spectra of *C.a.*HydG with SAM bound.[27]

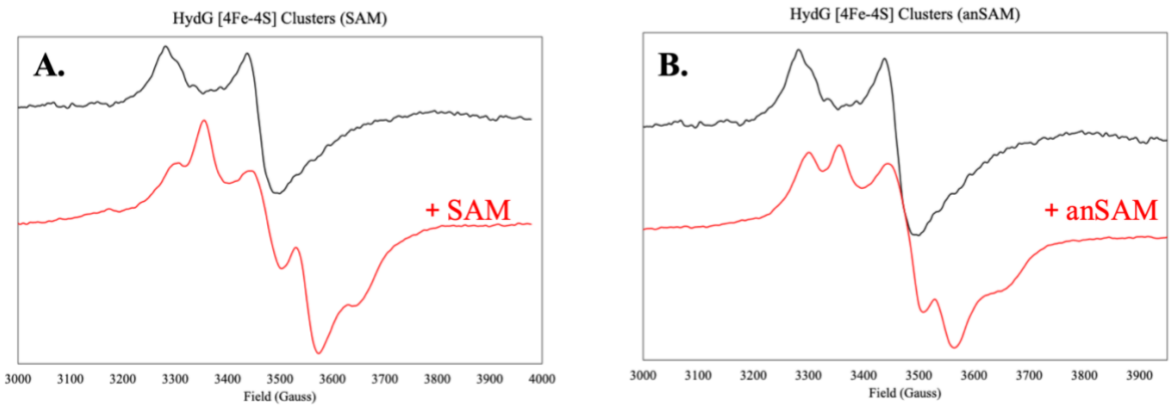

Figure 2.7. EPR spectra of *s.o.*HydG $[4Fe\text{-}4S]^+$-based radicals . A) HydG $[4Fe\text{-}4S]^+$ cluster with and without SAM bound. B) HydG $[4Fe\text{-}4S]^+$ cluster with and without anSAM bound. EPR parameters: 10 K, 1 mW, 10 G, 9.37 GHz.

When the *S.o.*HydG $[4Fe\text{-}4S]^+$-SAM complex is photolyzed at 10 K, we observe only the methyl radical product by EPR; this result, unlike that for PFL-AE, aligns with previously published work.[15] Upon annealing at 75 K for one hour—several times longer than the half-life

of the methyl radical in *C.a.*HydH in the previously published work—some methyl radical remains within the active site of *S.o.*HydG (Figure 2.8).[15] The apparently more stable •CH_3 formed upon photolysis of SAM in *S.o.*HydG could reflect that the active site of *S.o.*HydG is more constrained than that of *C.a.*HydG, thus preventing the methyl radical from diffusing away and being rapidly quenched at annealing temperatures of 75 K.

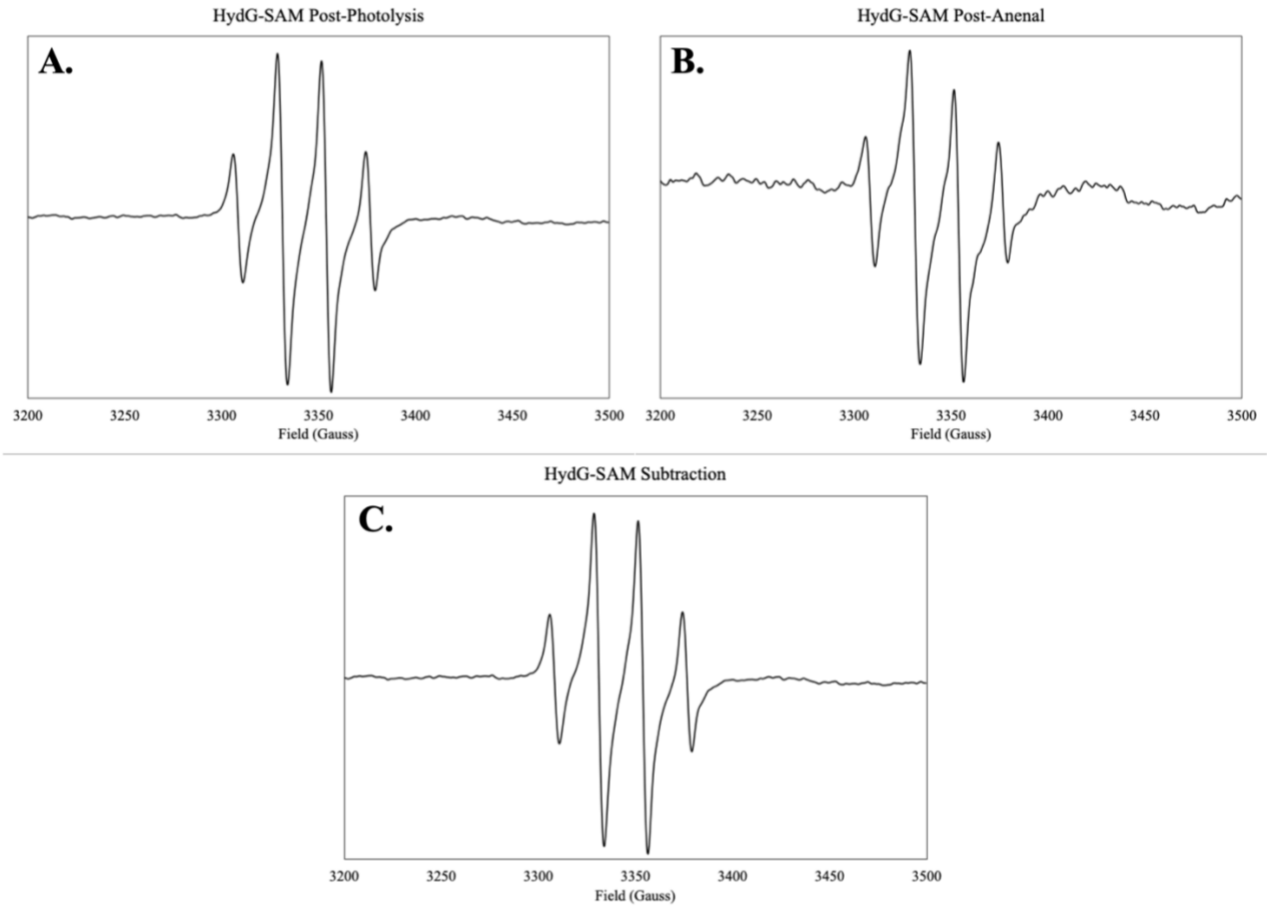

Figure 2.8. EPR spectra of *s.o.*HydG photolyzed with SAM. (A) Spectrum directly after 30 minutes of photolysis. (B) Spectrum after annealing for 1 hour at 75 K (B). (C) subtracted spectrum. EPR conditions: 40 K, 3 mW, 3 G, 9.37 GHz.

Photolysis of *s.o.*HydG/anSAM complex

Due to the lack of ring pucker in the ribose moiety of anSAM we expected to see a mixture of •dAdo and •CH_3 EPR signals when *S.o.*HydG was photolyzed with anSAM. However, upon photolysis of reduced *S.o.*HydG with anSAM we still only see the methyl radical formed by EPR spectroscopy (Figure 2.9). The EPR signal immediately after photolysis is lower in intensity than that observed after photolysis with SAM. Indicating that less •CH_3 was formed; after annealing for 1 hour no methyl radical signal remains. Regardless of the lower amount of methyl radical formed when using anSAM vs. SAM, in both cases there is only the CH_3 signal present. These results indicate that the absence of the 3′-OH and the restricted ribose conformation in anSAM are not sufficient to alter the regioselectivity of bond cleavage in HydG, suggesting that other active-site factors dictate which S–C bond undergoes photoreductive cleavage, as discussed further below.

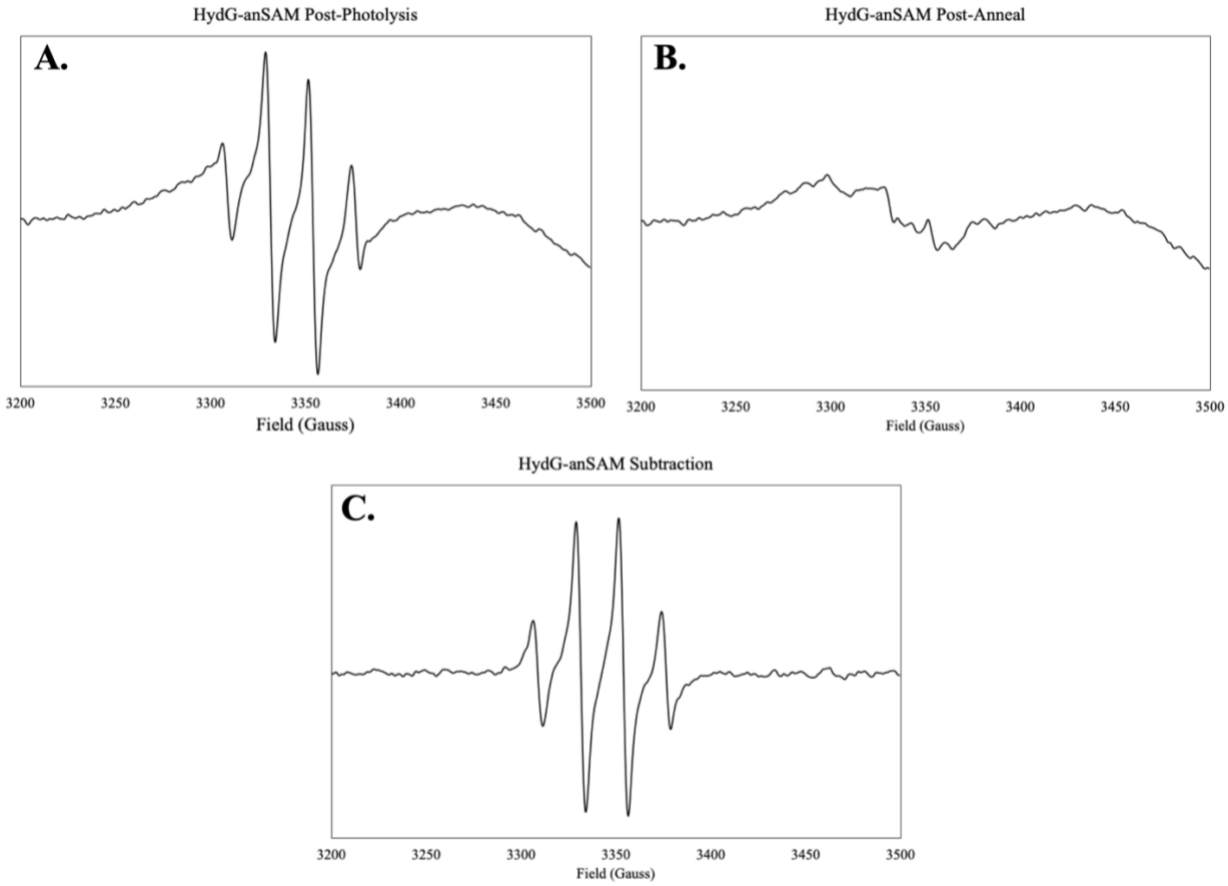

Figure 2.9) EPR spectra of *s.o.*HydG photolyzed with anSAM. (A) Spectrum directly after 30 minutes of photolysis. (B) Spectrum after annealing for 1 hour at 75 K (B). (C) subtracted spectrum. EPR conditions: 40 K, 3 mW, 3 G, 9.37 GHz.

Discussion

Radical SAM enzymes play an essential role in catalyzing over 70 types of reactions across all domains of life.[1, 8, 28] All use a catalytically essential [4Fe–4S] cluster and SAM as a cofactor or cosubstrate to generate the highly reactive 5′-deoxyadenosyl radical (5′dAdo•) intermediate, which is used to abstract a hydrogen atom from the substrate.[5, 7, 29, 30] Prior to 2019, no direct evidence had demonstrated the 5'-dAdo• was indeed an intermediate in radical SAM enzymatic catalysis but evidence suggested its existence and catalytic relevance.[17, 18] This

changed when photolysis under substrate free conditions of the $[4Fe\text{-}4S]^{+}$-SAM bound cluster in PFL-AE at 10 K promoted electron transfer and subsequent homolysis of the S-5'C bond allowing the 5-dAdo• radical to be trapped and characterized within the active site of PFL-AE.[14] Further work showed that when these experiments were conducted with HydG, a different S-C bond was cleaved and the $\bullet CH_3$ radical is produced.[15] This was extremely surprising given that both enzymes produce the 5'-dAdo• radical catalytically. This unexpected difference prompted further consideration of how the electronic and structural properties of the SAM sulfonium center and its active-site environment dictate the site of bond cleavage.

Upon reduction of the sulfonium center, an electron is added to the LUMO which has ^{2}E symmetry, resulting in a doubly degenerate and Jahn-Teller active state.[16] While the Jahn-Teller effect itself isn't responsible for the regioselectivity observed in sulfonium reductive cleavage, under the photolysis conditions discussed, the Jahn-Teller distortion is proposed to be localized onto one of the three S-C bonds of SAM due to active-site interactions, causing it to be the priority bond for homolytic cleavage. Structural evidence from radical SAM crystal structures shows there is a correlation between SAM ribose ring conformations in the active site and the cleavage product produced upon photolysis.[16]

To further examine this relationship between SAM conformation and regioselectivity of S-C bond cleavage, we revisited the photolysis behavior of PFL-AE. Previous studies reported that only a single product was detected following photolysis;[14] however, ongoing unpublished work collaborative between our lab and the Hoffman lab indicates that additional species were likely present even in those original samples. In our experiments with PFL-AE and anSAM, we clearly observe photoreductive cleavage of both the S–5′C and S–CH_3 bonds, producing 5′-

deoxyadenosyl (5′dAdo•) and methyl (•CH_3) radicals in relative yields of 84.1% and 15.6%, respectively (Figure 2.xxx). Given the structural differences between SAM and anSAM, we anticipated that photolysis of PFL-AE with anSAM would favor methyl radical formation. Indeed, the product ratio shifted accordingly to 65.6% 5′dAdo• and 34.3% •CH_3, consistent with our hypothesis (figure 2.xxx)

To determine whether similar alteration of regioselectivity would be observed in methyl-forming radical SAM enzymes, we next performed analogous photolysis experiments with HydG. Based on our observations with PFL-AE, we expected a shift in product distribution toward increased formation of the 5′dAdo• radical when anSAM was photolyzed with HydG. However, despite the structural differences between SAM and anSAM, photolysis of HydG resulted exclusively in cleavage of the S–CH_3 bond in both cases, yielding only the methyl radical (Figures 2.7 and 2.8). This contrast highlights fundamental differences in how PFL-AE and HydG interact with SAM and its analogs during photolysis, suggesting that the active-site environment plays a dominant role in dictating regioselectivity.

The difference in photolysis behaviors of PFL-AE and HydG suggests that differences in the details of SAM binding within the active site may influence which S–C bond undergoes reductive cleavage. To explore this possibility, we examined the hydrogen-bonding and electrostatic interactions to the 3′-OH of SAM in both enzymes (Figure 2.10). Note that there is no published structure of *S. oneidensis* HydG; thus, the structure depicted is from a homologous HydG enzyme from *Thermoanaerobacter italicus*. In PFL-AE, the 3′-OH group of SAM forms four notable contacts: the carboxylates of D104 and D129, and with the guanidino group of R166, at distances of 5.0 Å, 4.0 Å, and 3.3 Å, respectively. An additional electrostatic interaction

occurs between the 3′-OH and a nearby sodium ion located 4.2 Å away. These residues are positioned appropriately to influence the local electrostatic environment of the 3′-OH group and, by extension, the ribose conformation of SAM. In contrast, SAM bound to HydG displays only two contacts to the 3′-OH group, involving the carboxylate of E194 at 2.4 Å and the hydroxyl of Y96 at 5.3 Å. The reduced number and altered geometry of these interactions may permit greater flexibility of the ribose ring in HydG, allowing a conformation closer to the 2′-endo state. Such differences in the hydrogen-bonding network surrounding the ribose likely modulate the electronic structure of the sulfonium center, contributing to the distinct regioselectivity of S–C bond cleavage observed between PFL-AE and HydG.

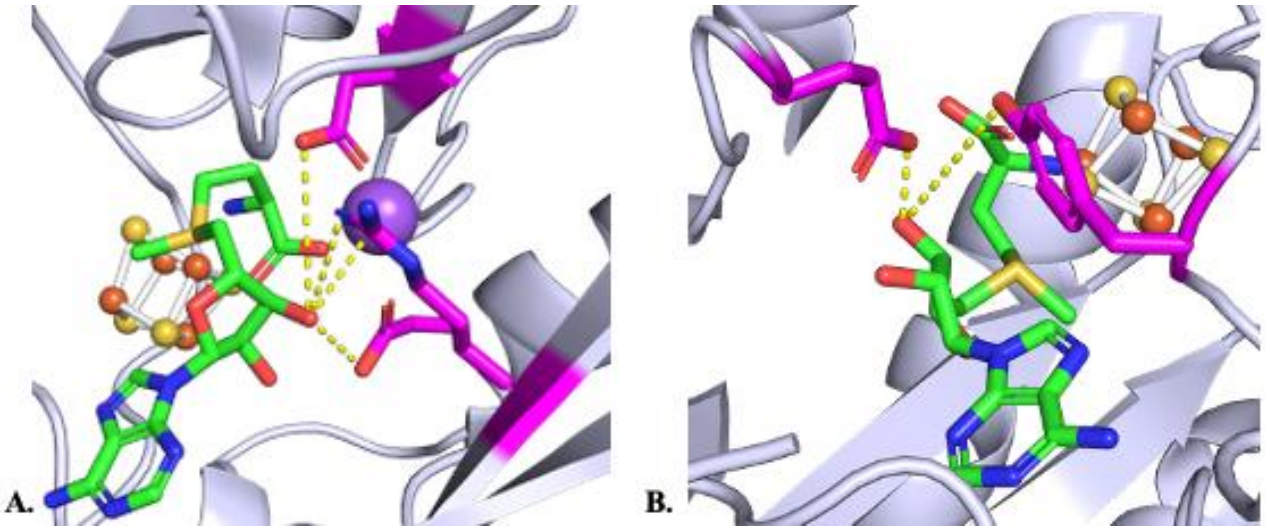

Figure 2.10. Specific contacts to the 3'-OH of SAM in (A) PFL-AE (PDB: 3CBD), and (B) HydG (PDB: 4WCX). SAM is depicted in green sticks, the [4Fe-4S] cluster is shown in the ball and stick model with sulfur atoms in yellow, and iron atoms in rust. Residues in contact with the 3'-OH of SAM are shown in magenta, and the sodium cation in PFL-AE is shown in purple.

DFT minimizations have been previously carried out using SAM structures from SPL (a 5'-dAdo• former) and HydE (a •CH_3 former).[16] The SAM bound to HydE retained a geometry close to its intrinsic, most stable conformation in solution, whereas SAM bound to SPL

underwent a significant ribose ring flip (2′-endo → 3′-endo) and reorientation of the C4′–C5′ bond. These results suggest that CH_3-forming enzymes such as HydE accommodate SAM without major distortion, whereas 5′-dAdo•-forming enzymes like SPL and PFL-AE induce substantial ribose ring conformational changes in SAM upon binding.[16]

Mechanistically these observations align with the longstanding proposal by Frey and co-workers,[31] with thorough investigations by Miller and Bandarian[32] that the $[4Fe\text{-}4S]^+$ cluster is not a sufficiently strong reductant to reduce the sulfonium of SAM in solution. To overcome this barrier, Frey proposed that Fe–S coordination stabilizes the cation–cation interactions, suggesting a mechanism in which substrate binding induces a conformational change in SAM that positions the sulfonium lone pair near an iron center, allowing inner-sphere electron transfer.[31]

Although the sulfur of SAM has three distinct substituents, canonical radical SAM enzymes cleave only the S-C5' bond during catalysis. While bond dissociation energies can influence sulfonium cleavage,[33-35] this factor alone does not explain the observed selectivity under these conditions. Instead, structural data indicate that although SAM's overall positioning is conserved across enzyme classes, the conformation of the ribose ring varies significantly. This suggests that electronic factors associated with the ribose ring influence the electronic structure of the sulfonium center, thereby modulating the regioselectivity of S–C bond cleavage in radical SAM enzymes.

Given that the ribose ring plays a key role in modulating the reductive cleavage of the sulfonium, we next considered how structural modifications to SAM—specifically the introduction of a 3′,4′ double bond in anSAM—might alter this balance. The 3′,4′ double bond in

anSAM removes the ring's flexibility and prevents interconversion between 2′-endo and 3′-endo conformations. This constraint likely alters orbital overlap between the ribose C4′–C5′ bond and the sulfonium center, thereby changing the electronic distribution within SAM.[16] Such an effect could bias cleavage toward the S–CH_3 bond, consistent with the increased methyl radical formation observed in PFL-AE photolysis and the lack of 5'dAdo• formation in HydG. These results suggest that even subtle changes to ribose ring electronics can significantly impact the electronic coupling between SAM and the [4Fe–4S] cluster. Understanding how this rigidity modifies the energy landscape of S–C bond homolysis could provide new strategies for designing SAM analogs that modulate radical formation pathways in distinct enzyme classes.

References

(1) Broderick, J. B.; Duffus, B. R.; Duschene, K. S.; Shepard, E. M. Radical S-Adenosylmethionine Enzymes. *Chem. Rev.* **2014**, *114* (8), 4229-4317, Review.

(2) Nicolet, Y. Structure-function relationships of radical SAM enzymes. *Nat. Catal.* **2020**, *3* (4), 337-350, Review.

(3) Landgraf, B. J.; McCarthy, E. L.; Booker, S. J. Radical S-Adenosylmethionine Enzymes in Human Health and Disease. *Annu. Rev. Biochem.* **2016**, *85* (1), 485-514.

(4) Holliday, G. L.; Akiva, E.; Meng, E. C.; Brown, S. D.; Calhoun, S.; Pieper, U.; Sali, A.; Booker, S. J.; Babbitt, P. C. Atlas of the Radical SAM Superfamily: Divergent Evolution of Function Using a "Plug and Play" Domain. Elsevier, 2018; pp 1-71.

(5) Krebs, C.; Broderick, W. E.; Henshaw, T. F.; Broderick, J. B.; Huynh, B. H. Coordination of adenosylmethionine to a unique iron site of the 4Fe-4S of pyruvate formate-lyase activating enzyme: A Mossbauer spectroscopic study. *J. Am. Chem. Soc.* **2002**, *124* (6), 912-913.

(6) Walsby, C. J.; Hong, W.; Broderick, W. E.; Cheek, J.; Ortillo, D.; Broderick, J. B.; Hoffman, B. M. Electron-nuclear double resonance spectroscopic evidence that S-adenosylmethionine binds in contact with the catalytically active 4Fe-4S + cluster of pyruvate formate-lyase activating enzyme. *J. Am. Chem. Soc.* **2002**, *124* (12), 3143-3151.

(7) Silakov, A.; Lanz, N. D.; Booker, S. J. Characterization of Radical S-adenosylmethionine Enzymes and Intermediates in their Reactions by Continuous Wave and Pulse Electron Paramagnetic Resonance Spectroscopies. Springer International Publishing, 2017; pp 143-186.

(8) Sofia, H. J. Radical SAM, a novel protein superfamily linking unresolved steps in familiar biosynthetic pathways with radical mechanisms: functional characterization using new analysis and information visualization methods. *Nucleic Acids Research* **2001**, *29* (5), 1097-1106.

(9) Byer, A. S.; Yang, H.; McDaniel, E. C.; Kathiresan, V.; Impano, S.; Pagnier, A.; Watts, H.; Denler, C.; Vagstad, A. L.; Piel, J.; et al. Paradigm Shift for Radical S-Adenosyl-L-methionine Reactions: The Organometallic Intermediate Ω Is Central to Catalysis. *J. Am. Chem. Soc.* **2018**, *140* (28), 8634-8638.

(10) Horitani, M.; Shisler, K.; Broderick, W. E.; Hutcheson, R. U.; Duschene, K. S.; Marts, A. R.; Hoffman, B. M.; Broderick, J. B. Radical SAM catalysis via an organometallic intermediate with an Fe–[5′-C]-deoxyadenosyl bond. *Science* **2016**, *352* (6287), 822-825.

(11) Brown, K. L. Chemistry and Enzymology of Vitamin B₁₂. *Chem. Rev.* **2005**, *105* (6), 2075-2150.

(12) Banerjee, R.; Ragsdale, S. W. The Many Faces of Vitamin B₁₂: Catalysis by Cobalamin-Dependent Enzymes. *Annu. Rev. Biochem.* **2003**, *72* (1), 209-247.

(13) Frey, P. A.; Abeles, R. H. The Role of the B12 Coenzyme in the Conversion of 1,2-Propanediol to Propionaldehyde. *Journal of Biological Chemistry* **1966**, *241* (11), 2732-2733.

(14) Yang, H.; McDaniel, E. C.; Impano, S.; Byer, A. S.; Jodts, R. J.; Yokoyama, K.; Broderick, W. E.; Broderick, J. B.; Hoffman, B. M. The Elusive 5'-Deoxyadenosyl Radical: Captured and Characterized by Electron Paramagnetic Resonance and Electron Nuclear Double Resonance Spectroscopies. *J Am Chem Soc* **2019**, *141* (30), 12139-12146.

(15) Yang, H.; Impano, S.; Shepard, E. M.; James, C. D.; Broderick, W. E.; Broderick, J. B.; Hoffman, B. M. Photoinduced Electron Transfer in a Radical SAM Enzyme Generates an S-Adenosylmethionine Derived Methyl Radical. *J Am Chem Soc* **2019**, *141* (40), 16117-16124.

(16) Impano, S.; Yang, H.; Jodts, R. J.; Pagnier, A.; Swimley, R.; McDaniel, E. C.; Shepard, E. M.; Broderick, W. E.; Broderick, J. B.; Hoffman, B. M. Active-Site Controlled, Jahn-Teller Enabled Regioselectivity in Reductive S-C Bond Cleavage of S-Adenosylmethionine in Radical SAM Enzymes. *J Am Chem Soc* **2021**, *143* (1), 335-348.

(17) Magnusson, O. T.; Reed, G. H.; Frey, P. A. Spectroscopic evidence for the participation of an allylic analogue of the 5′-deoxyadenosyl radical in the reaction of lysine 2,3-aminomutase. *J. Am. Chem. Soc.* **1999**, *121* (41), 9764-9765.

(18) Magnusson, O. T.; Reed, G. H.; Frey, P. A. Characterization of an Allylic Analogue of the 5‘-Deoxyadenosyl Radical: An Intermediate in the Reaction of Lysine 2,3-Aminomutase. *Biochemistry* **2001**, *40* (26), 7773-7782.

(19) Byer, A. S.; McDaniel, E. C.; Impano, S.; Broderick, W. E.; Broderick, J. B. Mechanistic Studies of Radical SAM Enzymes: Pyruvate Formate-Lyase Activating Enzyme and Lysine 2,3-Aminomutase Case Studies. In *Radical Sam Enzymes*, Bandarian, V. Ed.; Methods in Enzymology, Vol. 606; Elsevier Academic Press Inc, 2018; pp 269-318.

(20) Kuchenreuther, J. M.; Myers, W. K.; Suess, D. L. M.; Stich, T. A.; Pelmenschikov, V.; Shiigi, S. A.; Cramer, S. P.; Swartz, J. R.; Britt, R. D.; George, S. J. The HydG Enzyme Generates an Fe(CO)2(CN) Synthon in Assembly of the FeFe Hydrogenase H-Cluster. *Science* **2014**, *343* (6169), 424-427.

(21) Zor, T.; Seliger, Z. Linearization of the bradford protein assay increases its sensitivity: Theoretical and experimental studies. *Anal. Biochem.* **1996**, *236* (2), 302-308.

(22) Juarez-Facio, A. T.; de Lagarde, V. M.; Monteil, C.; Vaugeois, J. M.; Corbiere, C.; Rogez-Florent, T. Validation of a Fast and Simple HPLC-UV Method for the Quantification of Adenosine Phosphates in Human Bronchial Epithelial Cells. *Molecules* **2021**, *26* (20), 8.

(23) Stoll, S.; Schweiger, A. EasySpin, a comprehensive software package for spectral simulation and analysis in EPR. *J. Magn. Reson.* **2006**, *178* (1), 42-55.

(24) Wagner, A. F.; Frey, M.; Neugebauer, F. A.; Schäfer, W.; Knappe, J. The free radical in pyruvate formate-lyase is located on glycine-734. *Proceedings of the National Academy of Sciences* **1992**, *89* (3), 996-1000.

(25) Henshaw, T. F.; Cheek, J.; Broderick, J. B. The [4Fe-4S]¹⁺ Cluster of Pyruvate Formate-Lyase Activating Enzyme Generates the Glycyl Radical on Pyruvate Formate-Lyase: EPR-Detected Single Turnover. *J. Am. Chem. Soc.* **2000**, *122* (34), 8331-8332.

(26) Duboc-Toia, C.; Hassan, A. K.; Mulliez, E.; Ollagnier-De Choudens, S.; Fontecave, M.; Leutwein, C.; Heider, J. Very High-Field EPR Study of Glycyl Radical Enzymes. *J. Am. Chem. Soc.* **2003**, *125* (1), 38-39.

(27) Shepard, E. M.; Impano, S.; Duffus, B. R.; Pagnier, A.; Duschene, K. S.; Betz, J. N.; Byer, A. S.; Galambas, A.; McDaniel, E. C.; Watts, H.; et al. HydG, the “dangler” iron, and catalytic production of free CO and CN[−]: implications for [FeFe]-hydrogenase maturation. *Dalton Transactions* **2021**, *50* (30), 10405-10422.

(28) Bridwell-Rabb, J.; Grell, T. A. J.; Drennan, C. L. A Rich Man, Poor Man Story of S-Adenosylmethionine and Cobalamin Revisited. *Annu. Rev. Biochem.* **2018**, *87* (1), 555-584.

(29) Vey, J. L.; Drennan, C. L. Structural Insights into Radical Generation by the Radical SAM Superfamily. *Chem. Rev.* **2011**, *111* (4), 2487-2506. DOI: 10.1021/cr9002616.
(30) Frey, P. A. Radical Mechanisms of Enzymatic Catalysis. *Annu. Rev. Biochem.* **2001**, *70* (1), 121-148.

(31) Cosper, N. J.; Booker, S. J.; Ruzicka, F.; Frey, P. A.; Scott, R. A. Direct FeS Cluster Involvement in Generation of a Radical in Lysine 2,3-Aminomutase. *Biochemistry* **2000**, *39* (51), 15668-15673.

(32) Miller, S. A.; Bandarian, V. Analysis of Electrochemical Properties of S-Adenosyl-<scp>l</scp>-methionine and Implications for Its Role in Radical SAM Enzymes. *J. Am. Chem. Soc.* **2019**, *141* (28), 11019-11026. DOI: 10.1021/jacs.9b00933.
(33) Saeva, F. D.; Morgan, B. P. Mechanism of one-electron electrochemical reductive cleavage reactions of sulfonium salts. *J. Am. Chem. Soc.* **1984**, *106* (15), 4121-4125.

(34) Wang, X.; Saeva, F. D.; Kampmeier, J. A. Photosensitized Reduction of Sulfonium Salts: Evidence for Nondissociative Electron Transfer. *J. Am. Chem. Soc.* **1999**, *121* (18), 4364-4368.

(35) Donck, S.; Baroudi, A.; Fensterbank, L.; Goddard, J. P.; Ollivier, C. Visible-Light Photocatalytic Reduction of Sulfonium Salts as a Source of Aryl Radicals. *Advanced Synthesis & Catalysis* **2013**, *355* (8), 1477-1482.

CHAPTER THREE

SPECTROSCOPIC AND BIOCHEMICAL CHARACTERIZSTION OF ORIGAMIN EPIMERASE OPGD

Abstract

Ribosomally synthesized and post-translationally modified peptides (RiPPs) represent a structurally and functionally diverse family of natural products with broad-ranging biological activities, including antimicrobial, antiviral, and cytotoxic activities. Epimerization of the L-amino acids to their D-forms is a common post-translational modification in RiPPs Of the three characterized rSAM epimerase families—proteusins, eppipeptides, and the more recently characterized origamins—the origamins are mechanistically and structurally unknown.

Here we present the first biochemical and spectroscopic characterization of OpgD, a predicted origamin radical SAM epimerase. We demonstrate OpgD houses two [4Fe-4S] clusters and that both are reducible by sodium dithionite and that SAM binds to one of the clusters as would be expected from typical rSAM enzyme behavior. Biochemical assays show that the epimerization reaction on a truncated substrate OpgA-t12 is catalyzed by OpgD, but the specific epimerization sites remain unidentified. Collectively, these findings provide the first glimpses into the origamin family of radical SAM epimerases and pave the way for elucidation of their involvement in intricate RiPP biosynthesis.

Introduction

Organisms synthesize natural products to gain an ecological advantage, enabling them to defend against threats, compete for resources, communicate, or adapt to environmental

stressors.[1, 2] Two distinct biosynthetic pathways are responsible for the production of peptide natural products: ribosomal and non-ribosomal. The non-ribosomal pathway involves large, multienzyme megacomplexes in which each module incorporates a specific amino acid into the growing peptide chain.[3] In contrast, the ribosomal pathway—which is the focus of this chapter—relies on the ribosome for synthesis of a peptide precursor, which is then modified through enzymatic processes. These resulting compounds, known as **ri**bosomally synthesized and **p**ost-translational modified **p**eptides (RiPPs), represent a diverse class of natural products with a broad range of bioactivities, including antimicrobial, antiviral, and apoptosis-inducing properties.[4-7]

A significant post-translational modification occurring in RiPP natural products is epimerization, in which the stereochemistry of amino acid side chains at the Cα positions are changed from the naturally occurring L-amino acid configuration to the D-amino acid. D-amino acids are known to provide stability against degradation because proteases are unable to recognize the non-natural configuration.[8]

Several classes of epimerases have been discovered, including those involved in maturing proteusins, eppipeptides, and origamin RiPP natural products. Proteusins epimerases typically act on a large, complex substrates that undergo numerous post-translational modifications (PTMs), including C- and N-methylations, aminations, cysteine crosslinks, and epimerizations.[9] Eppipeptide epimerases generally modify simpler core regions with fewer PTMs, and can have of a twitch domain harboring an auxiliary [4Fe-4S] cluster in addition to the radical SAM domain. To date, the only crystal structure of a radical SAM epimerase is of the eppipeptide epimerase EpeE with and without a truncated version of its substrate (EpeX) bound in the active

site (PDB 8AI1 and 8AI2). Origamins are a newly discovered family of epimerases united by an interlocking NX_5N motif that facilitates the formation of stabilizing β-helical secondary structures in the peptide substrate.[10, 11] Origamin biosynthetic gene clusters are found widespread in the human microbiome, however is currently no published work on this class of epimerases.[12]

The origamin epimerase enzymes of features present in both the proteusin and eppipeptide epimerases, suggesting that origamins may behave catalytically in the same manner. A newly discovered member of origamin family, OpgD, was recently discovered by Jorn Piel's lab at ETH Zurich.[12] The predicted structure of OpgD reflects key characteristics of the eppipeptide epimerase structure, including an auxiliary [4Fe-4S] cluster, and shows perfect positioning of a cysteine residue for proposed H-atom abstraction from a Cα position on the peptide substrate (Figure 3.1).

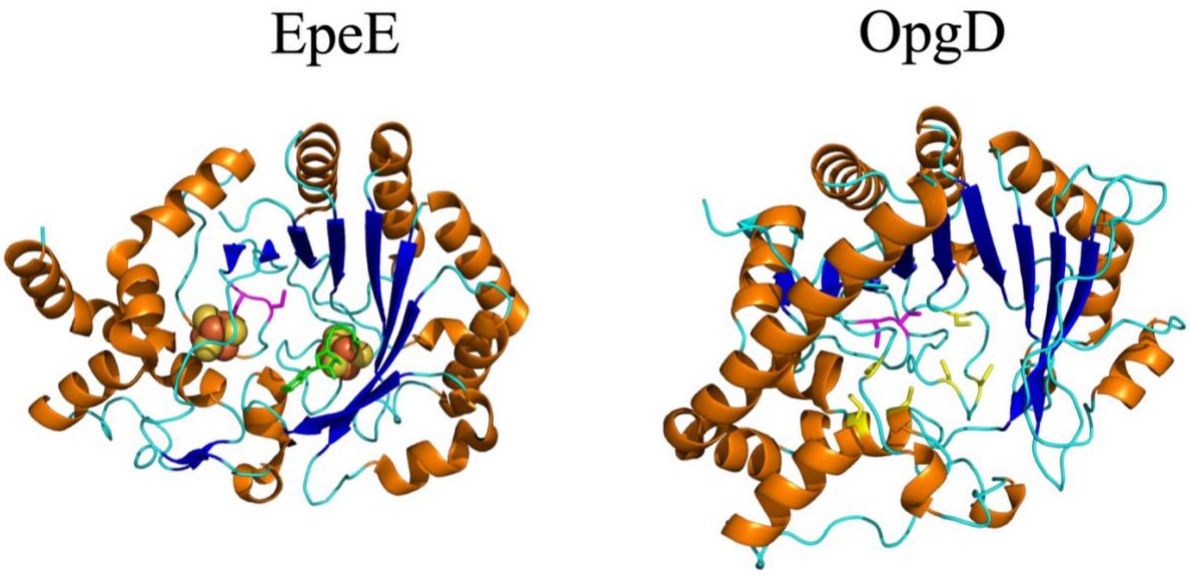

Figure 3.1. Crystal structure of EpeE (PDB: 8AI1) and AlphaFold3 predicted structure of OpgD.[13] The cysteine residues responsible for coordinating the [4Fe-4S] radical SAM and auxiliary cluster are in yellow, similar secondary structures colored in orange and blue, and the hydrogen donor that quenches the proposed Cα radical is in magenta.

OpgD sits in a biosynthetic gene cluster (BSG) with other maturating enzymes Figure 3.2A) and its substrate, OpgA, is a large peptide that is heavily modified during its maturation, much like the substrates of the proteusin family (Figure 3.2B). OpgA incorporates a total of 18 epimerizations, 13 N-methylations, and 13 C-methylations installed by 3 dedicated maturases. The fully modified OpgA product has the same epimerization pattern as polytheonamide (a well-characterized proteusin RiPP natural product), further emphasizing the similarities between origamins and proteusins.[14, 15] OpgD epimerizes alanine, proline, and threonine in the core of OpgA, but the scope of tolerable residues and epimerization sites, as well as the mechanism of epimerization, is currently unknown.[12]

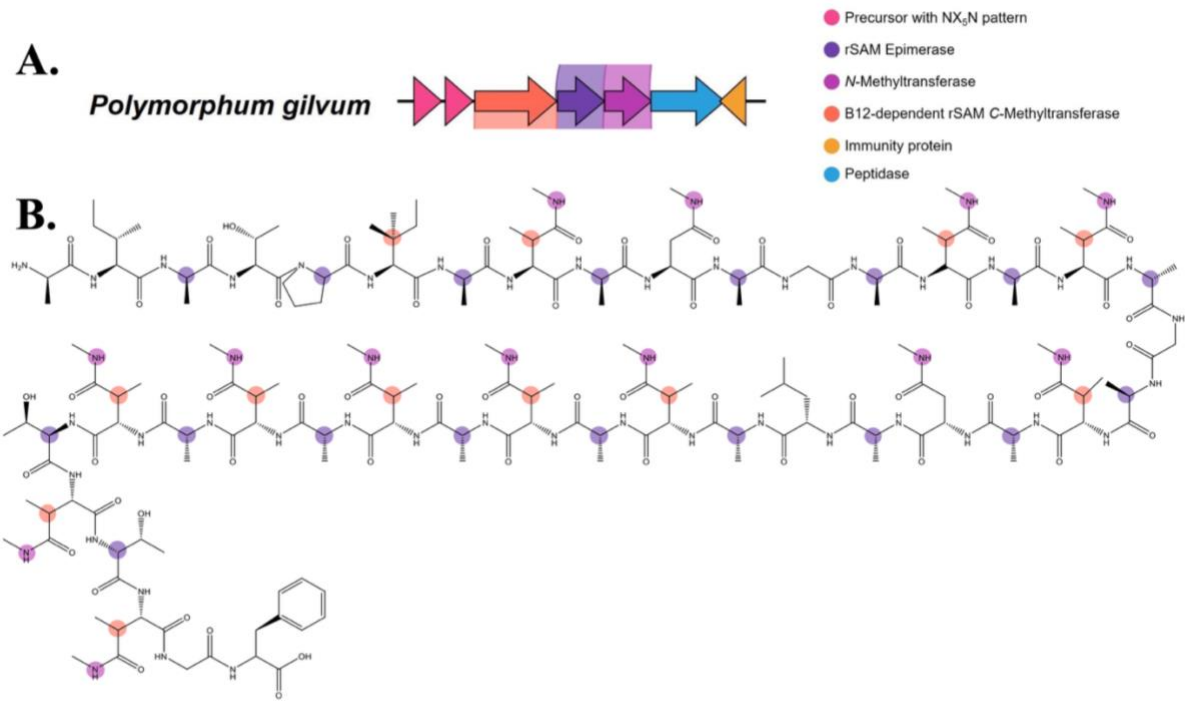

Figure 3.2. The *Polymorphum gilvum* origamin biosynthetic gene cluster (A) encodes multiple maturases, including the radical SAM epimerase OpgD. The predicted mature OpgA peptide (B) undergoes extensive epimerization and methylation, resembling proteusin-type RiPP natural products.

Epimerization of the precursor peptide can occur through either polar or radical-based mechanisms, with latter often involving radical SAM enzymes. Previous experiments performed on both proteusin and eppipeptide epimerases have provided evidence that epimerization occurs through a Cα intermediate. Based on the similarities of OpgD to the proteusins and eppipeptides, its mechanism is proposed to be the same as the other epimerase families. The proposed mechanism of radical-based epimerization of amino acid residues during RiPP maturation is shown in Figure 3.3 and begins with the reductive cleavage of SAM to form the organometallic intermediate **Ω**, which releases 5'-dAdo•. The 5'-dAdo• is proposed to abstract the Cα hydrogen from the target amino acid reside of the peptide substrate, forming a Cα radical intermediate. A conserved cysteine residue in the primary sequence of the epimerase is proposed to stereospecifically quenches the Cα radical through a hydrogen atom transfer step to yield a D-amino acid and a thiyl radical, which is proposed to be quenched by proton-coupled electron transfer (PCET) or by electron transfer from an auxiliary FeS cluster.

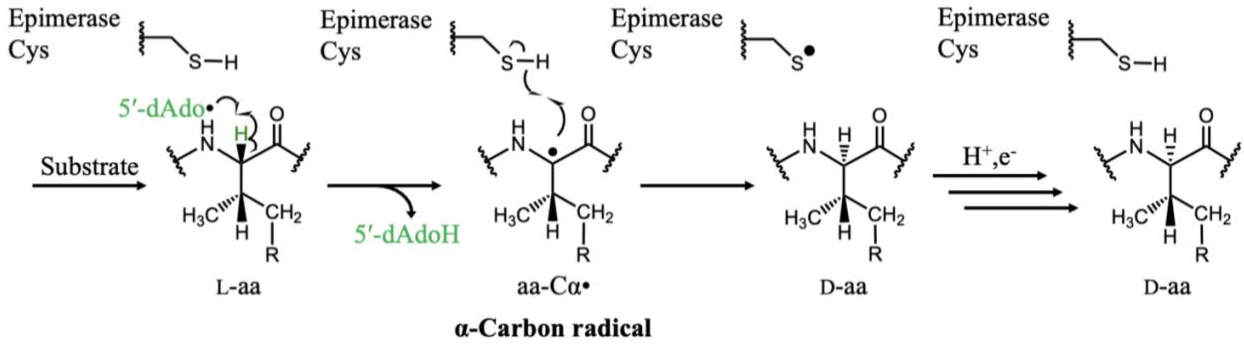

Figure 3.3. Proposed mechanism of radical epimerization by radical SAM enzymes. 5'-dAdo• abstracts a hydrogen from the Cα of the target amino acid of the peptide substrate, generating a peptidyl Cα radical, which is in turn quenched by a cysteine residue of the epimerase on the backside of the peptide, thus inverting the stereochemistry at the Cα. For this figure, R is either -CH3 representing an isoleucine residue, or a hydrogen indicating a valine residue.

In this chapter, my efforts towards cloning, expressing, and purifying OpgD for initial biochemical characterization are described. We have identified working methods for purification, iron reconstitution, and activity assessment for OpgD with a truncated OpgA peptide core, along with providing evidence the enzyme houses two [4Fe-4S] clusters. Additionally, we show both [4Fe-4S] clusters are visible via electron paramagnetic resonance spectroscopy (EPR), and SAM binds to one of the [4Fe-4S] clusters. Due to solubility issues, the work presented in this chapter The modified substrate of OpgD, OpgA t12, is a truncated, soluble version of the WT OpgA substrate, as the core region of the WT peptide harbored too many nonpolar residues and was insoluble.[12] The sequences of the two substrates are shown in Table 3.1. Both versions of the substrate have epimerization sites (Table 3.1, red) appearing throughout the sequence, with the truncated version missing the C-terminal region harboring a series of alanine and asparagine residues. OpgA t12 has 6 total epimerization sites with at least one of each epimerized residue (alanine, proline, and threonine).

Table 3.1. Comparison of OpgA and OpgA t12 core region. Residues in red represent the epimerization sites, and the section between the slashes in OpgA indicates the cut-out residues in the OpgA t12 construct.

Substrate	Sequence
OpgA	**AIATPIANANAG/ANANAGANANALANANANANANTN/TNGF**
OpgA t12	**AIATPIANANAG/TNGF**

Materials and Methods

Preparation of Plasmids

Initial plasmids: pACYC-OpgA2-truncated, pACYC-SUMO-OpgA2, pET28b-OpgD-WT, pET28b-OpgD-C249S, pET28b-OpgDC21/24A (ΔRS), and pET28b-OpgD-C314/317

(ΔAux) were received from the Piel Lab at ETH Zurich. pCA24N-FlvA and pCA24N-FlvR were purchased from the ASKA E. coli clone collection.[16] All plasmids were transformed by adding 50-100 ng of plasmid DNA to thawed BL21(DE3) cells and incubating for 30 min. Cells were then heat shocked for 45 seconds, followed by a 2-minute incubation on ice. 250 μL of LB media was added to the cells and shaken at 250 rpm at 37°C for 1 hour. 50 μl of cells was plated on LB + agar plates with 50 μg/mL of spectinomycin and incubated overnight at 37°C.

OpgD Plasmid Construction

Due to solubility issues, primers were designed to amplify the OpgD and SUMO-OpgD obtained from the Piel group out of its pET28b vector with 20 bp overhangs to ligate into an in-house pCDF-MBP plasmid. The pET28b-OpgD vector was diluted to 1 ng/μL and PCR amplified according to the following parameters: 98°C for 30s, followed by 30 cycles of 98°C for 10s, 67.4°C for 25s, 72°C for 35s, and finally 2 min at 72°C. 5 μL of the PCR product was visualized on a 1% agarose gel stained with thiazole orange. The gene was inserted into an in-house pcDF-MBP vector, which was digested with NdeI and XhoI restriction enzymes (ThermoFischer) via Gibson assembly. Approximately 50 ng of the pcDF-MBP vector, 84 ng of the OpgD PCR product, and 5.7μL of 2x HiFi master mix were combined and incubated at 50°C for 30 min, then stored at 4°C. The primers used do not overlap with any mutations or coordinating cysteines, and therefore the same primers were used for all OpgD constructs. The product from the Gibson assembly was then transformed into NEB5α cells (New England Biolabs) and plated on LB + agar plates. 5 mL starter cultures of LB media were inoculated with a single colony and grown overnight at 37°C while shaking at 220 rpm. The plasmid was mini-

prepped from the starter culture using the GeneJet mini prep kit standard protocol. Plasmids were stored at -20°C.

OpgD Growth and Purification

Plasmid DNA (pACYc-MBP-OpgD_C249S or pACYc-MBP-OpgD) was transformed into chemically competent BL21(DE3) cells and plated on selective LB-agar plates. A single colony was used to inoculate LB medium supplemented with 50 μg/mL spectinomycin and grown at 37°C at 250 rpm overnight. 2L of TB medium (12 g/L tryptone, 24 g/L yeast extract, 0.4% (v/v) glycerol, 0.017 M KH_2PO_4, 0.072 M K_2HPO_4) was supplemented with 50 μg/mL spectinomycin and inoculated with an overnight culture (1% v/v). Cultures were grown at 37°C, shaking at 200 rpm until OD_{600} = 0.8, and placed on ice for 15 minutes. Growth was supplemented with 250 μM ferrous ammonium sulfate, 300 μM *L*-cysteine, and 0.5 mM IPTG and left shaking at 16°C at 180 rpm for 20 hours. Cells were pelleted via centrifugation (6754 x g, 4°C, 15 min), flash frozen in liquid nitrogen, and stored at -80°C.

Cell pellets were lysed in buffer containing 50 mM HEPES pH 8, 300 mM KCl, 20% glycerol, 5 mM imidazole, 1 mM PMSF in MeOH, 1 protease inhibitor tab, 10 mg/mL Triton x-100, 1.15 mg/mL $MgCl_2$, 0.5 mg/mL lysozyme, and 0.01 mg/mL DNase at a ratio of 5 mL/g cell paste. Cells were homogenized with an 18-gauge needle and allowed to stir in an anaerobic chamber (COY Laboratories, Inc.) for 1 hour. The slurry was sonicated for 5 minutes (5s on, 15s off, 40% amplitude) and the lysate was clarified via centrifugation (26,790 x g, 4°C, 45 min). The lysate was loaded onto a Ni-NTA column (Cytiva) equilibrated in buffer A (50 mM HEPES, 300 mM KCl, 20% glycerol, pH 8) at a flow rate of 1 mL/min using a superloop. The column

was washed with 2% and 8% buffer B (50 mM HEPES, 300 mm KCl, 500 mM Imidazole, 20% glycerol, pH 8), and protein was eluted with 50% buffer B. The purified enzyme was desalted using a HiPrep 26/10 desalting column (Cytiva) into buffer A* (50 mM HEPES, 300 mM KCl, 10% glycerol, 1 mM DTT, pH 8) and concentrated with a 50 KDa spin filter (Amicon) to a concentration of about 300 μM. The protein was then aliquoted, flash frozen in liquid nitrogen and stored at -80°C.

FlvA and FlvR Growth and Purification

FlvA and FlvR were grown and purified to serve as an alternative reduction system to NaDT and DTT. A single colony from transformations of FlvA and FlvR were used to inoculate 25 mL of autoclaved LB media supplemented with chloramphenicol (33 μg/mL) overnight at 37°C, 220 rpm. Large cultures were inoculated with the precultures (1% v/v) supplemented with chloramphenicol (33 μg/mL) and grown at 37°C, 220 rpm, until OD_{600} = 0.8, at which point 10 μM FMN was added to the FlvA cultures, and 10 μM FAD for the FlvR culture. Each culture was induced with 0.5 mM IPTG and grown at 20°C at 180 rpm overnight. Cells were harvested via centrifugation (6,000 rpm, 15 min, 4°C). Separately, cells were lysed in buffer A (50 mM HEPES, 300 mM KCl, 10% glycerol, pH 8), containing 5 mM imidazole, 10 mg/mL Triton x-100, 1.15 mg/mL $MgCl_2 \bullet 6H_2O$, 0.5 mg/mL lysozyme, 0.01 mg/mL DNAse, and 1 Pierce protease inhibitor tablet in a ratio of 2 mL/1 g cell paste. Cells were stirred for 1 hr in an anaerobic chamber (COY Laboratory Products) and sonicated on ice for 10 min (5s on, 15s off, 40% amplitude). The lysate was centrifuged at 15,000 rpm, 1 hr, at 4°C and the supernatant was filtered through a 45 μm filter and loaded onto a 5 mL NiNTA (for FlvR) or NiNTA 16/10 (for

FlvA) column (Cytiva). Column was washed with 5% B (50 mM HEPES, 300 mM KCl, 10% glycerol, 500 mM imidazole, pH 8), then eluted with 50% B. Protein was desalted on a HiPrep 26/10 desalting column (Cytiva) into 50 mM HEPES, 150 mM KCl, 10% glycerol, pH 8, and concentrated with an Amicon 10 kDa MWCO spin filter, aliquoted, flash frozen in liquid nitrogen, and stored at -80°C.

Protein Quantification

Proteins were quantified according to the protocol from Zor and Selinger using Pierce bovine serum albumin (ThermoFisher) as a standard.[17]

Iron Analysis

The iron content of the purified protein was determined using an Agilent 240FS atomic absorption spectrometer. A standard curve was created with an iron atomic absorption standard (Ricca, 1000 ppm in 3% HNO_3) diluted in MQ water, ranging from 0.4 ppm to 2.0 ppm. Protein samples were diluted to 1-2 μM in buffer, in triplicate for analysis. Any absorption from the buffer was subtracted from the sample absorption, and iron content per protein was calculated by dividing the moles of iron by the moles of protein.

D_2O Buffer Preparation and Protein Buffer Exchange

Buffered D_2O was prepared by removing water from 50 mL of 50 mM HEPES, pH_{app} = 8.2, 300 mM KCl, 10% glycerol by rotary evaporation for 45 min. The residual glycerol and salt were dissolved in 4 mL of D_2O, and then removed by rotary evaporation, 3 times. After 3 washes, the solution was diluted to its original volume with D_2O, and the pH_{app} was measured to be 8.1-

8.3. The pH_{app} was adjusted following the recommendation by Rubinson, K. A., *Analytical Methods* **2017**, *9* (18), 2744-2750.[18] The buffered D_2O was degassed on a Schlenk line using the freeze-pump-thaw method. MBP-OpgD-WT was exchanged into buffered D_2O using PD MiniTrap columns, following the manufacturer's protocol, and concentrated back to its original volume using 10 kDa MWCO 0.5 mL spin filters. The MBP-OpgA t12 substrate was exchanged into buffered D_2O by diluting it 2x and reconcentrating to the original volume using 10 kDa MWCO 0.5 mL spin filters, a total of 4 times. The concentration of the D_2O-exchanged proteins was remeasured by Bradford (MBP-OpgD-WT) or Nanodrop (OpgA t12).

Activity Assays

In the glove box, assays contained 100 µM of MBP-OpgD WT or C249S, 200 µM OpgA, 5 mM SAM, 5 mM NaDT, and 5 mM DTT in buffer A, at a volume of 50 µL. SAM was added last to initiate the reaction and incubated overnight. Activity assays without NaDT contained 20 µM of FldA, 2 µM of FlvR, and 2 mM NADPH. 25 µL of the reaction (about 0.1 mg of OpgA t12) was mixed with 1 µg trypsin, 20 mM $CaCl_2$, and diluted with water to 50 µL. The digest was incubated at 37°C for 1 hour before being quenched with 5 µL of 10% trifluoroacetic acid (TFA). Peptides were desalted using 100 µL C18 Zip Tips (Thermo Scientific) and eluted into 25 µL of 60% acetonitrile, 0.1% formic acid, in water. 5 µL was injected for analysis by LC-MS.

Liquid Chromatography-Mass Spectrometry

An aliquot (5 µL) was injected onto an Agilent UHPLC 1290 Infinity II equipped with a Zorbax RRHD Eclipse Plus C18 column (2.1 x 50 mm, 1.8 µm, 95 Å) coupled to an Agilent 6538 UHD Accurate-mass Q-TOF mass spectrometer. The sample was eluted using the following

program: linear gradient from 2-10% B from 0-2 min, linear gradient to 40% B from 2-22 min, linear gradient from 40-98% B from 22-23 min, 98% B from 23-24.5 min, 98-2% B from 24.5-24.51 min, and was with 2% B from 24.51-25 min. Solvent A is 0.1% formic acid in water and solvent B is acetonitrile with 0.1% formic acid. The separation was carried out with 0.4 mL/ min flow rate and column temperature of 50°C. Mass spectra was collected with 2 Hz scan rate and a mass range of 103-1700 m/z. Expected m/z were calculated using the Fiehn laboratory's excel ESI-adduct calculator. B- and y- ions were calculated using the University of Washington's Proteomics Resource peptide fragmentation tool (https://proteomicsresource.washington.edu/cgi-bin/fragment.cgi).

EPR Sample Prep and Analysis

In an anaerobic mBraun chamber, protein samples for intracavity photolysis and EPR spectroscopic analysis were prepared by mixing buffer (50 mM HEPES, 150 mM KCl, 10% glycerol, pH 8) with Na-dithionite and dithiothreitol (DTT) to final concentrations of 3 mM and 3 mM respectively. Protein was added to final concentrations of 200 μM for MBP-OpgD-WT, MBP-OpgD-C249S, 180 μM -MBP-OpgD-ΔRS, and 500 μM for OpgA t12 and allowed to reduce for 10 minutes. Following reduction of the [4Fe-4S] cluster, SAM was added to a final concentration of 2 mM, the solution was mixed, transferred to an EPR tube and frozen in liquid nitrogen at stated time scales. Photoreduced samples contained 100 μM of 5-deazariboflavin, no NaDT and were reduced in the absence of SAM for 1 hr with a UV light approximately 3 cm from the sample. Following the photoreduction, SAM was added to a final concentration of 2 mM, and the samples were flash frozen in liquid nitrogen at specified times. Continuous wave

EPR X-band EPR spectroscopy was performed using a Bruker EMX EPR spectrometer equipped with a Bruker/ColdEdge (Sumitomo Cyrogenics) 10 K waveguide cryogen free system with an Oxford MercuryiTC controller unit and helium Stinger recirculating unit (Sumitomo Cyrogenics, ColdEdge Technologies). All spectra were recorded at 9.378 GHz83microwave frequency and 100 kHz modulation frequency. The spectrometer was calibrated with an external standard of 2,2-diphenyl-1-picrylhydrazyl (DPPH) with a *g*-value of 2.0036 (Bruker). Experimental spectra were simulated with Easyspin (5.2.35) within the Matlab R2020b software suite (Mathworks, Inc.).[19] Iron-Sulfur cluster signals were recorded at 10 K with 10 G modulation amplitude and 1 mW microwave power.

Results

The expression vectors containing OpgA t12, OpgD-WT, OpgD-C249S, OpgD-C21/24A (ΔRS), and OpgD-C314/317A (ΔAux) were received from Jörn Piel's lab at ETH Zurich. All vectors were transformed into *E. coli* BL21(DE3) cells for expression. Following expression and cell lysis, but except OpgA t12 proved to be insoluble with little to no protein being observed in the supernatant after pelleting the cellular debris (Figure 3.4A). To improve the solubility of OpgD, each construct was appended with an N-terminal maltose-binding protein (MBP) tag, and the resulting MBP-OpgD constructs were found to be soluble, as shown in Figure 3.4B.

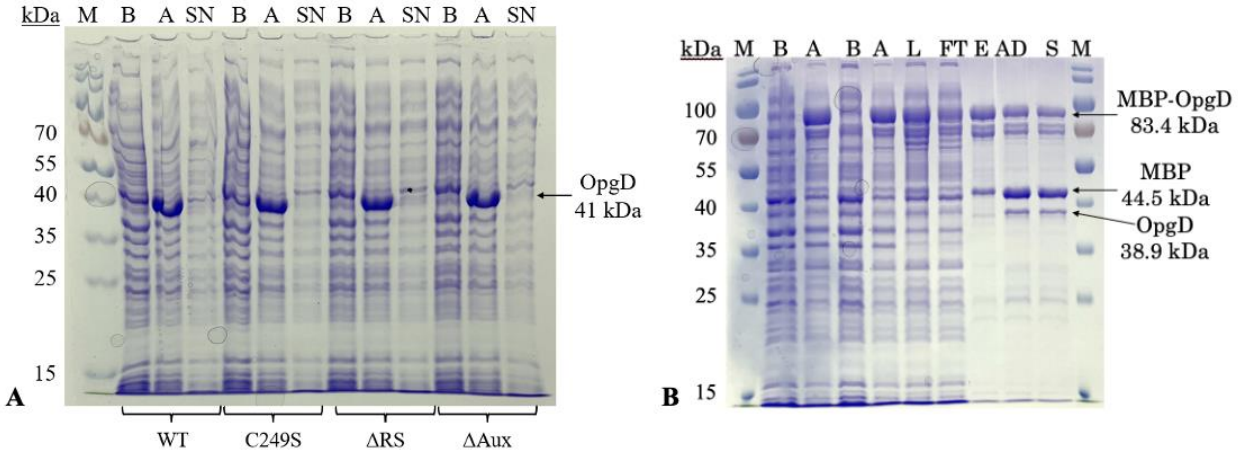

Figure 3.4. SDS-PAGE gels of OpgD and MBP-OpgD expression, solubility, and purification. (A) Expression of OpgD constructs, with lanes marked B and A for before and after induction, and SN for the supernatant following lysis. (B) Expression and purification of MBP-OpgD, with lanes marked B and A for before and after induction, L for the soluble lysate, FT for the column flow through, E for the elution fraction, AD for the after TEV digestion, and S for the soluble fraction after TEV digest. The ladder is in the left-most lane (M) of each gel.

Cells were harvested from a 2L growth in TB media and purified on an Ni-NTA column (Cytiva). Unfortunately, a significant amount of protein precipitated on the top of the column and only 95 mg of MBP-OpgD was recovered containing 2.5 $\pm$ 0.4 Fe/monomer. There are visible contaminants in the purified protein fraction, in addition to bands aligning with isolated MBP and the MBP-OpgD construct indicating only partial TEV cleavage of MBP-OpgD. Future purifications included glycerol in the buffer components which helped to prevent precipitation on the column, but the TEV digest has yet to be optimized.

The OpgD-MBP constructs from the purification were successfully reconstituted with iron and sulfide resulting in 9.7 $\pm$ 1.3 Fe/monomer based on atomic absorbance analysis of the resulting protein. This is higher than the expected 8 Fe/monomer and is could be due to contamination from other proteins that may bind or coordinate some iron ions. Reconstitution was also evidenced by the increase in absorbance at 410 nm (Figure 3.5). Addition of the

reducing agent dithionite to both MBP-OpgD and MBP-OpgD-C249S *in vitro* results in the appearance of an EPR signal characteristic of $[4Fe\text{-}4S]^{+}$ clusters, demonstrating that the radical SAM $[4Fe\text{-}4S]^{2+}$ clusters can be reduced to the paramagnetic $[4Fe\text{-}4S]^{+}$ state. Distinct perturbations in each spectrum when SAM is added to the samples indicate that SAM also binds to the radical SAM cluster, a key precursor for catalysis (Figure 3.6).

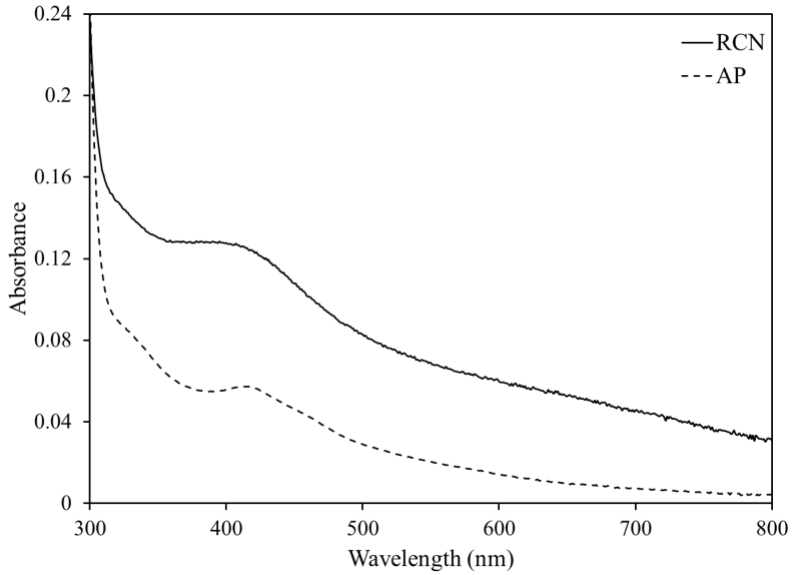

Figure 3.5 UV-visible evidence for reconstitution of MBP-OpgD-WT. Absorption at 410 nm increases from the as-purified protein (AP) to the reconstituted protein (RCN), indicating successful reconstitution. Iron numbers increased from 2.5 $\pm$ 0.4 Fe/monomer to 9.7 $\pm$ 1.3 Fe/monomer.

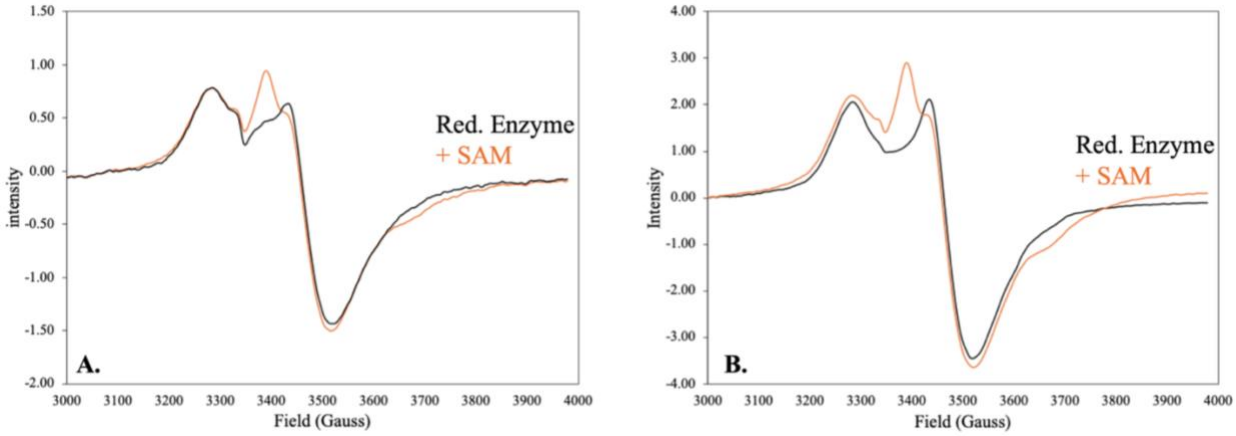

Figure 3.6. EPR spectra of (A) MBP-OpgD-WT and (B) MBP-OpgD-C249S. Each enzyme was reduced for 5 min with dithionite before the addition of SAM and then frozen in liquid nitrogen. For each spectrum, the reduced enzyme is shown in the black trace, and the +SAM spectra are in orange. EPR parameters: T = 10 K; microwave frequency, 9.37 GHz; modulation amplitude, 10 G, microwave power, 1 mW.

OpgD and OpgD-C249S Activity Assays

Activity assays were carried out using both MBP-OpgD-WT, and MBP-OpgD-C249S to determine if the MBP tag interfered with activity. Briefly, MBP-OpgD WT was incubated with OpgA t12 along with DTT, NaDT, and SAM for 17 hours. OpgA t12 was digested with trypsin protease to isolate the peptide core fragment for analysis by liquid chromatography mass spectrometry (LC-MS). First, no-substrate controls were run and only one peak for the core peptide was detected. Following incubations with the enzyme overnight, multiple peaks appeared in the extracted ion chromatogram with the same mass, suggestive of epimerization of isomerization events (Figure 3.7). Epimerization events will increase the retention time when run with either a chiral mobile or stationary phase, as previous evidence suggests,[20] however, when an epimerization event occurs, there is no overall mass change to the substrate.

The control was run with no enzyme to determine the retention time of the unmodified peptide, as any modification to one of the 6 epimerization sites would shift the retention time.

The shift from 6.98 min to 7.18 min after the 17-hour reaction indicates some amount of epimerization events in the MBP-OpgD assay (Figure 3.7A), and similar shifts were seen in the MBP-OpgD-C249S activity assay (Figure 3.7B) from 12.61 min to 12.81 min. the appearance of multiple peaks in the extracted ion chromatogram indicates the MBP tag does abolish the activity of OpgD *in vitro.*

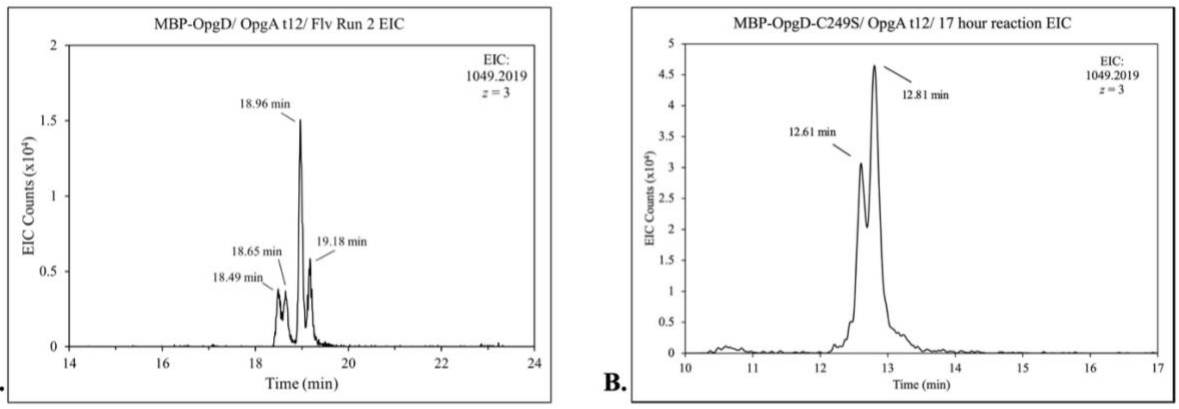

Figure 3.7 Extracted ion chromatogram of (A) MBP-OpgD/OpgA t12 and (B) MBP-pgD-C249S/OpgA t12 reactions.

EPR Characterization of OpgD

Following confirmation that both MBP-OpgD-WT and MBP-OpgD-C249S were active with OpgA t12, attempts were made to trap a radical intermediate using the C249S mutant. The cysteine to serine mutation in other radical SAM enzymes has previously been shown to slow the hydrogen atom transfer step in the epimerization reaction due to the stronger O-H bond of serine, allowing the Cα radical to accumulate enough that it could be observed via EPR.[21] Briefly, EPR protein was reduced with dithionite for 10 min before SAM and OpgA were added. The sample was then frozen in liquid nitrogen at a predetermined time. SAM-bound [4Fe-4S]$^{+}$ clusters were recorded at 10 K at different incubation times with SAM (Figure 3.). When the temperature was

increased to 75 K to observe organic-based radicals, there was no signal. It was hypothesized that the organic radical intermediate may have been either too transient to detect or had not yet formed under the initial conditions; therefore, quenching experiments were performed with both shorter and longer reaction times. Using hand-quench technique, the sample was frozen in liquid nitrogen in 13.4 seconds, 1 minute, and 10 minutes (Figure 3.8). However, one of these samples accumulated enough radical intermediate to be observed at 75 k.

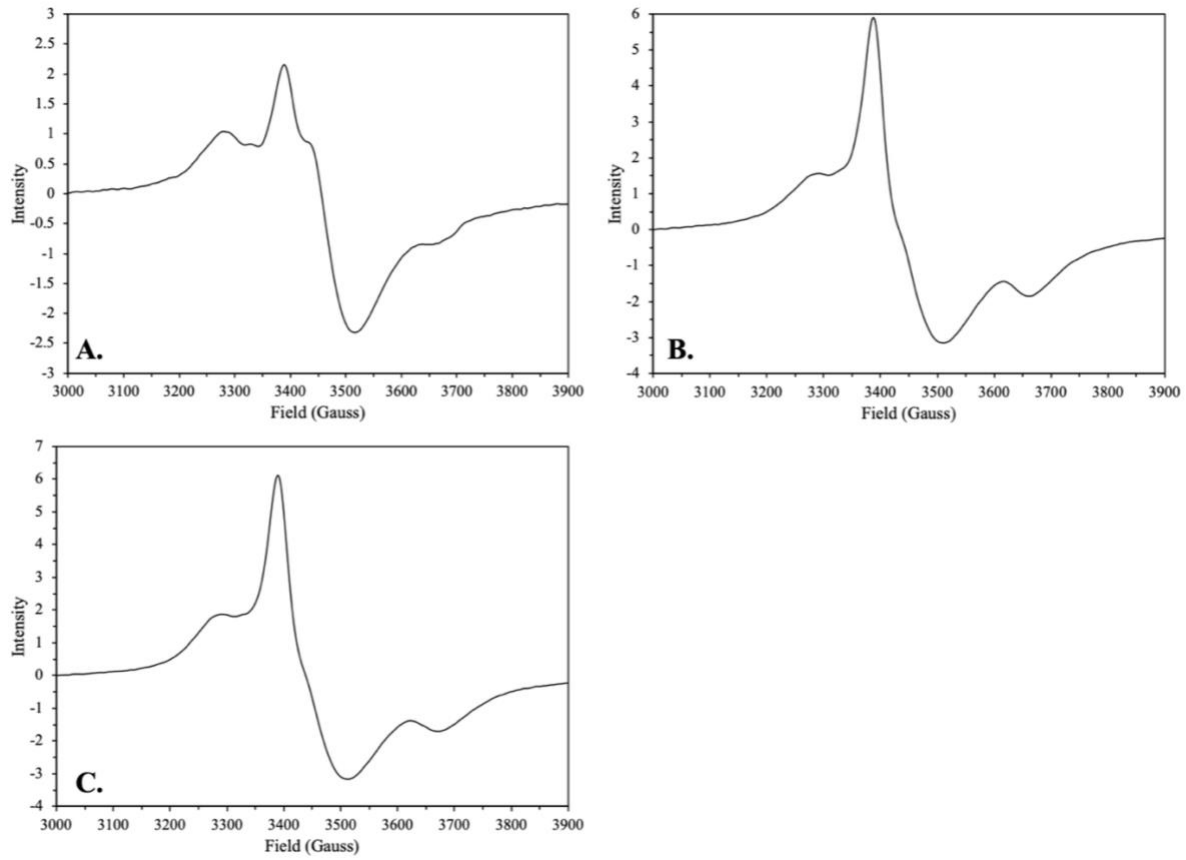

Figure 3.8. MBP-OpgD-C249S quenched at 13.4 sec (A), 1 min (B) and 10 min (C) after the addition of SAM and OpgA. Each sample was reduced for 10 minutes with NaDT and frozen in liquid nitrogen. EPR parameters: T = 10 K; microwave frequency, 9.37 GHz; modulation amplitude, 10 G, microwave power, 1 mW.

Despite failed attempts to catch any radical intermediate thus far, it was observed in the ΔRS mutant that the auxiliary cluster of OpgD is reducible by NaDT (Figure 3.9). By mutating radical SAM cluster coordinating cysteine residues C21 and C24 to alanine, we effectively knock out the rSAM cluster. Atomic absorbance data shows a reduction of Fe/monomer from about 9 to 4.5 $\pm$ 0.2 which is consistent with the loss of one [4Fe-4S] cluster. EPR analysis shows the signal from the ΔRS mutant has g-values and temperature broadening which are both properties consistent with $[4Fe\text{-}4S]^{+}$ clusters.

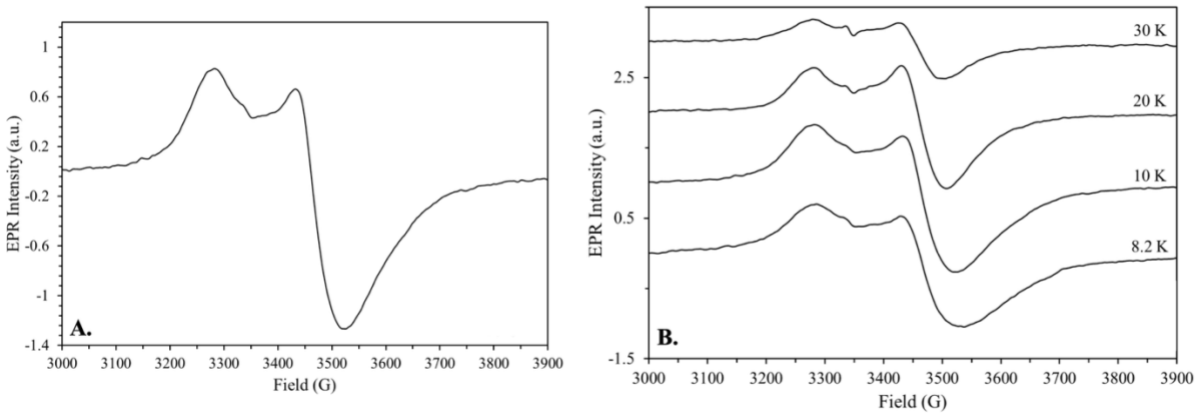

Figure 3.9. (A) Reduced auxiliary cluster from MBP-OpgD-ΔRS mutant. G-values = 2.047, 1.935, and 1.905 are consistent with a $[4Fe\text{-}4S]^{+}$ cluster. (B) The spectrum broadens when the temperature is increased, consistent with a metal-based signal due to the faster relaxation between ground and excited states. EPR parameters: 10 k, 1 mW, 10 G, 9.37 GHz.

To test if elements in the solution are quenching and substrate radicals before they can be observed on EPR, 5-deazariboflavin was introduced as reductant due to its limited single-electron reducing abilities. Using 5-deazariboflavin over NaDT or DTT could prevent continuous reduction conditions and allow for single turnover events. EPR samples were made using several different combinations of DTT, NaDT, and 5-deazariboflavin with both the C249S mutant and WT enzyme (Table 3.2). Each of these samples produced SAM-bound [4Fe-4S] spectra like

those seen in Figures 3.6, 3.7, and 3.8, but none had any organic-based radical formation when the samples were observed at 75 K.

Table 3.2. Reduction conditions for MBP-OpgD-C249S EPR samples.

Protein	Reductant	DTT present?	Reduction Time	Quench Time
MBP-OpgD-C249S	NaDT	✓	5 min	13.4 sec
MBP-OpgD-C249S	NaDT	✓	10 min	1 min
MBP-OpgD-C249S	NaDT	×	10 min	14.3 sec
MBP-OpgD-C249S	5-deazariboflavin	×	60 min	1 min
MBP-OpgD-C249S	NaDT	✓	10 min	10 min
MBP-OpgD-C249S	NaDT	✓	10 min	14.2 sec
MBP-OpgD-WT	NaDT	✓	10 min	29.35 sec
MBP-OpgD-WT	NaDT	✓	10 min	67 min

Discussion

Epimerization is a key reaction in both organic synthesis and the biosynthesis of natural products, and it can proceed through either polar or radical-based mechanisms. Radical-based epimerization reactions are widely utilized in Nature and can occur in several structural contexts, including unactivated C(sp^3)–H bonds.[22] In RiPP natural products, the epimerization of L-amino acid residues is a common modification, and both radical- and non-radical–mediated mechanisms have been described.[6] Radical SAM epimerases are commonly employed in RiPP natural product maturation and belong to one of three families: eppipeptides, proteusins, and origamins. Members of both the eppipeptide and proteusin families have been biochemically characterized and are not closely related.[9, 23-25]

In contrast, little is known about the recently discovered origamin family and its role in Nature. The origamins have been predicted to share elements characteristic of both the proteusins and eppipeptides. They act on large, heavily modified peptides like proteusins, but have similar predicted folds and structures as eppipeptides. Despite their differences, each family is expected to epimerize *L*-amino acids similarly. This hypothesis comes from the structural homology between OpgD and EpeE (Figure 3.1) and similarities in PTMs of proteusin PoyD's substrate PoyA and OpgA. The proposed mechanism begins with H-atom abstraction from the Cα position by the 5'-dAdo• radical generated by the reductive cleavage of SAM. This radical is then proposed to be quenched on the backside by a conserved cysteine residue, thus inverting the stereochemistry (Figure 3.3).

Our characterization of the unstudied origamin epimerase OpgD, suggests the presence of two [4Fe–4S] clusters (Figure 3.5), each of which can be reduced upon treatment with sodium dithionite (Figures 3.6 and 3.9). Additionally, we have shown SAM can bind to one of the [4Fe-4S] clusters and our results have shown that both MBP-OpgD-WT and MBP-OpgD-C249S are active and catalyze epimerizations on OpgA t12 (Figure 3.7). The specific location and number of epimerization events are unknown, but the shift in retention time and presence of multiple peaks in Figure 3.7A, and the various peaks seen in 3.7B indicate some epimerization of OpgA t12. With six possible epimerization sites in OpgA t12, it is impossible to determine which sites have been epimerized without conducting future experiments in D_2O, which will be the focus of future experiments. The cysteine/serine at position 249 is proposed to have a solvent-exchangeable hydrogen which would exchange with a deuterium and thus quench a Cα radical

with a 1 Da heavier atom. Upon LC-MS/MS peptide fragmentation, the number and location of epimerization events could be determined.

Despite seeing SAM binding (Figure 3.6 and 3.8), and activity (Figure 3.7) with OpgD, we were unable to detect a there was no radical intermediate observed on the 13-second to 1-hour timeline. It is possible that the reaction could be transpiring faster than 10 seconds, and the radical is being missed in which case rapid freeze-quench techniques should be employed. Another possibility is that the rate of reaction is so slow that after 1 hour the radical intermediate hasn't been formed yet. The only timescale that OpgD has proven active is after 17 hours (Figure 3.7), so both longer and shorter quench times should be attempted.

Based on the predicted structure of MBP-OpgD and OpgA (Figure 3.10), the active site appears to be exposed to the solvent around it. Any radical may form and immediately be quenched by the solution. To address this, samples were made without external reductants such as DTT and NaDT (Table 3.2) and quenched at different times. However, none of these samples caught a radical intermediate.

Based on predicted structures (Figure 3.10) of OpgA docked in MBP-OpgD,[13] there is potential that a radical formed within the active site of MBP-OpgD could be quenched by the solvent faster than it is possible to freeze the sample due to the predicted accessibility of the OpgD active site. If the core of OpgA is exposed to solvent, it is plausible that any quenching of the radical intermediate results from interaction with DTT of DT. Generally, DTT is added to the EPR samples to scrub any residual oxygen contamination in the protein, substrate, or buffer solutions. However, when DTT and NaDT were eliminated from the solutions and replaced with

5'-deazariboflavin as a reductant, there were still no organic radicals observed (Figure 3.8) suggesting the solvent components are not quenching substate-based radicals.

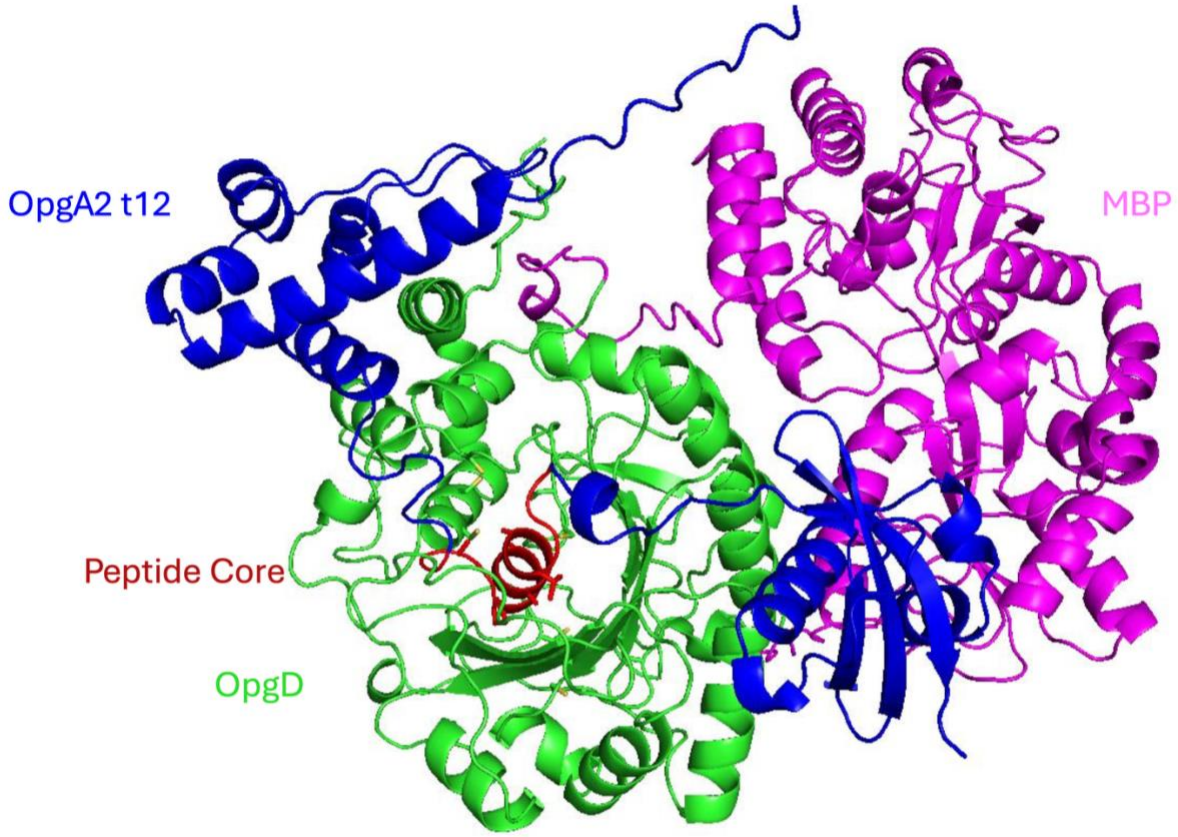

Figure 3.10. Docking model of MBP-OpgD and OpgA t12.[13] Peptide core of OpgA t12 (red) inserts into the active site of OpgD (green) with leader and follower sequences of OpgA t12 (blue) remaining outside the active site. MBP tag (pink) does not appear to interfere with substrate binding.

Given our failed attempts to catch radial intermediates, further experiments should be conducted to investigate the rates of the OpgD reaction. In this study, the products of the reaction have only been observed after 17 hours. A time-course experiment where aliquots are removed and quenched at pre-determined time points would give crucial insights into the rate of the OpgD reaction and inform which quench times should be attempted in the future. Additionally, the role

of the auxiliary cluster is unknown, and using the ΔAux construct could provide insights into its role. It is possible that using the ΔAux construct could prevent downstream events and slow or halt product turnover such that intermediate radicals could accumulate. Radical SAM peptide epimerases play a crucial role in the post-translational modification of RiPP (ribosomally synthesized and post-translationally modified peptide) natural products, introducing stereochemical diversity that can dramatically influence biological activity, stability, and target specificity. Understanding their mechanisms provides fundamental insight into radical chemistry in biology and opens opportunities to engineer new peptide-based therapeutics with tailored functions.

References

(1) Singh, K. S.; van der Hooft, J. J. J.; van Wees, S. C. M.; Medema, M. H. Integrative omics approaches for biosynthetic pathway discovery in plants. *Natural Product Reports* **2022**, *39* (9), 1876-1896.

(2) Amelia, T. S. M.; Suaberon, F. A. C.; Vad, J.; Fahmi, A. D. M.; Saludes, J. P.; Bhubalan, K. Recent Advances of Marine Sponge-Associated Microorganisms as a Source of Commercially Viable Natural Products. *Marine Biotechnology* **2022**, *24* (3), 492-512.

(3) Ruijne, F.; Kuipers, O. P. Combinatorial biosynthesis for the generation of new-to-nature peptide antimicrobials. *Biochemical Society Transactions* **2021**, *49* (1), 203-215.

(4) Ayikpoe, R. S.; Shi, C. Y.; Battiste, A. J.; Eslami, S. M.; Ramesh, S.; Simon, M. A.; Bothwell, I. R.; Lee, H.; Rice, A. J.; Ren, H. Q.; et al. A scalable platform to discover antimicrobials of ribosomal origin. *Nat. Commun.* **2022**, *13* (1), 15.

(5) Pfeiffer, I. P. M.; Schröder, M. P.; Mordhorst, S. Opportunities and challenges of RiPP-based therapeutics. *Natural Product Reports* **2024**, *41* (7), 990-1019.

(6) Montalbán-López, M.; Scott, T. A.; Ramesh, S.; Rahman, I. R.; van Heel, A. J.; Viel, J. H.; Bandarian, V.; Dittmann, E.; Genilloud, O.; Goto, Y.; et al. New developments in RiPP discovery, enzymology and engineering. *Natural Product Reports* **2021**, *38* (1), 130-239.

(7) Arnison, P. G.; Bibb, M. J.; Bierbaum, G.; Bowers, A. A.; Bugni, T. S.; Bulaj, G.; Camarero, J. A.; Campopiano, D. J.; Challis, G. L.; Clardy, J.; et al. Ribosomally synthesized and post-translationally modified peptide natural products: overview and recommendations for a universal nomenclature. *Natural Product Reports* **2013**, *30* (1), 108-160.

(8) Lu, J. G.; Xu, H. J.; Xia, J. H.; Ma, J.; Xu, J.; Li, Y. N.; Feng, J. D- and Unnatural Amino Acid Substituted Antimicrobial Peptides With Improved Proteolytic Resistance and Their Proteolytic Degradation Characteristics. *Frontiers in Microbiology* **2020**, *11*.

(9) Freeman, M. F.; Gurgui, C.; Helf, M. J.; Morinaka, B. I.; Uria, A. R.; Oldham, N. J.; Sahl, H. G.; Matsunaga, S.; Piel, J. Metagenome Mining Reveals Polytheonamides as Posttranslationally Modified Ribosomal Peptides. *Science* **2012**, *338* (6105), 387-390.

(10) Bhushan, A.; Egli, P. J.; Peters, E. E.; Freeman, M. F.; Piel, J. Genome mining- and synthetic biology-enabled production of hypermodified peptides. *Nature Chemistry* **2019**, *11* (10), 931-939.

(11) Hubrich, F.; Lotti, A.; Scott, T. A.; Piel, J. Uncovering Novel Peptide Chemistry from Bacterial Natural Products. *CHIMIA* **2021**, *75* (6), 543. DOI: 10.2533/chimia.2021.543.
(12) Piel, C. M. a. J. Broderick, J., Ed.; 2025.

(13) Abramson, J.; Adler, J.; Dunger, J.; Evans, R.; Green, T.; Pritzel, A.; Ronneberger, O.; Willmore, L.; Ballard, A. J.; Bambrick, J.; et al. Accurate structure prediction of biomolecular interactions with AlphaFold 3. *Nature* **2024**, *630* (8016), 493-500.

(14) Freeman, M. F.; Vagstad, A. L.; Piel, J. Polytheonamide biosynthesis showcasing the metabolic potential of sponge-associated uncultivated 'Entotheonella' bacteria. *Current Opinion in Chemical Biology* **2016**, *31*, 8-14.

(15) Parent, A.; Benjdia, A.; Guillot, A.; Kubiak, X.; Balty, C.; Lefranc, B.; Leprince, J.; Berteau, O. Mechanistic Investigations of PoyD, a Radical S-Adenosyl-<scp>l</scp>-methionine Enzyme Catalyzing Iterative and Directional Epimerizations in Polytheonamide A Biosynthesis. *J. Am. Chem. Soc.* **2018**, *140* (7), 2469-2477.

(16) Kitagawa, M.; Ara, T.; Arifuzzaman, M.; Ioka-Nakamichi, T.; Inamoto, E.; Toyonaga, H.; Mori, H. Complete set of ORF clones of Escherichia coli ASKA library (A complete Set of E. coli K-12 ORF archive):: Unique resources for biological research. *DNA Research* **2005**, *12* (5), 291-299.

(17) Zor, T.; Seliger, Z. Linearization of the bradford protein assay increases its sensitivity: Theoretical and experimental studies. *Anal. Biochem.* **1996**, *236* (2), 302-308.

(18) Rubinson, K. A. Practical corrections for p(H, D) measurements in mixed H2O/D2O biological buffers. *Anal. Methods* **2017**, *9* (18), 2744-2750. DOI: 10.1039/c7ay00669a.
(19) Stoll, S.; Schweiger, A. EasySpin, a comprehensive software package for spectral simulation and analysis in EPR. *J. Magn. Reson.* **2006**, *178* (1), 42-55.

(20) Hare, P. E.; Gilav, E. SEPARATION OF D-AMINO AND L-AMINO-ACIDS BY LIQUID-CHROMATOGRAPHY - USE OF CHIRAL ELUANTS. *Science* **1979**, *204* (4398), 1226-1228.

(21) Walls, W. G.; Vagstad, A. L.; Delridge, T.; Piel, J.; Broderick, W. E.; Broderick, J. B. Direct Detection of the α-Carbon Radical Intermediate Formed by OspD: Mechanistic Insights into Radical S-Adenosyl-<sc>l</sc>-methionine Peptide Epimerization. *J. Am. Chem. Soc.* **2024**, *146* (8), 5550-5559.

(22) Wang, Y.; Hu, X.; Morales-Rivera, C. A.; Li, G.-X.; Huang, X.; He, G.; Liu, P.; Chen, G. Epimerization of Tertiary Carbon Centers via Reversible Radical Cleavage of Unactivated C(sp³)–H Bonds. *J. Am. Chem. Soc.* **2018**, *140* (30), 9678-9684.

(23) Morinaka, B. I.; Vagstad, A. L.; Helf, M. J.; Gugger, M.; Kegler, C.; Freeman, M. F.; Bode, H. B.; Piel, J. Radical S-Adenosyl Methionine Epimerases: Regioselective Introduction of Diverse <scp>D</scp>-Amino Acid Patterns into Peptide Natural Products. *Angewandte Chemie International Edition* **2014**, *53* (32), 8503-8507.

(24) Benjdia, A.; Balty, C.; Berteau, O. Radical SAM Enzymes in the Biosynthesis of Ribosomally Synthesized and Post-translationally Modified Peptides (RiPPs). *Frontiers in Chemistry* **2017**, *5*.

(25) Pei, Z.-F.; Zhu, L.; Nair, S. K. Core-dependent post-translational modifications guide the biosynthesis of a new class of hypermodified peptides. *Nat. Commun.* **2023**, *14* (1).

REFERENCES CITED

Abramson, J.; Adler, J.; Dunger, J.; Evans, R.; Green, T.; Pritzel, A.; Ronneberger, O.; Willmore, L.; Ballard, A. J.; Bambrick, J.; et al. Accurate structure prediction of biomolecular interactions with AlphaFold 3. *Nature* **2024**, *630* (8016), 493-500.

Amelia, T. S. M.; Suaberon, F. A. C.; Vad, J.; Fahmi, A. D. M.; Saludes, J. P.; Bhubalan, K. Recent Advances of Marine Sponge-Associated Microorganisms as a Source of Commercially Viable Natural Products. *Marine Biotechnology* **2022**, *24* (3), 492-512.

Arnison, P. G.; Bibb, M. J.; Bierbaum, G.; Bowers, A. A.; Bugni, T. S.; Bulaj, G.; Camarero, J. A.; Campopiano, D. J.; Challis, G. L.; Clardy, J.; et al. Ribosomally synthesized and post-translationally modified peptide natural products: overview and recommendations for a universal nomenclature. *Natural Product Reports* **2013**, *30* (1), 108-160.

Ayikpoe, R. S.; Shi, C. Y.; Battiste, A. J.; Eslami, S. M.; Ramesh, S.; Simon, M. A.; Bothwell, I. R.; Lee, H.; Rice, A. J.; Ren, H. Q.; et al. A scalable platform to discover antimicrobials of ribosomal origin. *Nat. Commun.* **2022**, *13* (1), 15.

Backman, L. R. F.; Funk, M. A.; Dawson, C. D.; Drennan, C. L. New tricks for the glycyl radical enzyme family. *Critical Reviews in Biochemistry and Molecular Biology* **2017**, *52* (6), 674-695.

Balo, A. R.; Caruso, A.; Tao, L.; Tantillo, D. J.; Seyedsayamdost, M. R.; Britt, R. D. Trapping a cross-linked lysine–tryptophan radical in the catalytic cycle of the radical SAM enzyme SuiB. *Proceedings of the National Academy of Sciences* **2021**, *118* (21), e2101571118.

Banerjee, R.; Ragsdale, S. W. The Many Faces of Vitamin B₁₂: Catalysis by Cobalamin-Dependent Enzymes. *Annu. Rev. Biochem.* **2003**, *72* (1), 209-247.

Bhushan, A.; Egli, P. J.; Peters, E. E.; Freeman, M. F.; Piel, J. Genome mining- and synthetic biology-enabled production of hypermodified peptides. *Nature Chemistry* **2019**, *11* (10), 931-939.

Blum, M.; Andreeva, A.; Laise; Sara; Grego, T.; Hobbs, E.; Beatriz; Orr, A.; Paysan-Lafosse, T.; Ponamareva, I.; et al. InterPro: the protein sequence classification resource in 2025. *Nucleic Acids Research* **2025**, *53* (D1), D444-D456.

Booker, S. J.; Lloyd, C. T. Twenty Years of Radical SAM! The Genesis of the Superfamily. *ACS Bio & Med Chem Au* **2022**, *2* (6), 538-547.

Brazzolotto, X.; Rubach, J. K.; Gaillard, J.; Gambarelli, S.; Atta, M.; Fontecave, M. The Fe-Fe -hydrogenase maturation protein HydF from Thermotoga maritima is a GTPase with an iron-sulfur cluster. *Journal of Biological Chemistry* **2006**, *281* (2), 769-774.

Bridwell-Rabb, J.; Grell, T. A. J.; Drennan, C. L. A Rich Man, Poor Man Story of S-Adenosylmethionine and Cobalamin Revisited. *Annu. Rev. Biochem.* **2018**, *87* (1), 555-584.

Broderick, J. B.; Duderstadt, R. E.; Fernandez, D. C.; Wojtuszewski, K.; Henshaw, T. F.; Johnson, M. K. Pyruvate formate-lyase activating enzyme is an iron-sulfur protein. *J. Am. Chem. Soc.* **1997**, *119* (31), 7396-7397.

Broderick, J. B.; Duffus, B. R.; Duschene, K. S.; Shepard, E. M. Radical S-Adenosylmethionine Enzymes. *Chem. Rev.* **2014**, *114* (8), 4229-4317, Review.

Brown, K. L. Chemistry and Enzymology of Vitamin B₁₂. *Chem. Rev.* **2005**, *105* (6), 2075-2150.

Bruender, N. A.; Young, A. P.; Bandarian, V. Chemical and Biological Reduction of the Radical SAM Enzyme CPH₄ Synthase. *Biochemistry* **2015**, *54* (18), 2903-2910.

Burdette, S. C.; Lippard, S. J. Meeting of the minds: Metalloneurochemistry. *Proceedings of the National Academy of Sciences* **2003**, *100* (7), 3605-3610.

Byer, A. S.; McDaniel, E. C.; Impano, S.; Broderick, W. E.; Broderick, J. B. Mechanistic Studies of Radical SAM Enzymes: Pyruvate Formate-Lyase Activating Enzyme and Lysine 2,3-Aminomutase Case Studies. In *Radical Sam Enzymes*, Bandarian, V. Ed.; Methods in Enzymology, Vol. 606; Elsevier Academic Press Inc, 2018; pp 269-318.

Byer, A. S.; Shepard, E. M.; Peters, J. W.; Broderick, J. B. Radical S-Adenosyl-L-methionine Chemistry in the Synthesis of Hydrogenase and Nitrogenase Metal Cofactors. *Journal of Biological Chemistry* **2015**, *290* (7), 3987-3994.

Byer, A. S.; Yang, H.; McDaniel, E. C.; Kathiresan, V.; Impano, S.; Pagnier, A.; Watts, H.; Denler, C.; Vagstad, A. L.; Piel, J.; et al. Paradigm Shift for Radical S-Adenosyl-L-methionine Reactions: The Organometallic Intermediate Ω Is Central to Catalysis. *J. Am. Chem. Soc.* **2018**, *140* (28), 8634-8638.

Cosper, N. J.; Booker, S. J.; Ruzicka, F.; Frey, P. A.; Scott, R. A. Direct FeS Cluster Involvement in Generation of a Radical in Lysine 2,3-Aminomutase. *Biochemistry* **2000**, *39* (51), 15668-15673.

Donck, S.; Baroudi, A.; Fensterbank, L.; Goddard, J. P.; Ollivier, C. Visible-Light Photocatalytic Reduction of Sulfonium Salts as a Source of Aryl Radicals. *Advanced Synthesis & Catalysis* **2013**, *355* (8), 1477-1482.

Dowling, D. P.; Bruender, N. A.; Young, A. P.; McCarty, R. M.; Bandarian, V.; Drennan, C. L. Radical SAM enzyme QueE defines a new minimal core fold and metal-dependent mechanism. *Nature Chemical Biology* **2014**, *10* (2), 106-112.

Duboc-Toia, C.; Hassan, A. K.; Mulliez, E.; Ollagnier-De Choudens, S.; Fontecave, M.; Leutwein, C.; Heider, J. Very High-Field EPR Study of Glycyl Radical Enzymes. *J. Am. Chem. Soc.* **2003**, *125* (1), 38-39.

Eastman, K. A. S.; Jochimsen, A. S.; Bandarian, V. Intermolecular electron transfer in radical SAM enzymes as a new paradigm for reductive activation. *Journal of Biological Chemistry* **2023**, *299* (9), 105058.

Fenwick, M. K.; Mehta, A. P.; Zhang, Y.; Abdelwahed, S. H.; Begley, T. P.; Ealick, S. E. Non-canonical active site architecture of the radical SAM thiamin pyrimidine synthase. *Nat. Commun.* **2015**, *6* (1), 6480.

Finkelstein, J. Metalloproteins. *Nature* **2009**, *460* (7257), 813-813.

Fontecave, M. Iron-sulfur clusters: ever-expanding roles. *Nature Chemical Biology* **2006**, *2* (4), 171-174.

Freeman, M. F.; Gurgui, C.; Helf, M. J.; Morinaka, B. I.; Uria, A. R.; Oldham, N. J.; Sahl, H. G.; Matsunaga, S.; Piel, J. Metagenome Mining Reveals Polytheonamides as Posttranslationally Modified Ribosomal Peptides. *Science* **2012**, *338* (6105), 387-390.

Freeman, M. F.; Vagstad, A. L.; Piel, J. Polytheonamide biosynthesis showcasing the metabolic potential of sponge-associated uncultivated 'Entotheonella' bacteria. *Current Opinion in Chemical Biology* **2016**, *31*, 8-14.

Frey, P. A.; Abeles, R. H. The Role of the B12 Coenzyme in the Conversion of 1,2-Propanediol to Propionaldehyde. *Journal of Biological Chemistry* **1966**, *241* (11), 2732-2733.

Frey, P. A.; Hegeman, A. D.; Ruzicka, F. J. The Radical SAM Superfamily. *Critical Reviews in Biochemistry and Molecular Biology* **2008**, *43* (1), 63-88.

Frey, P. A. Radical Mechanisms of Enzymatic Catalysis. *Annu. Rev. Biochem.* **2001**, *70* (1), 121-148.

Grell, T. A. J.; Goldman, P. J.; Drennan, C. L. SPASM and Twitch Domains in S-Adenosylmethionine (SAM) Radical Enzymes. *Journal of Biological Chemistry* **2015**, *290* (7), 3964-3971.

Hare, P. E.; Gilav, E. SEPARATION OF D-AMINO AND L-AMINO-ACIDS BY LIQUID-CHROMATOGRAPHY - USE OF CHIRAL ELUANTS. *Science* **1979**, *204* (4398), 1226-1228.

Henshaw, T. F.; Cheek, J.; Broderick, J. B. The [4Fe-4S]¹⁺ Cluster of Pyruvate Formate-Lyase Activating Enzyme Generates the Glycyl Radical on Pyruvate Formate-Lyase: EPR-Detected Single Turnover. *J. Am. Chem. Soc.* **2000**, *122* (34), 8331-8332.

Hioe, J.; Savasci, G.; Brand, H.; Zipse, H. The Stability of C_α Peptide Radicals: Why Glycyl Radical Enzymes? *Chemistry-a European Journal* **2011**, *17* (13), 3781-3789.

Hoffman, B. M.; Broderick, W. E.; Broderick, J. B. Mechanism of Radical Initiation in the Radical SAM Enzyme Superfamily. *Annu. Rev. Biochem.* **2023**, *92*, 333-349, Review.

Holliday, G. L.; Akiva, E.; Meng, E. C.; Brown, S. D.; Calhoun, S.; Pieper, U.; Sali, A.; Booker, S. J.; Babbitt, P. C. Atlas of the Radical SAM Superfamily: Divergent Evolution of Function Using a "Plug and Play" Domain. Elsevier, 2018; pp 1-71.

Horitani, M.; Shisler, K.; Broderick, W. E.; Hutcheson, R. U.; Duschene, K. S.; Marts, A. R.; Hoffman, B. M.; Broderick, J. B. Radical SAM catalysis via an organometallic intermediate with an Fe–[5′-C]-deoxyadenosyl bond. *Science* **2016**, *352* (6287), 822-825.

Hubrich, F.; Lotti, A.; Scott, T. A.; Piel, J. Uncovering Novel Peptide Chemistry from Bacterial Natural Products. *CHIMIA* **2021**, *75* (6), 543. DOI: 10.2533/chimia.2021.543.

Impano, S.; Yang, H.; Jodts, R. J.; Pagnier, A.; Swimley, R.; McDaniel, E. C.; Shepard, E. M.; Broderick, W. E.; Broderick, J. B.; Hoffman, B. M. Active-Site Controlled, Jahn-Teller Enabled Regioselectivity in Reductive S-C Bond Cleavage of S-Adenosylmethionine in Radical SAM Enzymes. *J Am Chem Soc* **2021**, *143* (1), 335-348.

Juarez-Facio, A. T.; de Lagarde, V. M.; Monteil, C.; Vaugeois, J. M.; Corbiere, C.; Rogez-Florent, T. Validation of a Fast and Simple HPLC-UV Method for the Quantification of Adenosine Phosphates in Human Bronchial Epithelial Cells. *Molecules* **2021**, *26* (20), 8.

Kamat, S. S.; Raushel, F. M. PhnJ – A novel radical SAM enzyme from the C–P lyase complex. *Perspectives in Science* **2015**, *4*, 32-37.

King, P. W.; Posewitz, M. C.; Ghirardi, M. L.; Seibert, M. Functional studies of FeFe hydrogenase maturation in an Escherichia coli biosynthetic system. *Journal of Bacteriology* **2006**, *188* (6), 2163-2172.

Kitagawa, M.; Ara, T.; Arifuzzaman, M.; Ioka-Nakamichi, T.; Inamoto, E.; Toyonaga, H.; Mori, H. Complete set of ORF clones of Escherichia coli ASKA library (A complete Set of E. coli K-12 ORF archive):: Unique resources for biological research. *DNA Research* **2005**, *12* (5), 291-299.

Knappe, J.; Blaschkowski, H. P. Pyruvate formate-lyase from Escherischia coli and its activation system. *Methods in enzymology* **1975**, *41*, 508-518.

Krebs, C.; Broderick, W. E.; Henshaw, T. F.; Broderick, J. B.; Huynh, B. H. Coordination of adenosylmethionine to a unique iron site of the 4Fe-4S of pyruvate formate-lyase activating enzyme: A Mossbauer spectroscopic study. *J. Am. Chem. Soc.* **2002**, *124* (6), 912-913.

Kuchenreuther, J. M.; Myers, W. K.; Suess, D. L. M.; Stich, T. A.; Pelmenschikov, V.; Shiigi, S. A.; Cramer, S. P.; Swartz, J. R.; Britt, R. D.; George, S. J. The HydG Enzyme Generates an Fe(CO)2(CN) Synthon in Assembly of the FeFe Hydrogenase H-Cluster. *Science* **2014**, *343* (6169), 424-427.

Landgraf, B. J.; McCarthy, E. L.; Booker, S. J. Radical S-Adenosylmethionine Enzymes in Human Health and Disease. *Annu. Rev. Biochem.* **2016**, *85* (1), 485-514.

Lanz, N. D.; Booker, S. J. Auxiliary iron–sulfur cofactors in radical SAM enzymes. *Biochimica et Biophysica Acta (BBA) - Molecular Cell Research* **2015**, *1853* (6), 1316-1334.

Latham, J. A.; Barr, I.; Klinman, J. P. At the confluence of ribosomally synthesized peptide modification and radical S-adenosylmethionine (SAM) enzymology. *Journal of Biological Chemistry* **2017**, *292* (40), 16397-16405.

Layer, G.; Heinz, D. W.; Jahn, D.; Schubert, W.-D. Structure and function of radical SAM enzymes. *Current Opinion in Chemical Biology* **2004**, *8* (5), 468-476.

Lu, J. G.; Xu, H. J.; Xia, J. H.; Ma, J.; Xu, J.; Li, Y. N.; Feng, J. D- and Unnatural Amino Acid Substituted Antimicrobial Peptides With Improved Proteolytic Resistance and Their Proteolytic Degradation Characteristics. *Frontiers in Microbiology* **2020**, *11*.

Magnusson, O. T.; Reed, G. H.; Frey, P. A. Characterization of an Allylic Analogue of the 5‘-Deoxyadenosyl Radical: An Intermediate in the Reaction of Lysine 2,3-Aminomutase. *Biochemistry* **2001**, *40* (26), 7773-7782.

Magnusson, O. T.; Reed, G. H.; Frey, P. A. Spectroscopic evidence for the participation of an allylic analogue of the 5′-deoxyadenosyl radical in the reaction of lysine 2,3-aminomutase. *J. Am. Chem. Soc.* **1999**, *121* (41), 9764-9765.

Mahanta, N.; Hudson, G. A.; Mitchell, D. A. Radical S-Adenosylmethionine Enzymes Involved in RiPP Biosynthesis. *Biochemistry* **2017**, *56* (40), 5229-5244.

McCarthy, E. L.; Booker, S. J. Biochemical Approaches for Understanding Iron–Sulfur Cluster Regeneration in Escherichia coli Lipoyl Synthase During Catalysis. Elsevier, 2018; pp 217-239.

Mészáros, L. S.; Németh, B.; Esmieu, C.; Ceccaldi, P.; Berggren, G. InVivo EPR Characterization of Semi-Synthetic FeFe Hydrogenases. *Angew. Chem.-Int. Edit.* **2018**, *57* (10), 2596-2599.

Miller, S. A.; Bandarian, V. Analysis of Electrochemical Properties of S-Adenosyl-<scp>l</scp>-methionine and Implications for Its Role in Radical SAM Enzymes. *J. Am. Chem. Soc.* **2019**, *141* (28), 11019-11026. DOI: 10.1021/jacs.9b00933.

Montalbán-López, M.; Scott, T. A.; Ramesh, S.; Rahman, I. R.; van Heel, A. J.; Viel, J. H.; Bandarian, V.; Dittmann, E.; Genilloud, O.; Goto, Y.; et al. New developments in RiPP discovery, enzymology and engineering. *Natural Product Reports* **2021**, *38* (1), 130-239.

Morinaka, B. I.; Vagstad, A. L.; Helf, M. J.; Gugger, M.; Kegler, C.; Freeman, M. F.; Bode, H. B.; Piel, J. Radical S-Adenosyl Methionine Epimerases: Regioselective Introduction of Diverse <scp>D</scp>-Amino Acid Patterns into Peptide Natural Products. *Angewandte Chemie International Edition* **2014**, *53* (32), 8503-8507.

Morra, S.; Valetti, F.; Gilardi, G. FeFe -hydrogenases as biocatalysts in bio-hydrogen production. *Rendiconti Lincei-Scienze Fisiche E Naturali* **2017**, *28*, 183-194.

Mulder, D. W.; Ortillo, D. O.; Gardenghi, D. J.; Naumov, A. V.; Ruebush, S. S.; Szilagyi, R. K.; Huynh, B.; Broderick, J. B.; Peters, J. W. Activation of HydA^{ΔEFG} Requires a Preformed 4Fe-4S Cluster. *Biochemistry* **2009**, *48* (26), 6240-6248.

Nicolet, Y. Structure-function relationships of radical SAM enzymes. *Nat. Catal.* **2020**, *3* (4), 337-350, Review.

Oberg, N.; Precord, T. W.; Mitchell, D. A.; Gerlt, J. A. RadicalSAM.org: A Resource to Interpret Sequence-Function Space and Discover New Radical SAM Enzyme Chemistry. *ACS Bio & Med Chem Au* **2022**, *2* (1), 22-35.

Parent, A.; Benjdia, A.; Guillot, A.; Kubiak, X.; Balty, C.; Lefranc, B.; Leprince, J.; Berteau, O. Mechanistic Investigations of PoyD, a Radical S-Adenosyl-<scp>l</scp>-methionine Enzyme Catalyzing Iterative and Directional Epimerizations in Polytheonamide A Biosynthesis. *J. Am. Chem. Soc.* **2018**, *140* (7), 2469-2477.

Pei, Z.-F.; Zhu, L.; Nair, S. K. Core-dependent post-translational modifications guide the biosynthesis of a new class of hypermodified peptides. *Nat. Commun.* **2023**, *14* (1).

Peng, Y.; Veneziano, S. E.; Gillispie, G. D.; Broderick, J. B. Pyruvate Formate-lyase, Evidence for an Open Conformation Favored in the Presence of Its Activating Enzyme. *Journal of Biological Chemistry* **2010**, *285* (35), 27224-27231. DOI: 10.1074/jbc.M109.096875.

Pfeiffer, I. P. M.; Schröder, M. P.; Mordhorst, S. Opportunities and challenges of RiPP-based therapeutics. *Natural Product Reports* **2024**, *41* (7), 990-1019. DOI: 10.1039/d3np00057e.

Piel, C. M. a. J. Broderick, J., Ed.; 2025.

Posewitz, M. C.; King, P. W.; Smolinski, S. L.; Zhang, L. P.; Seibert, M.; Ghirardi, M. L. Discovery of two novel radical S-adenosylmethionine proteins required for the assembly of an active Fe hydrogenase. *Journal of Biological Chemistry* **2004**, *279* (24), 25711-25720.

Rao, G.; Tao, L.; Yu, X.; Rauchfuss, T. B.; Britt, R. D. The Radical S-Adenosyl-<scp>l</scp>-methionine Enzyme HydE Forms an Fe(I)Fe(I) Dimer En Route to the [FeFe] Hydrogenase H-Cluster. *J. Am. Chem. Soc.* **2025**, *147* (36), 32737-32744.

Rodel, W.; Plaga, W.; Frank, R.; Knappe, J. PRIMARY STRUCTURES OF ESCHERICHIA-COLI PYRUVATE FORMATE-LYASE AND PYRUVATE-FORMATE-LYASE-ACTIVATING ENZYME DEDUCED FROM THE DNA NUCLEOTIDE-SEQUENCES. *European Journal of Biochemistry* **1988**, *177* (1), 153-158.

Rubach, J. K.; Brazzolotto, X.; Gaillard, J.; Fontecave, M. Biochemical characterization of the HydE and HydG iron-only hydrogenase maturation enzymes from Thermatoga maritima. *Febs Letters* **2005**, *579* (22), 5055-5060.

Rubinson, K. A. Practical corrections for p(H, D) measurements in mixed H2O/D2O biological buffers. *Anal. Methods* **2017**, *9* (18), 2744-2750. DOI: 10.1039/c7ay00669a.

Ruijne, F.; Kuipers, O. P. Combinatorial biosynthesis for the generation of new-to-nature peptide antimicrobials. *Biochemical Society Transactions* **2021**, *49* (1), 203-215.

Rush, K. W.; Eastman, K. A. S.; Kincannon, W. M.; Blackburn, N. J.; Bandarian, V. Peptide Selenocysteine Substitutions Reveal Direct Substrate–Enzyme Interactions at Auxiliary Clusters in Radical S-Adenosyl-<scp>l</scp>-methionine Maturases. *J. Am. Chem. Soc.* **2023**, *145* (18), 10167-10177.

Saeva, F. D.; Morgan, B. P. Mechanism of one-electron electrochemical reductive cleavage reactions of sulfonium salts. *J. Am. Chem. Soc.* **1984**, *106* (15), 4121-4125.

Shepard, E. M.; Impano, S.; Duffus, B. R.; Pagnier, A.; Duschene, K. S.; Betz, J. N.; Byer, A. S.; Galambas, A.; McDaniel, E. C.; Watts, H.; et al. HydG, the “dangler” iron, and catalytic production of free CO and CN[−]: implications for [FeFe]-hydrogenase maturation. *Dalton Transactions* **2021**, *50* (30), 10405-10422.

Shepard, E. M.; Mus, F.; Betz, J. N.; Byer, A. S.; Duffus, B. R.; Peters, J. W.; Broderick, J. B. FeFe -Hydrogenase Maturation. *Biochemistry* **2014**, *53* (25), 4090-4104.

Shisler, K. A.; Broderick, J. B. Glycyl radical activating enzymes: Structure, mechanism, and substrate interactions. *Archives of Biochemistry and Biophysics* **2014**, *546*, 64-71.

Silakov, A.; Lanz, N. D.; Booker, S. J. Characterization of Radical S-adenosylmethionine Enzymes and Intermediates in their Reactions by Continuous Wave and Pulse Electron Paramagnetic Resonance Spectroscopies. Springer International Publishing, 2017; pp 143-186.

Singh, K. S.; van der Hooft, J. J. J.; van Wees, S. C. M.; Medema, M. H. Integrative omics approaches for biosynthetic pathway discovery in plants. *Natural Product Reports* **2022**, *39* (9), 1876-1896.

Sofia, H. J. Radical SAM, a novel protein superfamily linking unresolved steps in familiar biosynthetic pathways with radical mechanisms: functional characterization using new analysis and information visualization methods. *Nucleic Acids Research* **2001**, *29* (5), 1097-1106.

Stoll, S.; Schweiger, A. EasySpin, a comprehensive software package for spectral simulation and analysis in EPR. *J. Magn. Reson.* **2006**, *178* (1), 42-55.

Valko, M.; Jomova, K.; Rhodes, C. J.; Kuča, K.; Musílek, K. Redox- and non-redox-metal-induced formation of free radicals and their role in human disease. *Archives of Toxicology* **2016**, *90* (1), 1-37.

Vey, J. L.; Drennan, C. L. Structural Insights into Radical Generation by the Radical SAM Superfamily. *Chem. Rev.* **2011**, *111* (4), 2487-2506. DOI: 10.1021/cr9002616.

Wagner, A. F.; Frey, M.; Neugebauer, F. A.; Schäfer, W.; Knappe, J. The free radical in pyruvate formate-lyase is located on glycine-734. *Proceedings of the National Academy of Sciences* **1992**, *89* (3), 996-1000.

Walls, W. G.; Vagstad, A. L.; Delridge, T.; Piel, J.; Broderick, W. E.; Broderick, J. B. Direct Detection of the α-Carbon Radical Intermediate Formed by OspD: Mechanistic Insights into Radical S-Adenosyl-<sc>l</sc>-methionine Peptide Epimerization. *J. Am. Chem. Soc.* **2024**, *146* (8), 5550-5559.

Walls, W. Mechanistic Investigation into post-Translational Modifications Catalyzed By Radical S-Adenosylmethionine Enzymes. Montana State Univeristy, 2025.

Walsby, C. J.; Hong, W.; Broderick, W. E.; Cheek, J.; Ortillo, D.; Broderick, J. B.; Hoffman, B. M. Electron-nuclear double resonance spectroscopic evidence that S-adenosylmethionine binds in contact with the catalytically active 4Fe-4S + cluster of pyruvate formate-lyase activating enzyme. *J. Am. Chem. Soc.* **2002**, *124* (12), 3143-3151.

Walsby, C. J.; Hong, W.; Broderick, W. E.; Cheek, J.; Ortillo, D.; Broderick, J. B.; Hoffman, B. M. Electron-nuclear double resonance spectroscopic evidence that S-adenosylmethionine binds in contact with the catalytically active 4Fe-4S + cluster of pyruvate formate-lyase activating enzyme. *J. Am. Chem. Soc.* **2002**, *124* (12), 3143-3151.

Wang, X.; Saeva, F. D.; Kampmeier, J. A. Photosensitized Reduction of Sulfonium Salts: Evidence for Nondissociative Electron Transfer. *J. Am. Chem. Soc.* **1999**, *121* (18), 4364-4368.

Wang, Y.; Hu, X.; Morales-Rivera, C. A.; Li, G.-X.; Huang, X.; He, G.; Liu, P.; Chen, G. Epimerization of Tertiary Carbon Centers via Reversible Radical Cleavage of Unactivated C(sp³)–H Bonds. *J. Am. Chem. Soc.* **2018**, *140* (30), 9678-9684.

Wang, Y.; Li, D.; Xu, K.; Wang, G.; Zhang, F. Copper homeostasis and neurodegenerative diseases. *Neural Regeneration Research* **2025**, *20* (11), 3124-3143.

Yang, H.; Impano, S.; Shepard, E. M.; James, C. D.; Broderick, W. E.; Broderick, J. B.; Hoffman, B. M. Photoinduced Electron Transfer in a Radical SAM Enzyme Generates an S-Adenosylmethionine Derived Methyl Radical. *J Am Chem Soc* **2019**, *141* (40), 16117-16124.

Yang, H.; McDaniel, E. C.; Impano, S.; Byer, A. S.; Jodts, R. J.; Yokoyama, K.; Broderick, W. E.; Broderick, J. B.; Hoffman, B. M. The Elusive 5'-Deoxyadenosyl Radical: Captured and Characterized by Electron Paramagnetic Resonance and Electron Nuclear Double Resonance Spectroscopies. *J Am Chem Soc* **2019**, *141* (30), 12139-12146.

Zor, T.; Seliger, Z. Linearization of the bradford protein assay increases its sensitivity: Theoretical and experimental studies. *Anal. Biochem.* **1996**, *236* (2), 302-308.